Cobalt catalysts on carbon-based materials for Fischer-Tropsch synthesis: a review

Amel Ghogia, Ange Nzihou, Philippe Serp, Katerina Soulantica, Doan Pham Minh

Cobalt catalysts on carbon-based materials for Fischer-Tropsch synthesis: a review

Amel Cydric Ghogia[a,b,c], Ange Nzihou[a,] Philippe Serp[b]* philippe.serp@ensiacet.fr, Katerina Soulantica[c]* ksoulant@insa-toulouse.fr, Doan Pham Minh[a]* doan.phamminh@mines-albi.fr

[a]Université de Toulouse, IMT Mines Albi, UMR CNRS 5302, Centre RAPSODEE, Campus Jarlard, F-81013 Albi, cedex 09, France.

[b]LCC, CNRS-UPR 8241, ENSIACET, Université de Toulouse, France.

[c]LPCNO, Université de Toulouse, CNRS, INSA, UPS, Toulouse.

*Corresponding author:

Graphical abstract

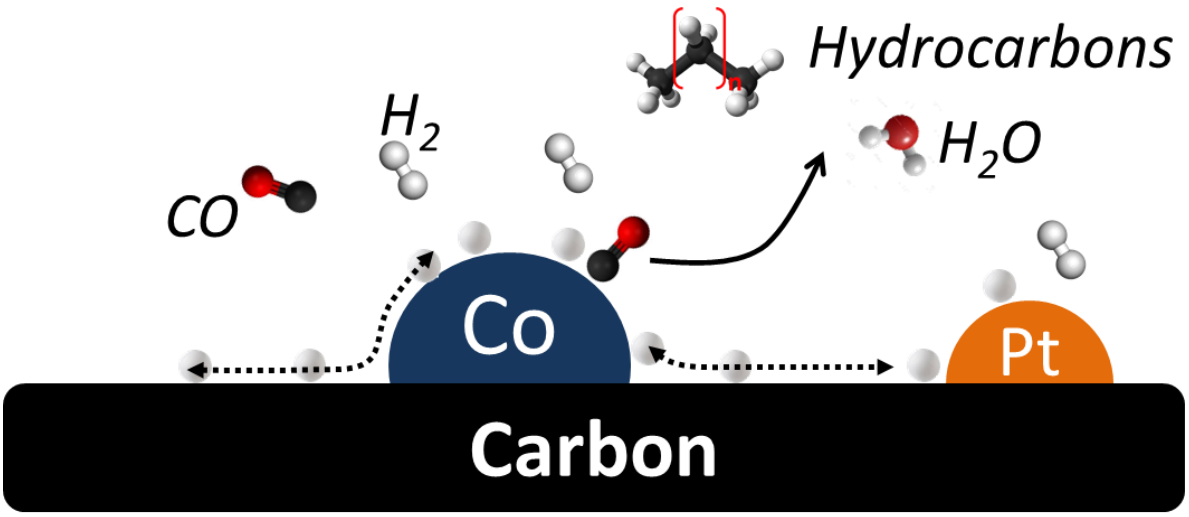

Highlights

- Challenges and opportunities in Co/C catalyzed Fischer-Tropsch synthesis
- Guidelines for the design of Co/C catalysts for Fischer-Tropsch synthesis
- The choice of carbon materials as Fischer-Tropsch synthesis support is rationalized
- The evolution of TOF and S_{C5+} with Co particle size is relatively complex
- Effect of confinement and spillover on catalyst performances are discussed

Abstract:

This review analyzes the literature from the 80's to the beginning of 2020 and covers the use of carbon materials as supports for cobalt-based catalysts used in the Fischer Tropsch reaction. The article is composed of two sections. The first one details the reactivity of carbon supported cobalt catalysts with a particular focus on: i) reaction mechanisms and conditions, ii) effect of cobalt particle size, iii) confinement effects, iv) hydrogen spillover, and v) deactivation mechanisms. In the second part, the different methods of Co/C catalyst

preparation are presented, and the influence of several parameters such as the type of supports and its functionalization, the metal loading or the catalyst activation on the catalytic performances is discussed. This work also provides some perspectives in the field.

Keywords: Cobalt catalysts, carbon materials, Fischer-Tropsch synthesis, catalyst support, catalyst preparation

1. Introduction

The Fischer-Tropsch Synthesis (FTS) is a surface catalyzed polymerization process enabling the conversion of syngas into higher hydrocarbons that can be further upgraded into liquid hydrocarbon transportation fuels with very low sulfur content, and various other chemical products [1]. Depending on the source of the syngas, the technology is often referred to as coal-to-liquids (CTL), gas-to-liquids (GTL), and more recently biomass-to-liquid (BTL) [2]. The FT reaction is highly exothermic with a reaction enthalpy of about 170 kJ mol^{-1}, therefore heat management is critical. In general, the reaction can be performed in fixed- or fluidized-bed reactors or in slurry reactors [3]. Due to their low mass and heat transfer, microstructured- and monolith-reactors have also been considered [4,5]. The FTS can be operated at low-temperature (LTFT, 220-260°C) using either cobalt-based or iron-based catalysts, at middle temperature (MTFT, 260–300 °C) [6] or at high-temperature (HTFT, 320-350 °C) on iron-based catalysts. The rate of formation and the selectivity of hydrocarbons, key challenges of the research in FTS, are dependent on the catalyst used. Ru [7], Ni [8], Fe [9], and Co [10] are the active metals most often used in FTS. Nickel is generally not desirable since it promotes CH_4 formation. Iron is cheap and has a high water-gas-shift activity and is therefore suitable for syngas feedstocks of a low H_2/CO ratio, such as those derived from coal gasification. Cobalt is more active, stable, and is generally preferred over Fe for LTFT [11] and over Ru because of the prohibitively high price of this latter metal. The cobalt-catalyzed LTFT involves syngas with a high H_2/CO ratio (~2), which is generally generated from natural gas.

In addition to cobalt (15-30 wt.%) and a support (generally a high surface area inorganic oxide such as Al_2O_3, SiO_2 or TiO_2), the catalysts often contain a number of promoters, including noble metals (0.05-0.1 wt.%), to improve Co reducibility, and structural oxide promoters (ZrO_2, La_2O_3, CeO_2, 1-10 wt.%) to improve Co dispersion or induce electronic effects [12,13]. As in many reactions, in FTS the nature of the support material directly influences the reducibility and activity, selectivity, and also stability (resistance to attrition, sintering, re-oxidation or poisoning) of catalysts [14] including Co-based catalysts [15]. In addition, the nature of the support can also influence heat and mass transfer, or diffusion of reagents and reaction products [16]. Metal-support interaction (MSI) strength and charge transfer [17], support textural properties (surface area and porosity) [18], acid/base properties [19], surface chemistry [20], thermal stability and conductivity [21], and catalyst resistance to attrition [22] are the main features that influence the reaction and transfer phenomena in the FT process, as well as catalyst stability [23].

Oxides, such as SiO_2, Al_2O_3, and TiO_2, are the most extensively investigated supports for Co catalysts. However, the main drawback of these oxide supports is the undesirable strong cobalt-support interaction that can lead to the formation of mixed metal oxides (such as $CoAl_2O_4$ when Al_2O_3 is used as support), which are inactive in FTS and cause rapid deactivation of the FT catalysts. For typical air calcined catalysts, Co oxide species have been found to have strong interactions with Al_2O_3, moderate ones with TiO_2, and relatively weak interactions with SiO_2 [24]. Although the interaction is relatively weak for Co/SiO_2 catalysts, the

hardly reducible Co_2SiO_4 can also be formed. Such detrimental interactions can be circumvented by surface modifications with inorganic oxides (MgO, ZrO_2, La_2O_3), or hydrothermal carbon coatings leading to carbon-oxide hybrid supports [16,25]. Considering this latter approach, carbon materials are generally considered to interact weakly with cobalt compared to conventional oxide supports, and thus overcome the drawbacks associated with the formation of inactive mixed oxides.

In catalysis, the most widely employed carbon support material is activated carbon (AC), followed by carbon black (CB) and graphite or graphitized materials [26]. Carbon materials such as carbon nanotubes (CNT) and nanofibers (CNF), graphene and mesoporous carbons have also recently attracted much attention as catalyst supports because of their unique properties [27]. In addition to a tailorable porous structure and surface chemistry, most of these carbon materials present several advantages as catalyst supports, such as: i) an easy reduction of the metallic phase; ii) a good resistance to acidic/basic media; iii) a stable structure even above 750 °C under inert atmosphere; iv) porous carbon catalysts can be prepared in different physical forms such as granules, cloth, fibers, pellets, etc.; v) the metal can be easily recovered; and vi) the cost of conventional carbon supports is usually lower than that of other conventional supports, such as Al_2O_3 and SiO_2 [28–30]. Nevertheless, this type of supports can also present some disadvantages such as: i) a weak metal support interaction that can lead to metal sintering; ii) they can be easily gasified, which makes them difficult to use in high temperature hydrogenation and oxidation reactions; iii) their reproducibility can be poor, especially activated carbon-based catalysts since different batches of the same material can contain varying ash amounts; and iv) relatively low bulk density in the powder form leading to high reactor volumes and high-pressure drops.

Graphite intercalation compounds, including with cobalt, were one of the first modified carbon materials used in FTS [31,32], and the first reports on the use of Co/C catalysts in FTS dates from the 80-90's [33,34]. A review of development in Co-based catalysts supported on carbon materials for FTS was published in 2015 with 93 references [35], (for Fe/C and ordered mesoporous cobalt based catalysts in FTS the readers are encouraged to read some recent reviews [36–38]) and since then more than 200 publications have been published on that subject (Figure 1).

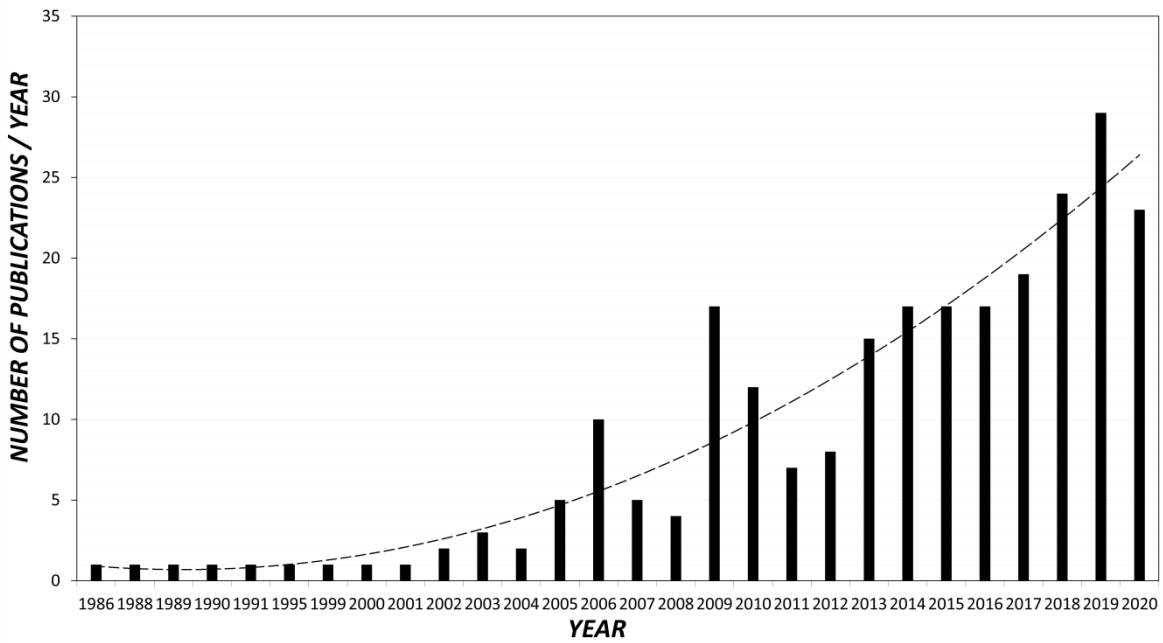

Figure 1. Published works between 1986 and October 2020 related to the use of carbon-supported cobalt-based catalysts for FTS. Source WoS.

The aim of the present review article is to provide a comprehensive overview on the impact of the use of carbon materials to support cobalt in FTS. The review is divided into two main sections, the first one dealing with catalyst reactivity and the second one analyzing Co/C FTS catalyst preparation, and activation methods. Major challenges for the use of Co/C catalyst in FTS are also discussed.

2. Catalyst reactivity

The catalyst reactivity is an important aspect for the development of a new FTS catalyst. It has been reported in the literature that the reactivity of Co/C catalysts strongly depends on several parameters such as Co particle size, crystal phase, reaction conditions, Co confinement, and its ability to favor hydrogen spillover [39,40]. The impact of these parameters on the catalyst reactivity will be discussed in the following section. Before addressing their reactivity, we will present an overview of the proposed mechanisms of the FTS reaction, and the impact of reaction conditions on the course of the reaction.

2.1 Reaction mechanisms

FTS is a complex reaction implying surface polymerization reactions, in which monomer units are produced *in*-situ from hydrogen and carbon monoxide on the catalyst surface *(*Figure 2a) [41]. This leads to a variety of hydrocarbons (*Eq.1*) for a wide range of applications. Hence, various hydrocarbons are formed by successive addition of C1 units to hydrocarbon chains on the catalyst surface (*Eq.1*) [41]. Other products such as carbon dioxide (*Eq.3*), water (*Eq.1* and *Eq.2*) and alcohols (*Eq.4*) [42] are also produced [41].

$CO + 2H_2 \rightarrow (-CH_2-) + H_2O$ $\Delta H^0_{298} = -152\ kJ\ mol^{-1}$

(*Eq.1*)

$CO + 3H_2 \rightarrow CH_4 + H_2O$ $\Delta H^0_{298} = -206\ kJ\ mol^{-1}$

(*Eq.2*)

$CO + H_2O \rightarrow CO_2 + H_2$ $\Delta H^0_{298} = -41\ kJ\ mol^{-1}$

(*Eq.3*)

$nCO + 2nH_2 \rightarrow C_nH_{2n+2}O + (n-1)\ H_2O$ $\Delta H^0_{227} = -370\ kJ\ mol^{-1}$

(*Eq.4*)

The mechanism of FTS has been debated over decades, and two main mechanisms have been envisaged (Figure 2a) [43]. The first one, called *carbide mechanism*, involves as a first step CO dissociative chemisorption, which can be either direct or H-assisted (Figure 2b), and then the resulting carbon species are hydrogenated to produce CH_x surface species. These latter moieties act as chain initiators and propagators in the formation of long-chain hydrocarbons. The H-assisted CO dissociative chemisorption involving HCO* or HCOH* species, which significantly lowers the activation energy for subsequent C-O bond scission, could explain the positive reaction order with respect to H_2, assuming that CO dissociation is the rate-determining step [44]. This H-assisted CO dissociative chemisorption could involve either direct hydrogenation (on highly CO-covered terraces) [44,45], or proton transfer from surface hydroxyl groups to O atoms [46]. The direct CO dissociation on Co-based catalysts would require high activation energies on the close-packed Co(0001) surface at moderate coverage. This mechanism is thus inconsistent under FTS conditions [47]. These observations led researchers to consider defect sites (steps and kinks) as the catalytically relevant sites [48–50], or to consider the role of the crystal structure (*fcc*-Co *vs hcp*-Co) since it has been shown that *hcp*-Co exposes sites that are more active for CO activation than *fcc*-Co [47,51]. In this case, the positive H_2 reaction order could be correlated to the fact that the hydrogenation of adsorbed C and O atoms is slower than CO dissociation [49]. The second mechanism proceeds *via* the insertion of CO into the growing chain, followed by cleavage of the C-O bond (*insertion mechanism*, Figure 2b) [52,53]. Whatever the mechanism(s), which can depend on many parameters such as the exact nature of the active sites, the Co phase but also particle size [54], or the coverage of the surface [55], the initial formation of a surface CH_x species is required to initiate chain propagation in FTS, and this species could be formed from numerous surface species present on the catalyst surface [56,57].

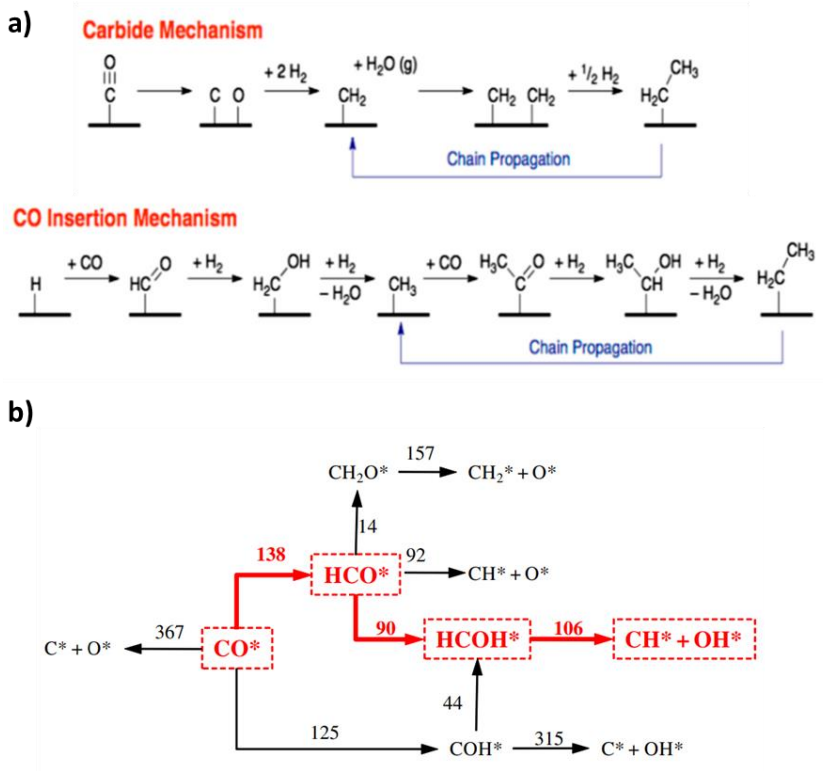

Figure 2. Schematic outline of the FTS mechanism: a) carbide and CO insertion mechanisms. Reprinted with permission from Ref [43]. Copyright 2015 Elsevier. b) direct and H-assisted CO dissociation on Co(0001). Values on the arrows refer to the individual barriers (in kJ mol^{-1}) for each elementary step. The preferred H-assisted CO dissociation path is highlighted in red. Reprinted with permission from Ref [44].Copyright 2010 Elsevier.

Various approaches including kinetics, microkinetics and DFT calculations, were used to elucidate the different paths in FTS in order to properly identify the relative importance of intermediates or to propose a predictive model [58]. Additionally, compared to conventional kinetics, the microkinetic approach implies that we limit ourselves to the intrinsic kinetics of the reaction that exclude mass and heat transfer effects [58]. In the following section, some results related to the conventional kinetics, microkinetic and DFT calculations for Co/C catalysts reported in the literature will be discussed.

From an engineering and industrial point of view, it is important to establish kinetic rate equations integrating the performance and the scale-up of the process *e.g.*, reactor modeling and process modeling [59]. Kinetic rate equations are most of the time described by empirical power law models based on Langmuir-Hinshelwood-type equations [60]. Moreover, the development of kinetic models has to consider the rate-limiting step of the reaction mechanism. For that, two different approaches were proposed by Wojciechowski *et al.* [61] and Rautavuoma *et al.* [62]. The first one stipulated that CO dissociation can be the rate-limiting step of FTS [60]. The second postulated that the rate-limiting step was the hydrogenation of the carbon atoms on the surface. To judge the applicability of a given model Trépanier *et al.* [60] used a conventional kinetic approach based on Langmuir–Hinshelwood-type equations. The rate of syngas consumption over RuKCo/CNT_{ox} (CNT_{ox} = oxidized carbon nanotubes) catalyst was measured in a fixed-bed reactor (T = 210-225 °C, P = 20-35 bar, H_2/CO = 1-2.5, and GHSV = 2700-3600 mL g^{-1} h^{-1}) in order to model the kinetics of the FT reaction. The Weisz-Prater criterion (CWP < 1) suggested that the pore diffusion resistance on the reaction rate can be neglected. The apparent activation energy obtained from all the kinetic models (**See Table 1**) was in the range of 80-85 kJ mol^{-1}, which is lower than the usual values reported in

the literature (98-104 kJ mol^{-1}) [60]. Furthermore, this range of activation energy (80-85 kJ mol^{-1}) is consistent with the absence of pore diffusion limitation. Based on the power law model, they concluded that CO is strongly adsorbed dissociatively on the catalyst surface, and the reaction rate is significantly influenced by the partial pressure of H_2. In another study, Rose *et al.* [59] used Langmuir-Hinshelwood and power rate equations (*Eq.5*) to describe the kinetics of FTS reaction on cobalt catalysts and manganese-doped cobalt catalysts supported on CNT_{ox}. This study was carried out in a wide range of pressure and temperature, since the FTS activity and selectivity strongly depend on the syngas pressure and temperature. In order to better predict the evolution of the activity as a function of the CO concentration over Co/CNT_{ox} catalysts three kinetic expressions including power law rate expressions (*Eqs.6-7)*, rate expressions by Yates and Satterfield (*Eq.8)*, and rate expressions by Rautavuoma and Van der Baan (*Eq.9*) were applied [59]. It was found that the activity at 1 bar of H_2/CO was significantly higher than that predicted by the models (Figure 3). The applied kinetic approaches lead to the same results (Figure 3). The Rautavuoma and Van der Baan model presenting lower residual sum of squares was more accurate in comparison with other kinetic models. This model assumes chemisorption of reactants on the catalyst surface at ambient pressure. Interestingly, it was also found that the apparent order of CO in the power law rate depends not only on CO concentration but also on temperature.

$$r_{m,CO} = -\frac{d_{\dot{n}_{CO}}}{d_{m_{cat}}} = k_{m,CO,ml} c_{CO}^{m} c_{H_2}^{l}$$

(Eq.5)

$$r_{m,CO} = -\frac{d_{\dot{n}_{CO}}}{d_{m_{cat}}} = k_{m,CO,ml} c_{CO}^{-0.2} c_{H_2}^{1}$$

(Eq.6)

$$k_{m,CO,ml} = 6.4 \times 10^{11} \frac{mol^{1.8} m^{2.4}}{s k_{g_{Co}}} \exp\left(\frac{-145 \frac{kJ}{mol}}{RT}\right)$$

(Eq.7)

$$r_{m,CO} = k_{m,CO,YS} = \frac{c_{CO} c_{H_2}}{(1+K_{CO,YS} c_{CO})^2}$$

(Eq.8)

$$r_{m,CO} = k_{m,CO,RB} = \frac{\sqrt{c_{CO} c_{H_2}}}{(1+K_{CO,RB}\sqrt{c_{CO}})^3}$$

(Eq.9)

In *Eqs. 5-9*, n denotes the molar flow of reactant, $k_{m\,1st}$ the apparent (first-order) rate constant, r_m the rate expression, m_{cat} the mass of active metal in the cobalt catalyst, *c* the respective concentration of CO and H_2, K_{CO} is the equilibrium constant, m and l are the order of carbon monoxide and hydrogen, respectively, RB is the Rautavuoma and Van der Baan, and YS is the Yates and Satterfield constants , $\dot{n}_{CO}$ is the molar flow [59].

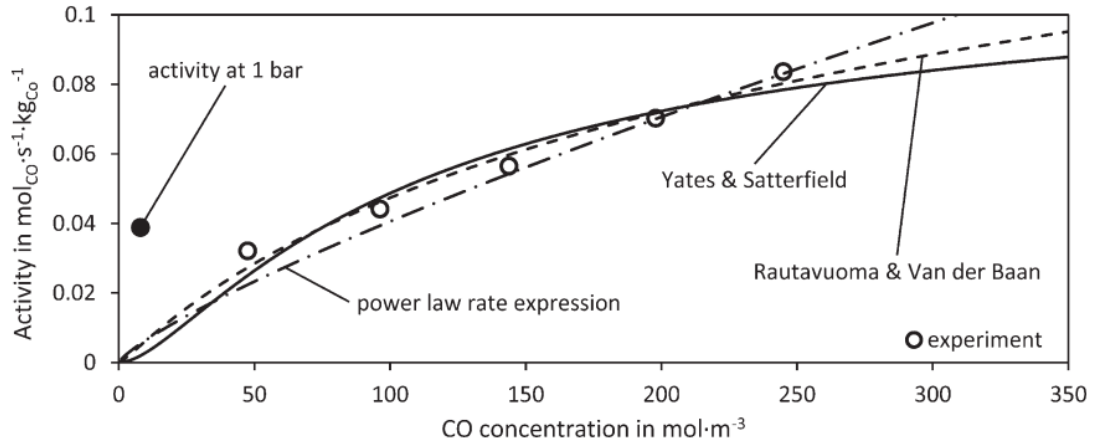

Figure 3. Dependence of mass-related activity at constant H_2 to CO ratio of the unpromoted Co/CNT$_{ox}$ system on CO concentration for power law rate expression (Eqs. (6) and (7)) and both Langmuir-Hinshelwood models (Yates and Satterfield (Eq. (8)), Rautavuoma and Van der Baan (Eq. (9)) and T = 230 °C, P_{H2}/P_{CO} = 2, P_{tot} = 1 and 30 bar, τ' = 150–380 kg$_{Co}$ s Nm^{-3}. Reprinted with permission from Ref[59]. Copyright 2014 John Wiley and Sons.

Contrary to the unpromoted Co/CNT$_{ox}$ catalysts, the rate of CO consumption on the Mn-promoted catalyst cannot be described by Yates and Satterfield and Rautavuoma and Van der Baan rate equations [59], because the chemisorption of CO proceeds dissociatively on Co/CNT$_{ox}$, while on Mn-Co/CNT$_{ox}$ the CO adsorbs in a non-dissociative way [59]. Based on Wojciechowski equation (*Eq.10*) and the power law rate, it was found that the rate slightly decreased with increasing CO concentration at a constant H_2/CO ratio of 2 (Figure 4).

$$-r_{m,CO,W} = \frac{k_{m,CO,W} c_{CO} \sqrt{c_{CO} c_{H_2}}}{(1+K_{CO,YS} c_{CO})^2} \qquad \textit{(Eq.10)}$$

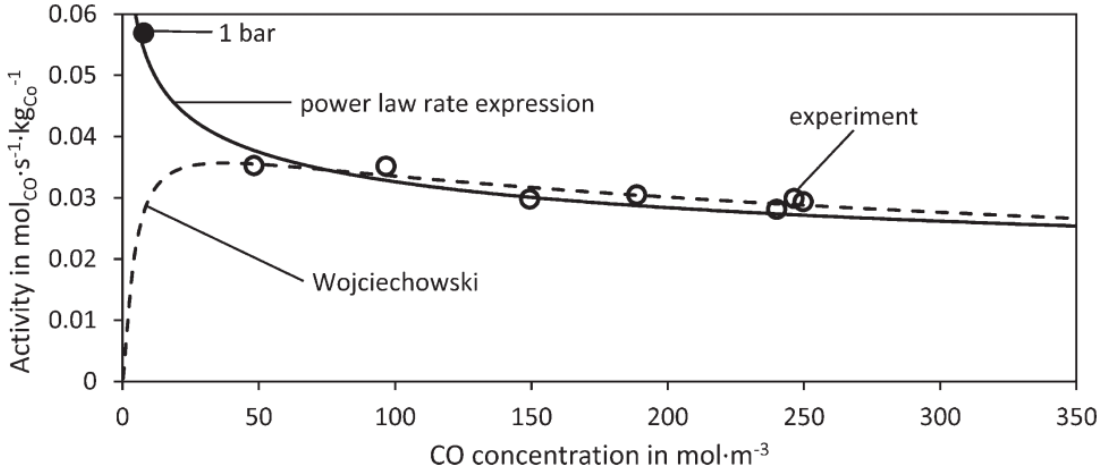

Figure 4. Plot of mass-related activity (experimentally obtained data, calculated data) *vs*.CO concentration at a constant syngas ratio for the kinetic approaches based on the non-dissociative CO chemisorption (Wojciechowski) (see *Eq.10*) for the manganese-promoted Mn-Co/CNT$_{ox}$ catalyst. The rate at ambient pressure is depicted additionally. T= 240 °C, P_{H2}/P_{CO} = 2, P_{tot} = 1 and 30 bar, τ' = 190-50 kg$_{Co}$ s Nm^{-3}. Reprinted with permission from Ref [59]. Copyright 2014 John Wiley and Sons.

In this context, the model derived from Rautavuoma and Van der Baan and the power law rate expressions appeared to be more suitable to describe the reaction rate on the Co/CNT_{ox} and Mn-Co/CNT_{ox}, respectively [59]. The kinetic models tested for Co/CNT_{ox} catalysts reported in the literature together with their advantages and drawbacks are presented in the Table 1.

Table 1. Kinetic models tested for cobalt particles supported on CNT and CNT$_{ox}$.

Catalyst	Equation rate	Advantages	Drawbacks	Ref.
0.5Ru0.0016K15Co/CNT$_{ox}$	• $-r_{H_{2+CO}} = \frac{aP_{H_2}^{\alpha}}{(1+bP_{CO}^{\beta})^2}$ • $-r_{H_{2+CO}} = \frac{aP_{H_2}^{\alpha}}{(1+bP_{CO}^{\beta}P_{H_2}^{0})^2}$	• This model fits well with the experimental results obtained from CNT-supported and promoted cobalt catalyst.	• The validity of this model is restricted to fixed bed reactor. • This model does not consider heat and mass transfer limitation, and catalyst deactivation.	[60]
Co/CNT$_{ox}$	• $r_{m,CO} = k_{m,CO,mn}c_{CO}^{m}c_{H_2}^{n}$ • $r_{m,CO} = \frac{c_{CO}c_{H_2}}{(1+K_{CO,YS}c_{CO})^2}$ • $r_{m,CO} = \frac{\sqrt{c_{CO}c_{H_2}}}{(1+K_{CO,RB}\sqrt{c_{CO}})^3}$	• The results obtained from this kinetic model are accurate for high pressure, which represents realistic FTS conditions.	• The rate expressions are not able to describe the experiment conducted at ambient pressure (dry FTS).	[59]
Mn-Co/CNT$_{ox}$	• $r_{m,CO} = k_{m,CO,mn}c_{CO}^{m}c_{H_2}^{n}$ • $-r_{m,CO,W} = \frac{k_{m,CO,W}c_{CO}\sqrt{c_{CO}c_{H_2}}}{(1+K_{CO,YS}c_{CO})^2}$	• This model can describe kinetic behavior, even at ambient pressure. • This model well predicts the behavior of the reaction over promoted cobalt catalyst.	• This model cannot be applied for a non-promoted cobalt catalyst due to the change in CO chemisorption from dissociative on pure cobalt catalyst to non-dissociative with addition of promoter.	[59]
Co/CNT **Co/CNT$_{ox}$**	• $r_{FTS} = \frac{k_{FTS}b}{\left(1+C\left(\frac{P_{H_2}P_{CO}}{P_{H_2}O}\right)\right)^2}\left(\frac{P_{H_2}^{3/2}P_{CO}}{P_{H_2}O}\right)$	• This model well predicts the behavior of the reaction over cobalt supported on CNT$_{ox}$ and CNT. • The obtained kinetic parameters show the behavior of the reaction as well.	• The rate expression does not consider the effect of energetically heterogeneous surfaces.	[63,64]

Since the FTS is a rather complex reaction, this approach does not account for the mechanisms of formation of different reaction products [41,59]. In order to overcome this problem, the new approaches consist in using microkinetics [65–67], DFT calculations [68,69], or to combine DFT calculations and microkinetics in order to elucidate the reaction mechanism [70]. Yang *et al.* [70] combined DFT, transient, and steady-state kinetic modeling to elucidate the reaction mechanism in FTS using a 20%Co/CNT_{ox} catalyst to collect the experimental data. In this study, the steady-state modeling was based on the Langmuir-Hinshelwood model of the steady-state CO conversion rate. The main challenge was to model the CO activation mechanism and the CH_4 formation. The H-assisted CO dissociation was identified as the dominating CO activation pathway. Interestingly, it was revealed that the availability of hydrogen on the surface was the key parameter in determining the CO reactivity and relative contribution of the two pathways for CH_4 formation at high CO pressures. Moreover, low H surface concentration and high CO pressure favor the decomposition of CHOH* species, followed by the CH* hydrogenation, which leads to methane formation. Several studies concerning Mn-Co/CNT catalysts for FTS experimentally showed that the addition of manganese as promoter enhances the S_{C5+} [71,72]. This microkinetic model has been mainly used for carbon nanotubes and oxides. It could be advantageously used for other carbon materials since it gives more precise information on the different steps of the reaction. The result obtained from microkinetic study was corroborated by a recent DFT study conducted by Liu *et al.* [69] They simulated the catalytic reactivity of a CNT-supported bimetallic center, M_1M_2/N_6h (M = Fe, Co, Mn and N_6h = N-doped (6,6)-CNT surface), for three C-C coupling reactions. They found that the electrons are transferred from the metal surface to adsorbates and the anti-bonding energy levels directly affect the reaction barrier for different C-C coupling mechanisms (Figure 5), leading to a suppressed C_1 selectivity in FTS when Co-Mn/N_6h systems was used.

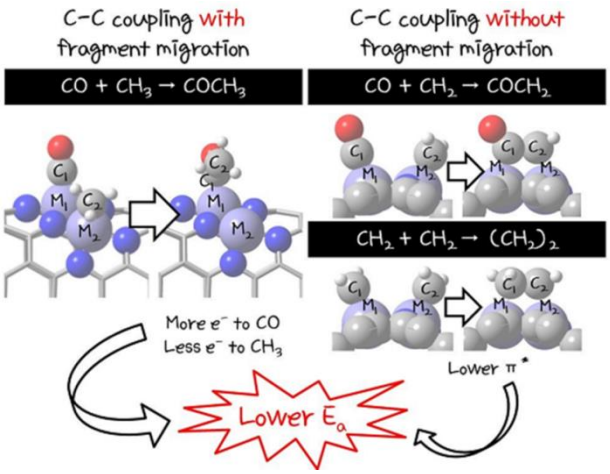

Figure 5. Schematic reaction mechanisms of C-C coupling between different adsorbates on M_1M_2/N_6h surfaces Reproduced by permission from Ref [69]. Copyright 2020 Royal Society of Chemistry.

In FTS, the primary products are olefins but they can be rapidly transformed to paraffins due to the hydrogenation ability of cobalt [41]. In fact, understanding the reactivity of these different hydrocarbons on the catalyst surface would allow better control of the selectivity toward heavy hydrocarbons. The physical adsorption of olefins and paraffins on the surface of a Co/CNT catalyst was investigated by Shariatinia *et al.* using DFT calculations [68]. The energetic, structural, and electronic properties of the catalyst and the products were also predicted. The

band gaps (E_g) of hydrocarbons was found to be higher (~12.5 eV) than that of α-olefins (~7.5 eV). This was attributed to the easier electron transfer through the π bonds in the case of α-olefins. Additionally, the α-olefin compounds have greater electronegativity and electrophilicity index values, but much lower hardness (η) and E_g values in comparison to their related paraffin counterparts. It is notable that lowering E_g, η, and the chemicals potential (μ) facilitates charge transfer and contributes to increase the species reactivity. This justifies that α-olefins have higher reactivity than paraffins.

2.2 Reaction conditions

The FT product distribution depends on many process variables such as temperature, total pressure of syngas, syngas composition, and residence time of syngas [73]. The physicochemical properties of the catalyst also influence the selectivity in FTS but this will be discussed latter. The distribution of FTS products can be described by the "chain growth probability" (α), which can be determined by Anderson-Schulz-Flory (ASF) plots [41]. For industrial applications using GTL technology, heavy waxes (C_{35}-C_{120}) are mostly targeted, which are then upgraded into different products such as kerosene/diesel as final products [74]. Consequently, liquid hydrocarbons with α higher than 0.9 are desired. Selected works on the effects of reaction conditions in FTS using Co/C catalysts are presented in Table 2.

Aluha *et al.* [75] investigated the effect of H_2/CO molar ratio on the distribution of FT products over plasma synthesized Co/C catalyst. The FTS was carried out in a 3-phase continuously-stirred tank slurry reactor operated isothermally at 220 °C and 20 bar. The H_2/CO molar ratio was varied in the range of 1-2. As shown in the Figure 6a, CO conversion increased with H_2/CO ratio. High H_2/CO ratio also allowed limiting the formation of coke because the hydrogenation rate of carbonaceous intermediates was increased [41]. H_2/CO molar ratio of 1.0 and 1.5 favored the production of heavier hydrocarbons including diesel (C_{13}-C_{20}) and waxes (C_{21+}), giving an α of 0.93 (Figure 6b). The same groups reported in another study that high temperatures enhanced CO conversion and gasoline production with low α value, while low temperatures favored diesel and wax fractions [76]. This trend was confirmed by other research groups [77,78]. For example, at 227 °C, a Co/C catalyst produced 8% gasoline, 61% diesel and 28% wax. At 247 °C, the same catalyst produced 22% gasoline, 50% diesel and 19% wax, while at 267 °C, it generated 24% gasoline, 34% diesel, and 11% wax. This result was attributed to high product desorption rates and low residence time on the catalyst surface at high temperatures [76,79].

As far as pressure is concerned, high pressure is beneficial for CO conversion, S_{C5+} and high α value. This was evidenced in the work conducted by Honsho *et al.* [80]. In fact, high partial H_2 pressure favors CO conversion, while high partial CO pressure favors S_{C5+}, in particular heavy hydrocarbons.

Qian *et al.* [66] investigated the effect of the GHSV in the range of 2000-3500 mL g^{-1} h^{-1}, maintaining constant all other operating parameters (T = 250 °C, P = 40 bar, H_2/CO = 2). As expected, increasing the GHSV led to a decrease in CO conversion. In another study, Farzad *et al.* [81] reported that S_{C5+} decreased by increasing the GHSV. However, the effect of GHSV in FTS is complex and controversial results have been obtained [41].

The syngas fed to the FT reactors generally contains CO_2. Díaz *et al.* [82] investigated the influence of CO_2 on the activity and selectivity of Co/CNF (CNF = carbon nanofibers). Under similar conditions (T = 220-250 °C, P = 20 bar, GHSV = 3000 mL g^{-1} h^{-1}) the presence of CO_2 provoked a decreased activity and increased the formation of lighter hydrocarbons. In fact, CO hydrogenation follows the FT mechanism while CO_2 hydrogenation follows the methanation mechanism.

The reduction of methane formation during FTS represents a challenge, and adding α-olefins can effectively reduce methane production and liquid yield [83]. Yang *et al*. [83] used 20%Co0.5%Re/CNT catalyst to study the effect of ethylene co-feeding on the product distribution. The FTS was carried out at T = 210 °C, P_{tot} = 1.85 bar, P_{CO} = 0.11 bar, P_{H2} = 0.22 bar, P_{C2H4} = 0 or 0.11 bar. A decrease in CO conversion in the presence of ethylene was observed due to the competitive adsorption of C_2H_4 and H_2, which inhibits the CO hydrogenation [83]. In contrast, an enhancement of olefin to paraffin ratio and chain growth probability was observed in the presence of ethylene. The increase in olefin to paraffin was due by an enhanced adsorption of the very reactive ethylene species as compared to H_2 species [84]. The enhancement of chain growth probability come from the fact that ethylene can hydrocrack into C1 species and be incorporated into the growing chain [83]. The enhancement of chain growth probability is explained by a combined effect of: i) a higher concentration of chain growth monomer C1 from ethylene cracking; ii) ethylene can function as chain initiator, and therefore a higher concentration of chain initiator is present; and iii) reduced chain termination due to reduced H coverage.

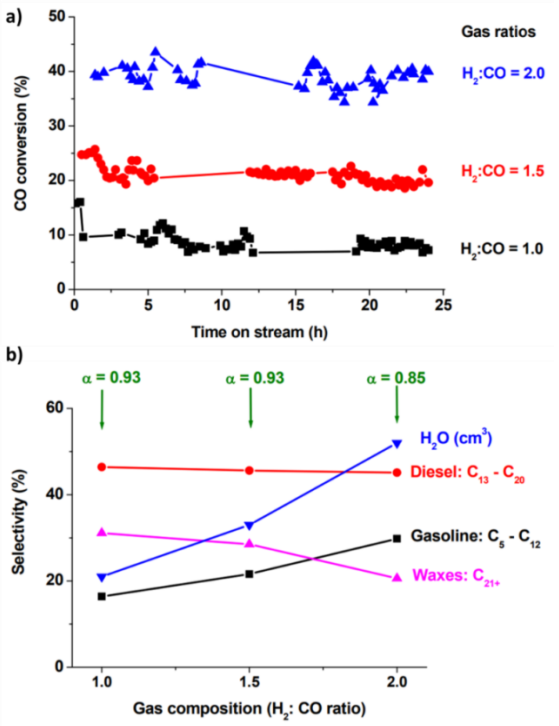

Figure 6.a) Plots showing the positive influence of H_2 on FTS reaction; and b) impact of gas composition on FTS product fractions after 24 h on stream with Co/C catalyst tested at 220 °C, 20 bar and GHSV of 3600 mL g^{-1} h^{-1}. Reproduced with permission from Ref [75].

Capturing and converting CO_2 into liquid hydrocarbon can be used as an alternative solution to reduce CO_2 emission to the atmosphere *via* FTS [85]. Generally, this reaction takes place in two steps in the same reactor: i) the transformation of CO_2 and H_2 into syngas (H_2/CO) *via* the reverse water-gas-shift reaction (rWGS); and ii) the resulting syngas is used directly through the FTS for the production of liquid hydrocarbons. For this reaction, few studies using Co/C catalysts have been reported in the literature. Han *et al.* [86] prepared *via* the hydrothermal method a Co/CNT catalyst for CO_2 hydrogenation. The Co/CNT catalyst was prepared *via* hydrothermal conditions by mixing CNT with $Co(acac)_2$ in N, N-

dimethylformamide (DMF) for 30 min followed by annealing the mixture at 200 °C for 12 h. The Co/CNT catalysts showed a good dispersion of Co nanoparticle. Under FTS conditions, the CO_2 conversion increased from 3% to 12% with increasing reaction temperature from 200 to 300 °C. This was due to the endothermicity of the rWGS reaction ($\Delta H^0_{300} = 38\, kJ\, mol^{-1}$). Furthermore, the Co/CNT catalyst also exhibited good stability during nine catalytic tests at 200 °C. However, no information as to the selectivity of this catalyst was given in this study.

In this section, we presented the influence of reaction conditions such as P, T, H_2/CO ratio and GHSV on the FTS activity and selectivity for Co/C catalysts. Thus, the influence of temperature on the FTS activity and selectivity was studied for Co/C, Co/Dia$_{ox}$ (Dia$_{ox}$ = oxidized diamond) and Co/GSi (GSi = graphene-silica) catalysts by different authors. The carbon supports used for the preparation of supported Co catalysts present differences in terms of morphology and the resulting catalysts have different textural properties and particle sizes: Co/C (S_{BET} = 75.7 $m^2\, g^{-1}$, d_{Co} = 11 nm); Co/Dia$_{ox}$ (S_{BET} = 25 $m^2\, g^{-1}$, d_{Co} = 23 nm), and Co/GSi (S_{BET} = 130 $m^2\, g^{-1}$, d_{Co} = 17 nm). Although these supports and catalysts present different morphologies and particles sizes, the influence of temperature on the FTS activity and selectivity is similar regardless of the Co/C catalysts used. The same tendency was observed for Co supported on oxide support such as the 0.5 % Pt–25 % Co/Al_2O_3 catalyst [87]. These studies show that the effect of the reaction conditions is more important than the physicochemical properties of the catalysts.

Table 2. The effects of reactions conditions on FTS activity and selectivity on Co/C catalysts

Catalyst	*Reactor*	*T °C*	*P bar*	*GHSV*	*H_2/CO*	*CO %*	*S_{CH4}*	*S_{C5+}*	*α*	*Remark*	*Ref*
Co/C	CSTSR[a]	220	20	3600[b]	1.0 1.5 2.0	9 22 38	1.8 4.0 3.6	93.9 95.7 95.5	0.93 0.93 0.85	The CO conversion increases with H_2/CO ratio, while higher values of H_2/CO ratio favor the formation of light-weight hydrocarbons (gasoline = C_4-C_{12}).	[75]
Co/C	CSTSR[a]	227 247 267	20	2000[b]	1.5 1.2 0.9	17.5 46.2 85.0	1.9 5.9 16.4	97.8 91.2 68.7	0.84 0.89 0.85	Work in FTS beyond 267 °C enhances CO_2 and CH_4, lowering S_{C5+}. The effect of temperature is more pronounced than that of the H_2/CO ratio on product selectivity.	[76]
Co/Dia$_{ox}$	Fixed-bed	240 250 260	10	4500[b]	2	38.0 50.0 70.0	20.0 20.0 50.0	66.0 62.0 18.0	0.76 0.75 0.60	An increase of reaction temperature contributes to improved CO conversion. High temperature FT using cobalt based catalysts leads to enhanced CH_4 selectivity.	[80]
Co/Dia$_{ox}$	Fixed-bed	250	5 10 20	4500[b]	2	38.0 52.0 78.0	48.0 20.0 10.0	18.0 60.0 70.0	0.73 0.74 0.80	High pressure FT is beneficial to activity, S_{C5+} as well as chain growth probability (α)	[80]
Co/GSi	Fixed-bed	205 215 225 235	20	2800[b]	2	50.0 60.0 80.0 85.0	4.0 5.0 6.0 7.0	92.0 90.0 98.0 85.0		Upon increasing temperature, the CO conversion and selectivity to CH_4 and CO_2 notably increase, and the S_{C5+} slightly decreases.	[88]
Co/AC	Fixed-bed	250	40	2500[b] 3000[b] 3500[b]	2.18	44.69 39.81 36.35				The CO conversion decreases with increasing GHSV because of the small residence time of syngas through the catalytic bed.	[66]

[a] 3-phase continuously-stirred tank slurry reactor. [b] mL g^{-1} h^{-1}. **Dia$_{ox}$** = Oxidized diamond; **GSi** = Graphene-silica nanocomposite ; **AC** = Activated carbon ; **C** = Carbon

2.3 Effects of Co particle sizes

Metal particle size is one of the most crucial properties of the catalyst and many studies reported in the literature claimed that the FTS activity and selectivity are highly dependent on Co particle size in the range 2-50 nm [35,89–92]. In the quest for the development of performant FT catalysts, a rational strategy is to enhance cobalt dispersion [89]. Xiong et *al*. [91] showed that, for both Co/CNT_{ox} and Co/CS_{ox} (CS_{ox} = oxidized carbon sphere), turnover frequency (TOF) was constant for cobalt particles above 10 nm, but it sharply decreased for cobalt particles smaller than 10 nm. Furthermore, an increase of S_{C5+} with Co particle sizes (3-18 nm) was observed for both Co/CNT_{ox} and Co/CS_{ox} catalysts [91]. Van Deelen *et al.* [90] prepared model Co/CNT catalysts for FTS with Co particle size in the range of 9-100 nm. The TOF_{CO} and S_{C5+} were evaluated only for catalysts presenting Co particle sizes of 9 and 12 nm. The TOF were similar for both Co particle sizes but S_{C5+} increased with the increase of particle size. The high cobalt time yield (CTY) obtained with Co/CNT catalyst presenting small Co particle size (d_{Co} = 9 nm) was attributed to its higher cobalt surface. Bezemer *et al.* [89] investigated Co/CNF_{ox} catalysts with Co particle size in the range of 2.6-27 nm. It was observed that the TOF was constant for Co particle size above 6 nm at 1 bar (Figure 7a) or 8 nm at 35 bar. On the other hand, below these sizes, both activity and selectivity evolved as a function of Co particle size. At 35 bar and when the cobalt particle size decreased from 16 to 2.6 nm, the TOF decreased from 23×10^{-3} to 1.4×10^{-3} s^{-1}, while S_{C5+} (Figure 7b) decreased from 85 to 51 %. In addition, the CTY was optimal with Co particle size around 8 nm as shown in the Figure 7c, d. The high CH_4 selectivity observed with small Co particles indicates their ability to favor the adsorption of carbon species that could be fully hydrogenated to CH_4 [89]. From this study, it was proposed that in order to optimize the catalyst performance in FTS, the Co particle size must be in the range of 6-8 nm. In another study, the effect of Co particle size of Co/CNT_{ox} catalysts (4.9-12.4 nm) was evaluated [93]. The reaction rate was optimal with the catalyst having Co particle size around 8 nm [94], which is consistent with the studies of Bezemer *et al*. [89] and den Breejen *et al.* [95].

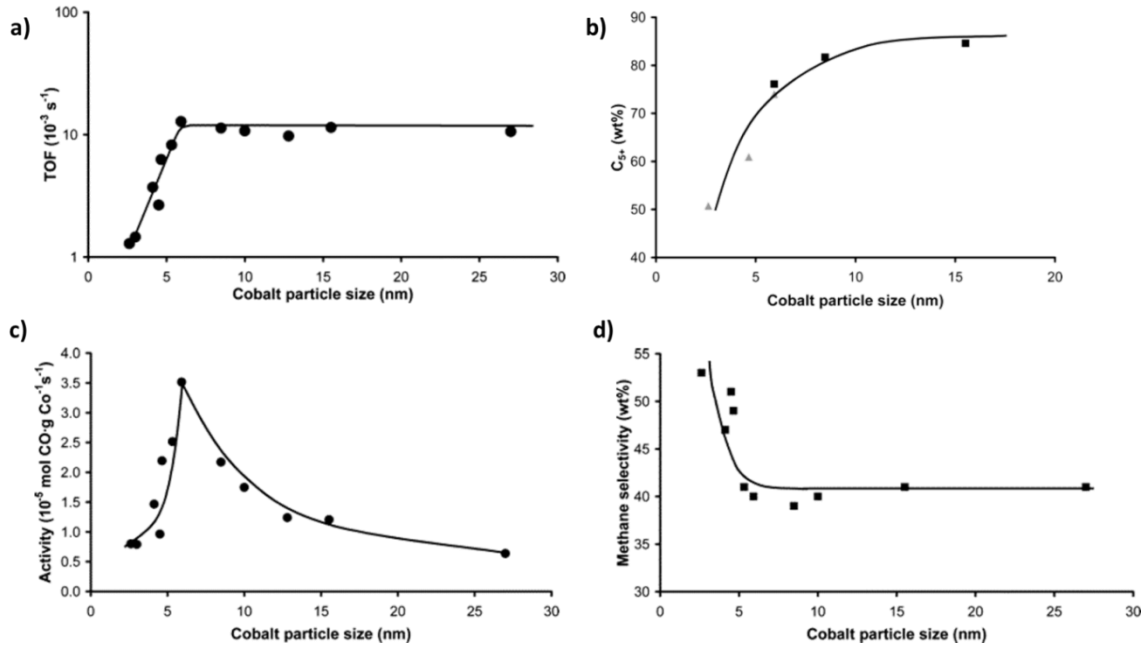

Figure 7. The influence of cobalt particle size on: a) the TOF (220 °C, H_2/CO = 2, 1 bar) ; b) S_{C5+} (measured at 35 bar; data markers in black at 210 °C and in gray at 250 °C); c) CTY (T = 220 °C, H_2/CO = 2, P = 1 bar); and d) methane selectivity (T = 220 °C, H_2/CO = 2, P = 1 bar). Reprinted with permission from Ref [89]. Copyright 2006 American Chemical Society.

In contrast, other studies showed that the TOF was optimal for Co particle size of 25 nm [96], 20 nm [97], 12 nm [98], 11 nm [99], and 45 nm [91], which are much higher than the value proposed by Bezemer *et al*. [89] To explain the origin of the Co particle size effect in FTS, den Breejen *et al.* [100] carried out steady-state isotopic kinetic transient (SSITKA) experiments for the methanation (H_2/CO = 10) and FT (H_2/CO = 2) reactions. They showed that the catalyst deactivation was linked to the irreversible dissociative adsorption of CO on Co particle of sizes < 6 nm. Their cubo-octahedral model showed that the fraction of atoms with low coordination numbers was significantly higher on smaller Co particle size. Consequently, metal atoms with low coordination numbers can bind irreversibly CO, which results in a partial blocking of the Co atoms surface and therefore a decrease in TOF on catalysts having small Co particle size [100]. They also showed that the selectivity towards methane increased for particles smaller than 5 nm because of high coverage of hydrogen on small particles [100]. In another work, based on *in-situ* CO chemisorption measured at 100 °C, the TOF_{CO} was found to increase by increasing Co particle size and SSITKA experiments showed that this was possibly due to an increased number of sites covered with CO [54]. At the same time, the TOF_{CH4} increased with the increase of Co particle size up to a limit value and then remained constant for large particle sizes. This is likely due to the effect of the site coverage, which increased with Co particle size leading to methane formation [54]. The authors speculated that the carbon support seemed to influence the CO hydrogenation over Co particles. These latter results are in contradiction with those obtained by Breejen *et al.* [100] and Radstake *et al.* [101], since the S_{CH4} should decrease with an increase of Co particle size. This suggests that taken alone, Co particle size cannot explain the observed FTS activity and selectivity. In another study, it was found that the high activity of Co/CNT catalysts having small Co particle size was related to the presence of metallic *hcp*-Co [102], since it is known that *hcp*-Co allows a higher CO dissociation rate than *fcc*-Co [47]. Figure 8 compiles the data concerning the influence of cobalt particle size on TOF and S_{C5+}, on several carbon-supported catalysts reported in the literature. The evolution of TOF and S_{C5+} with average Co particle size is very complex. These controversial results can be ascribed to the synergistic effect of different parameters such as, hydrogen spillover, Co confinement, support properties, and Co crystallographic phase.

It is important to extend this conclusion to the case of Co particles supported on oxides in order to bring out the key parameters that control the FTS activity and selectivity. The objective here is to compare the trends of the TOF and S_{C5+} obtained for carbon and metal oxide supports. As shown in Figure 9a, the TOF roughly increased with the Co particle size from 4 nm to 10 nm and became constant for Co particle size > 10 nm. Obviously, many points are out of trend, and this is likely due to the additional influence of the Co crystallographic phase [103] or the nature of the oxide support [104]. Pestman *et al.* [105] recently plotted the evolution of the TOF as a function of the Co particle size, supported on carbon and oxide supports. They observed that the TOF increased with the Co particle size from 4 nm up to 20 nm. Since the MSI is different in the carbon and oxide supports, they concluded that the MSI does not affect this trend [105]. Gnanamani *et al.* [103] prepared 20%Co/SiO_2 catalysts with different Co crystallographic phases (*hcp*-Co and *fcc*-Co) and different Co particle size. The Co particle size was 20.4 nm for *hcp*-Co and 26.9 for *fcc*-Co. The *hcp*-Co exhibited higher TOF and S_{C5+} in the FTS (T = 220°C, P = 20 bar, H_2/CO = 2, GHSV = 3000 mL g^{-1} h^{-1}) as compared to *fcc*-Co with larger Co particle size. This study shows that the Co crystallographic phase can be more important than the Co particle size effects in the FTS.

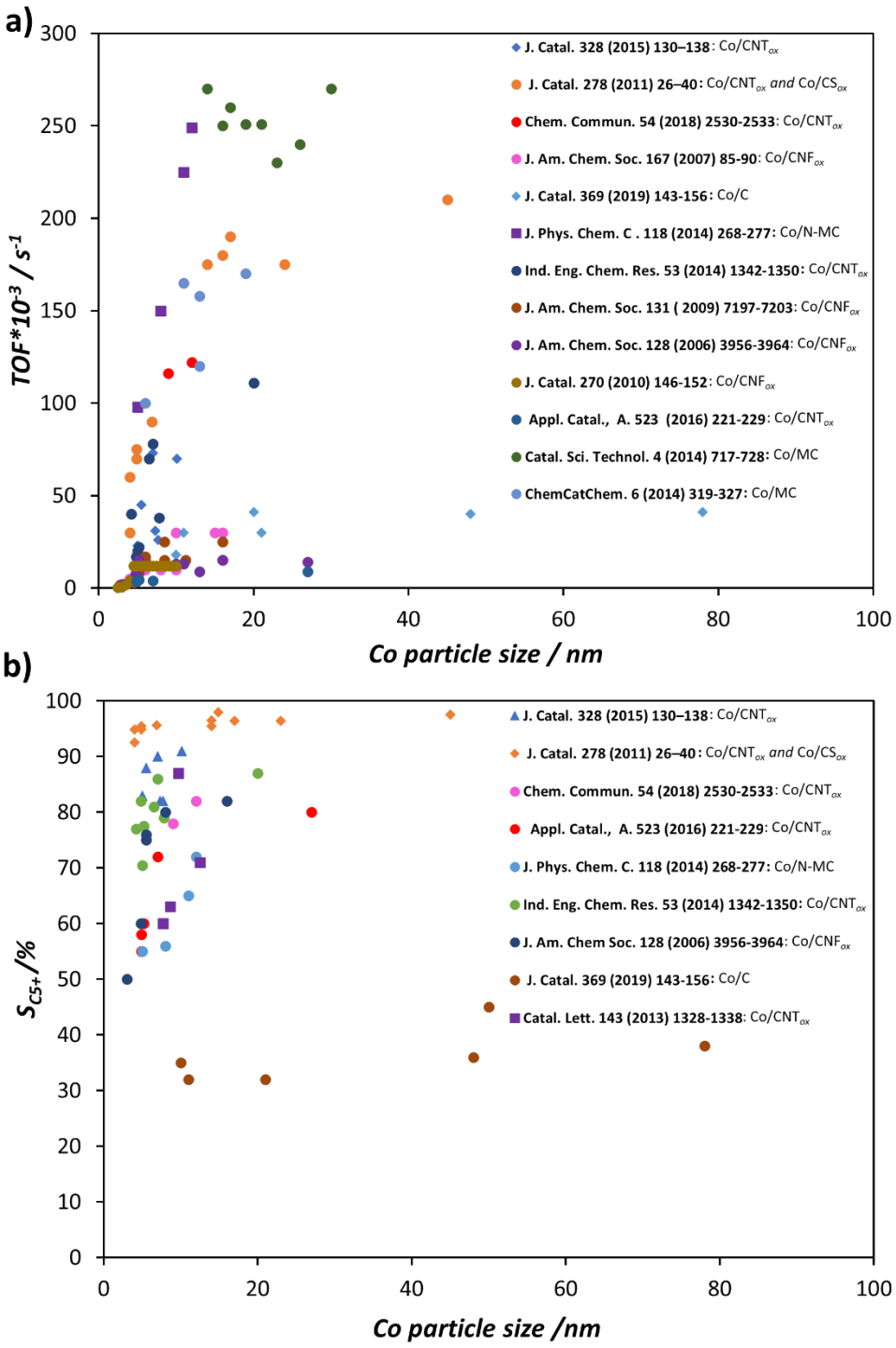

Figure 8. Correlation between Co particle size: a) TOF [89–91,95–101,106–108]; and b) S_{C5+} [89–92,96–99,106] on various Co/C catalysts reported in the literature.

Iglesia *et al.* [109] reported that the TOF is affected by the reaction conditions and the nature of the catalyst. On the other hand, the S_{C5+} increased with the Co particle size from 5 up to 20 nm and stabilizes beyond 20 nm (Figure 9b). This is a typical trend observed in the literature. Furthermore, the average pore size [110] and the surface area [111] of the metal oxide can

also affect the S_{C5+}. Based on these results it is obvious that the TOF and S_{C5+} for cobalt catalyst supported on carbon materials and metal oxides strongly depend on several parameters, which differ from one support to the other.

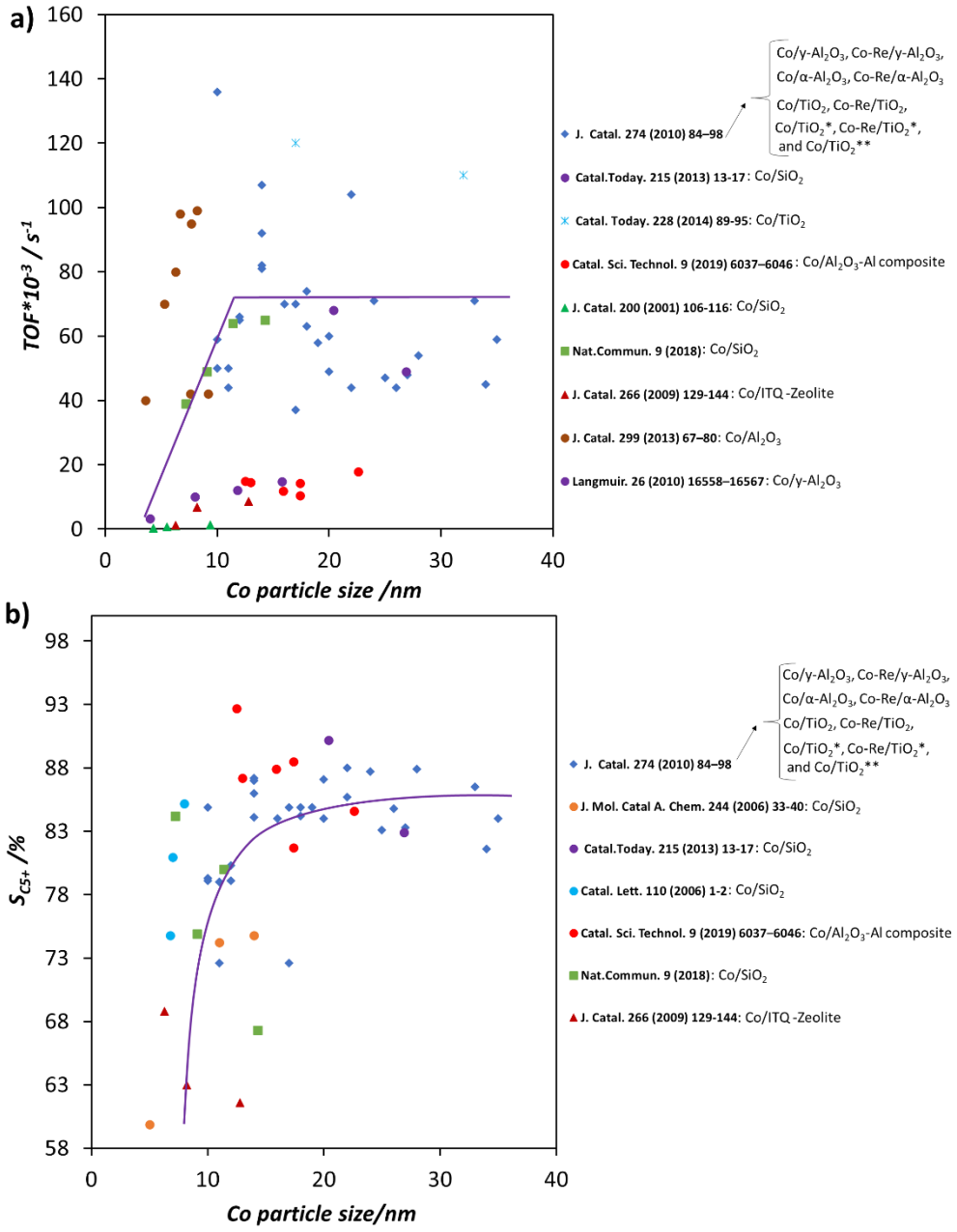

Figure 9. Correlation between Co particle size and a) TOF [103,104,112–118]; and b) S_{C5+} [103,112,114,116,117,119,120] for cobalt catalysts supported on metal oxides.

2.4 Confinement effects

The confinement effect of metal particles in CNT has gained increasing attention in catalysis [121]. In comparison with other types of carbon materials, CNT provide new possibilities to

finely tune MSI and to control metal particle location, either in their inner cavity or on their external surface [122]. Moreover, CNT possesses high external surface areas without micropores, which may be beneficial in FTS that encounters mass transfer limitations [122]. It was reported that the spatial restriction effect of CNT_{ox} channels led to an increase of the contact time between the reactants and the active sites, resulting in the production of heavier hydrocarbons [122]. On the other hand, the electron deficiency of the inner CNT surface could facilitate the reduction of metal oxides located in the inner cavity in comparison with the particles located on the outer surface of the tubes [123,124]. Indeed, according to Serp *et al.* [125] the confinement of metal particles enhanced the catalyst reducibility. However, the confinement of Co particles in CNT strongly depends on the CNT diameter and its surface properties. Various treatments such as thermal pretreatments [126], functionalization [127,128], and the preparation conditions [127,128] can be adapted to maximize the confinement of Co particles (Table 3). Thermal pre-treatments were applied by Akbarzadeh *et al.* [126] to control the confinement of Co particles in the CNT_{ox} channels. According to these authors, thermal treatment at high temperatures created more defects on CNT_{ox}, which can be subsequently used as anchoring sites for Co particles. The results showed that 70% of Co particles were confined in the CNT_{ox} channels when high temperature pre-treatment (900 °C) was applied. The combined acid treatment and thermal pre-treatment of the CNT support at 900°C improved the filling yield of Co inside the CNT_{ox}, which led to enhanced activity, S_{C5+} and stability of the catalyst. The narrow particle size distribution induced by the Co confinement, due to the MSI weakening, enhanced Co reducibility and increased Co dispersion inside CNT_{ox} channels. Besides, the high catalyst stability observed in this study was attributed to the spatial restriction of CNT_{ox} channels, which inhibited sintering during FTS. To highlight the influence of Co confinement inside CNT_{ox} in FTS, 10wt.% of Co was deposited either inside CNT_{ox} (*in*-10Co/CNT_{ox}) or outside CNT_{ox} (*out*-10Co/CNT_{ox}) [122]. For *in*-10Co/CNT_{ox}, 80% of the cobalt particles were distributed in the inner pores, thanks to capillary forces during the impregnation process. In contrast, 70% of Co particles were attached to the exterior surface of the *out*-10Co/CNT_{ox} catalyst. The latter was prepared with CNT_{ox} the inner pores of which were initially filled with water. Thus, aqueous solution of cobalt salt could only interact with the outside surface of CNT_{ox}. Cobalt species of *in*-10Co/CNT_{ox} were easier to reduce than those of *out*-10Co/CNT_{ox} (Figure 10a), which was attributed to the electron deficiency of the inner CNT_{ox} surface [122,129]. This electron density loss destabilizes the metal oxide nanoparticles and assists the auto-reduction of the encapsulated particles [130]. Under the same FTS conditions (T = 220 ºC, P = 20 bar and $H_2/CO = 2$), the *in*-10Co/CNT_{ox} catalyst showed higher CO conversion and higher selectivity into long-chain hydrocarbons (Figure 10b), in comparison to *out*-10Co/CNT_{ox}. This was ascribed to the combined effect of Co particles confinement and their electron-deficiency, which enhanced the dissociation of CO, resulting in the production of long-chain hydrocarbons.

In another study, Wei *et al.* [129] investigated the effects of CNT_{ox} average pore size and Co confinement in FTS. The catalysts (metal loading of 10 wt.%) were prepared by selectively impregnating preformed Co particles either inside or outside CNT_{ox}. The H_2-TPR analyses allowed identifying residual cobalt nitrate in the case of *in*-Co/CNT_{ox}, which was assigned to the enhanced thermal stability of NO_3^- inside CNT_{ox}, likely due to the electron deficiency, which varies depending on the location of cobalt nitrate (inside or outside the CNT_{ox}) [129]. As expected, the increase of the CNT_{ox} inner diameter provoked the increase of cobalt oxide particle size formed inside the CNT_{ox}. Thus, the reduction temperature of the catalyst increased. A similar trend was also found by Fu et *al.* [97] who investigated the effect of carbon

porosity and cobalt particle size on FTS performances. The small Co_3O_4 size obtained with small diameter CNT_{ox} was due to the spatial restriction of CNT_{ox} channels, which limited the growth of Co particle and improved Co confinement. Consequently, this catalyst showed high CO conversion and S_{C5+}.

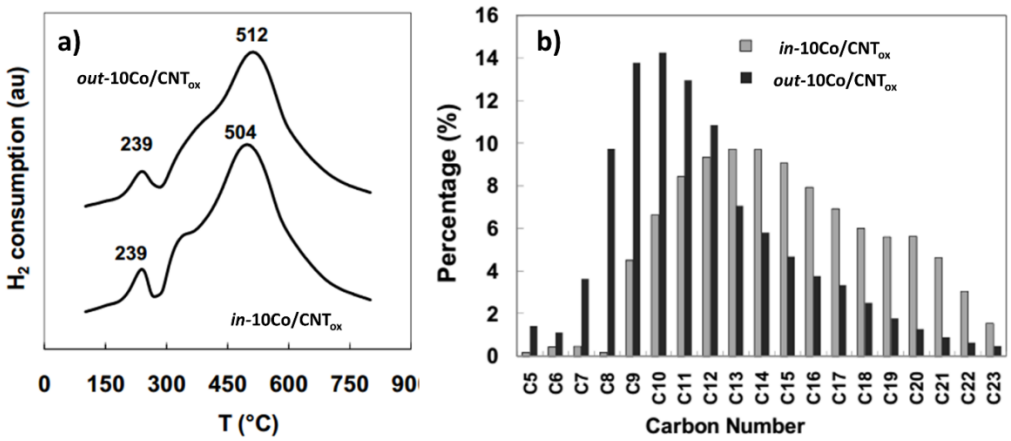

Figure 10. a) H_2-TPR profiles for *in*-10Co/CNT_{ox} and *out*-10Co/CNT_{ox} catalysts; and b) cold trap product distribution for both the *in*-10Co/CNT_{ox} and *out*-10Co/CNT_{ox} catalysts. (T = 220 ºC, P = 20 bar and H_2/CO = 2). Adapted from ref [122].

Confinement effects can also influence Co sintering and catalyst deactivation in FTS. By combining the functionalization by HNO_3 treatment with the incipient wetness impregnation (IWI) method, Tavasoli et *al.* [123] studied the effect of the electronic properties of the inner and outer surfaces of CNT_{ox} on the deactivation of Co/CNT_{ox} catalysts. About 65-70 % of the Co particles were distributed in the inner cavities of the CNT. Because of the tubular morphology of CNT_{ox} that can induce capillary forces during the impregnation process, the size of the cobalt oxide particles located inside the CNT_{ox} was fairly uniform in the range of 4-11 nm. In contrast, the mean diameter of the Co oxide particles located on the outer surface reached 16 nm. After FTS, the Co particle size of the spent catalysts were still small (4-11 nm) for Co particles inside the tubes, while the particles attached to the outer surfaces of CNT had significantly grown (> 40 nm). The low rate of sintering of the Co particles inside the CNT_{ox}, could be explained by two phenomena involving electronic and steric effects: i) the electron deficiency in the inner cavity of the CNT_{ox} leading to the strong interaction between Co particles and the support surface, which limit the sintering of cobalt particles [123], and ii) the steric effect induced by the inner cavity of the CNT_{ox}, which also contributes to limit the mobility of the particles [123]. This was not the case for Co particles located outside the tubes.

Using the inner cavity of CNT_{ox} as a nanoreactor for FTS is thus an exciting possibility that faces the challenge of selectively driving the metal particles inside the CNT_{ox} channel [35]. Various methods proposed to fill CNT_{ox} channel with Co particle are shown on Table 3. For example, the functionalization of the CNT external surface was performed by introducing different surface species (carboxylic acid groups and amide groups presenting a long alkyl chain) that induce weak interaction or repulsion between metal particles and the CNT external surface [35,131,132]. By this way, it was reported that metal particles could be selectively driven inside the functionalized CNT, and the percentage of particles located inside the tubes was close to 100% [35]. This enhanced the confinement, the reducibility and the dispersion of

Co^0 particles [35]. Another method was based on the appropriate selection of the solvent for the impregnation step. In comparison with 1-propanol and water, ethanol was reported as the best solvent for preparing well-dispersed and well-distributed supported cobalt oxide particles due to its low surface tension, which improved the contact between CNT_{ox} support and the solution containing the metal precursor [106].

Table 3. Different ways for enhancing the confinement of Co particles in CNT for FTS

Method for enhancing confinement	Effect on catalysts properties	Effects on catalyst performance	Ref.
Thermal pretreatments (eg. 600,700, 800 and 900 °C)	• Increase BET surface area of CNT_{ox} (eg. 900 °C) • Improve the formation of defects on the CNT_{ox} • Enhance encapsulation of Co inside the CNT_{ox} channels (70%) • Enhance Co reducibility and dispersion • Suppress Co sintering	• Enhance FTS activity and S_{C5+} • Avoid Co sintering and improves catalyst stability	[126]
CNT_{ox} properties (eg. diameter of CNT_{ox} = 8, 20, 60 nm) CNT_{ox} properties (eg. diameter of CNT_{ox} = 5, 11, 17 nm)	• Larger diameter CNT_{ox} increase Co size • Small diameter CNT_{ox} enhance Co reducibility and dispersion	• Larger Co particle size improves TOF and S_{C5+} • Larger Co particle size decreases CH_4 selectivity	[97,129]
CNT pretreatment with high HNO_3 concentration and temperature N-doped carbon nanotubes	• Increases the functional groups and defects on CNT_{ox} • Decreases the Co particle size • Enhances Co confinement • Improves Co dispersion and reducibility	• Enhances the FTS rate in comparison with untreated CNT	[127,128]
Catalyst preparation methods: microemulsion and sol-gel	• Both provide catalysts with narrow Co^0 distribution (2-6 nm) compared to IWI • Improve Co confinement • Extent the Co dispersion	• Increase CO conversion • Increase olefin/paraffin ratio and S_{C5+}	[133,134]

2.5 Hydrogen spillover in Fischer-Tropsch synthesis

Generally, spillover concerns hydrogen and oxygen species. Thereafter, only hydrogen spillover effects in FTS will be discussed. Hydrogen spillover is defined as the transport of activated H-species, adsorbed or formed on a surface, to another surface, which does not adsorb or form the activated H-species under the same conditions [135,136]. Gerber *et al.* [28] described the steps of hydrogen spillover on carbon materials. In the first step, molecular hydrogen is dissociatively adsorbed on a transition metal catalyst in close contact with a carbon support. In the second step, the migration of H-species from the catalyst particles to the support occurs. The last two steps consist in the diffusion and recombination of H-species on the support surface. Additionally, the spilled-over species formed on the metal may react with reactant adsorbed on the support, which could modify or promote the catalytic activity and selectivity [28]. In FTS, hydrogen spillover has been studied for cobalt catalysts supported on metal oxides [137,138], and on carbon [139,140]. In the case of metal oxides, hydrogen spillover allowed explaining the role of noble metals (Pt, Au) as promoters for Co reduction in Co/Al_2O_3 catalysts [137,138]. In the case of carbon-based supports, many factors can promote hydrogen spillover [139]. The capacity of a carbon support to reversibly store atomic H relies on a number of factors such as accessible surface area, geometric nanostructure, defects, dopants, surface chemistry, surface coverage and the interaction of metal particles and support [139,141]. Phaahlamohlaka *et al.* [140] studied the effects of hydrogen spillover on Co catalysts prepared from mesoporous hollow carbon spheres (MHCS) with cobalt loading of 15wt.% and different nominal Ru loadings (0.2wt.% Ru-Co/MHCS and 0.5wt.% Ru-Co/MHCS) [140]. This study also highlighted the influence of hydrogen spillover on the enhancement of the reduction of carbon supported cobalt using a noble metal such as Ru as promoter. Furthermore, the reduction of Co_3O_4 particles assisted by Ru could be performed according to two mechanisms: (i) primary or (ii) secondary hydrogen spillover (Figure 11). In comparison to secondary hydrogen spillover, it was reported that primary hydrogen spillover improved cobalt oxide reducibility due to the close contact between Ru and Co particles, which favors the rapid migration of H species from Ru particles to cobalt oxide particles (Figure 11a) [140].

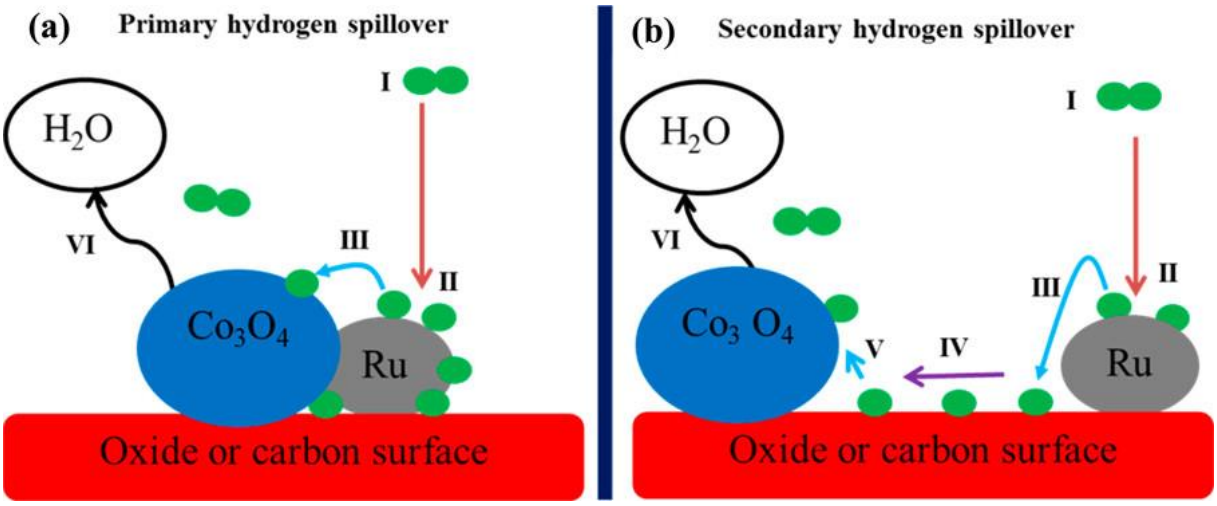

Figure 11. Pathways for spillover-assisted Co reduction on Ru-Co/C catalyst: a) primary; and b) secondary hydrogen spillover. (i) molecular hydrogen; (ii) dissociative chemisorption; (iii) spillover; (iv) hydrogen atom surface migration; (v) spillover; and (vi) reduction and water removal. Reprinted with permission from Ref [140]. Copyright 2017 American Chemical Society.

The small dimensions of MHCS ensured the short travelling distance on the carbon surface for the spilled-over hydrogen. Additionally, the encapsulation of Ru particles in Ru-Co/MHCS catalysts allowed physical separation of Ru from Co by a layer of mesoporous carbon, making the study of hydrogen spillover effects possible [140]. Figure 12 shows that the close contact between Ru and Co particles was optimal in Co@Ru/MHCS (Figure 12b) compared to the other Ru-Co/MHCS samples. Consequently, the metallic Co dispersion of the catalysts expressed in terms of the ratio of the H atoms adsorbed to Co atoms increased in the following order: Co/MHCS < 0.2wt.% Ru-Co/MHCS ≈ 0.5wt.% Ru-Co/MHCS < Co@Ru/MHCS. This order could be rationalized by considering that the increase of Co reducibility is due to the intimate contact between Ru as promoter and Co on Co@Ru/MHCS. This was confirmed by a recent study conducted by the same group using two Co catalysts promoted by Ru, placed inside or outside hollow carbon spheres [142]. Moreover, primary hydrogen spillover was invoked to explain the reduction of cobalt oxide on Co@Ru/MHCS, with the electronic effects determining the Co phase that forms during the process (*hcp*-Co when using a carbon support). On the other hand, for the reduction observed with Ru-Co/MHCS catalysts, secondary hydrogen spillover was invoked to explain the complete phase transformation of cobalt oxide nanoparticles to Co^0 (*hcp*-Co and *fcc*-Co) that were loaded outside the hollow carbon spheres (Figure 12c, d). The Co@Ru/MHCS system constituted the best environment for primary hydrogen spillover.

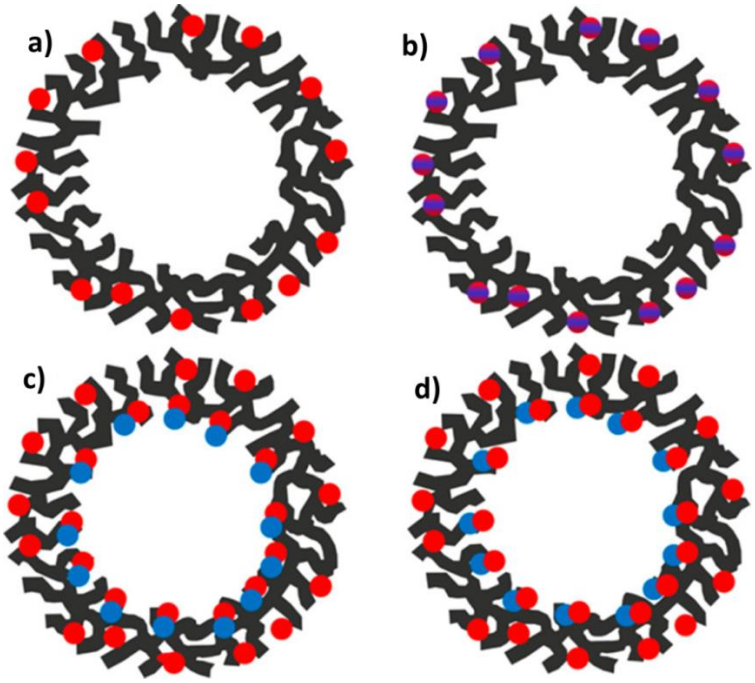

Figure 12. Schematic showing likely particle distributions (Co red and Ru blue) on the MHCS support: a) Co/MHCS; b) Co@Ru/MHCS; c) 0.2% Ru-Co/MHCS and d) 0.5% Ru-Co/MHCS. Reprinted with permission from Ref [140]. Copyright 2017 American Chemical Society.

In FTS (T = 220°C, P = 10 bar, H_2/CO = 2, GHSV = 1800mL g^{-1} h^{-1}), the high activity of CoRu/MHCS catalyst was attributed to the primary hydrogen spillover, while no accurate explanation was identified for its low S_{C5+}. In order to provide an answer to this question, the direct involvement of hydrogen spillover on FTS activity and selectivity on non-promoted

carbon-supported cobalt catalysts was recently demonstrated for the first time [139]. As mentioned above, the carbon support properties seem to influence the occurrence of H-spillover. For that, three different carbon supports, presenting various concentrations of surface oxygen groups and defects, were used to prepare 15%Co/C catalysts. These supports included a fibrous material (FM), CNT and CNF, which were functionalized by HNO_3. The functionalized carbon supports exhibit different textural properties: FM_{ox} (S_{BET} = 173 m^2 g^{-1}, V_p = 0.4 cm^3 g^{-1}, d_p = 8.9 nm); CNT_{ox} (S_{BET} = 220 m^2 g^{-1}, V_p = 1.2 cm^3 g^{-1}, d_p = 22.2 nm); and CNF_{ox} (S_{BET} = 71 m^2 g^{-1}, V_p = 0.3 cm^3 g^{-1}, d_p = 17.1 nm), which will influence the physicochemical properties of the catalysts. Cobalt catalysts were prepared by IWI with an aqueous solution of cobalt acetate. It is known that HNO_3 treatment creates specific functional groups on the carbon materials such as carboxylic, anhydrides, carbonyl, phenolic, quinone and lactone groups, resulting in high level of defects. In addition, the density of functional groups depends on the type of carbon materials. Defects and functional groups created during the HNO_3 treatment were crucial to assess the hydrogen spillover. These surface groups were quantified by TPD-MS (Figure 13a, b). The density of oxygen surface groups decreased following the order: Co/FM_{ox} > Co/CNT_{ox} > Co/CNF_{ox}. Subsequently, H_2-uptake obtained from TPD-MS (Figure 13c) followed the same order. From these analyses, it was clear that the hydrogen spillover was significantly more pronounced on Co/FM_{ox} than on Co/CNT_{ox} and Co/CNF_{ox}. This was attributed to the higher amount of oxygen surface groups and defects of FM support, which contribute to improve hydrogen spillover.

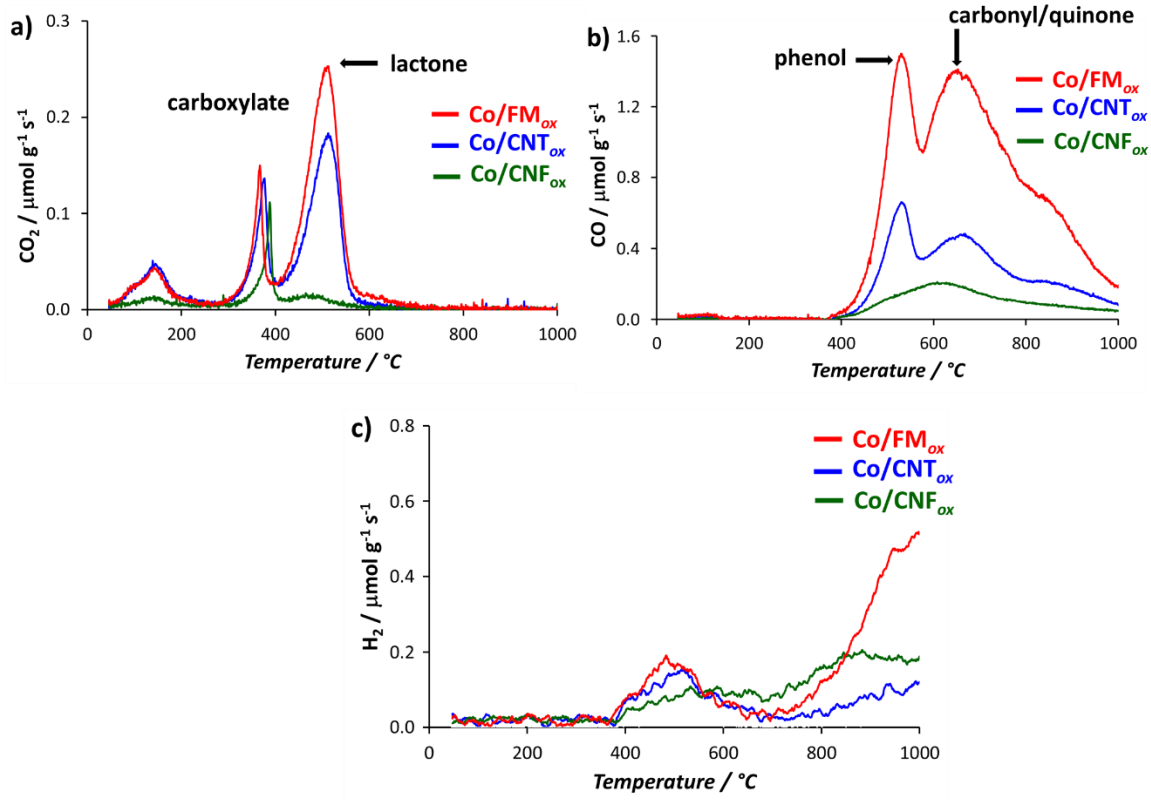

Figure 13. H_2-TPD-MS of Co/FM_{ox}, Co/CNT_{ox} and Co/CNF_{ox} catalysts (50-1050 °C): a) CO_2 b) CO; and c) H_2 released during the desorption step. Adapted with permission from Ref [139]. Copyright 2019 John Wiley and Sons.

The performances of these catalysts were evaluated in FTS (T = 220°C, P = 20 bar, H_2/CO = 2, GHSV = 1155 mL g^{-1} h^{-1}). The CTY decreased with the increase of the Co particle size, and the highest value of CTY was obtained with the 15%Co/FM_{ox} catalyst having a mean particle size of 11 nm (Figure 14a). On the other hand, TOF decreased with the increase of Co particle size as follows: Co/CNF_{ox} (17 nm) < Co/CNT_{ox} (14 nm) < Co/FM_{ox} (11 nm) (Figure 14b*)*. This is opposite to the expected tendency regarding the effect of Co particle size proposed by Bezemer *et al*. [89] and den Breejen *et al*. [95] for Co/CNF catalysts.

Since the evolution of TOF with respect to the average Co particle size was not in agreement with the literature, other factors such as H_2-uptake and crystallographic phase (Co_{hcp}/Co_{fcc}*)* were considered. No correlation was found between TOF and Co_{hcp}/Co_{fcc} ratio. Interestingly, TOF increased with the increase of hydrogen uptake (Figure 14c*)*. This result allows explaining the highest activity of 15%Co/FM_{ox} catalyst by its enhanced hydrogen spillover and small Co particle size which favor CO conversion. At the same time, it was also observed that S_{C5+} decreased with the increase of H_2-uptake as follows: Co/CNF_{ox} > Co/CNT_{ox} > Co/FM_{ox} (Figure 14d*)*. The low S_{C5+} of 15%Co/FM_{ox} was due to hydrogen spillover effect, which favors the hydrogenation of olefins formed during FTS. Based on these results, it appears that hydrogen spillover has a positive effect on FTS activity but a negative impact on S_{C5+}. Small Co particle size and strong MSI favor rapid transfer of H species between metal and support leading to an enhancement of hydrogen spillover.

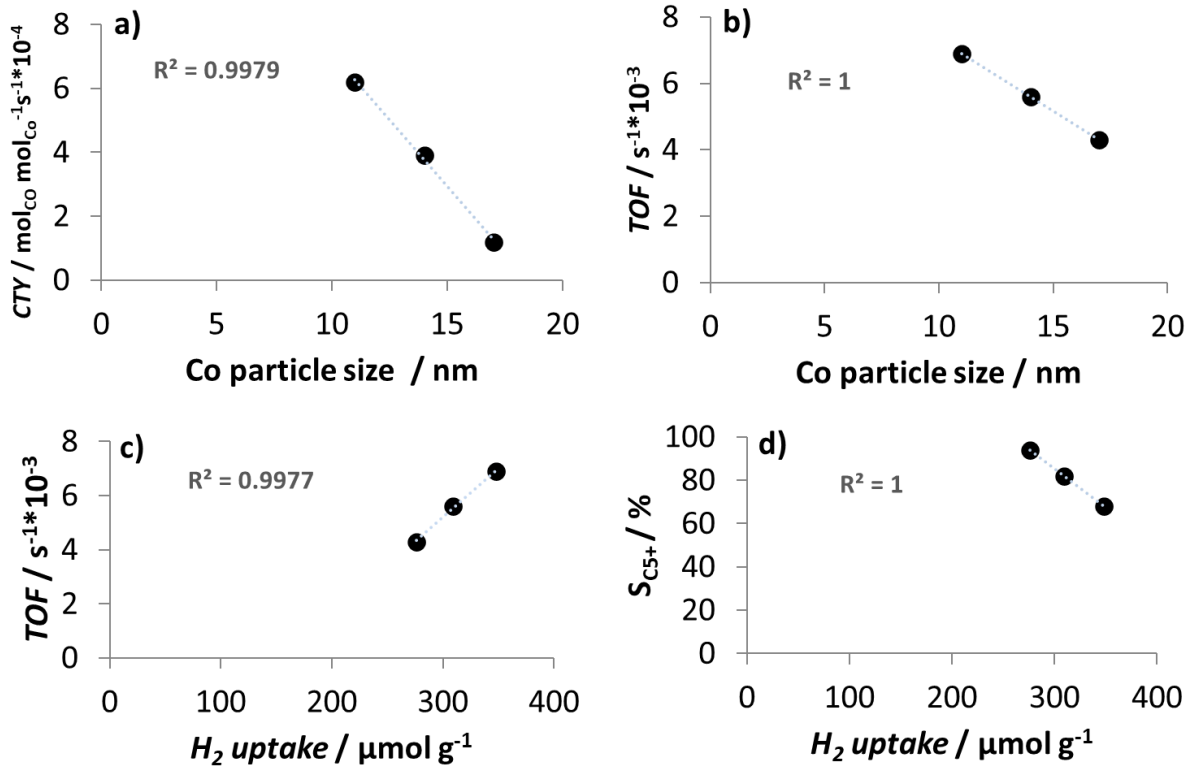

Figure 14. Influence of: a) cobalt particle size (after test) on CTY (steady state); b) cobalt particle size (after test) on TOF (steady state); c) H_2 uptake obtained by TPD-MS between 350 and 650 °C on TOF (steady state); and d) H_2 uptake obtained by TPD-MS between 350 and 650 °C on C_{5+} selectivity. Adapted with permission from Ref [139].

2.6 Deactivation

The deactivation of cobalt-based catalysts is a major challenge in the FTS. Combined with the relatively high price of cobalt, the catalytic stability is crucial for the competitiveness of FTS [15]. The most important factors contributing to the deactivation of cobalt FT catalysts include coke formation, re-oxidation, poisoning, and sintering [143,144]. In the case of Co particles supported on carbon materials, it has been reported that, because of weak MSI, sintering significantly contributes to the catalyst deactivation [145]. According to Trépanier *et al.* [146] cobalt re-oxidation and sintering are the main reasons for catalyst deactivation. In their study, the deactivation mechanisms of Co/CNT_{ox} catalysts was investigated during 480 h in a FTS fixed-bed microreactor (T = 220 °C, P = 20 bar, H_2/CO = 2). They found that the catalyst deactivation occurred in three distinct steps (see Figure 15a). In the first step (4 days) the CO conversion dropped by 10%, then by 4.7 % 0.73 %in the second and third steps, respectively, as shown in Figure 15a.

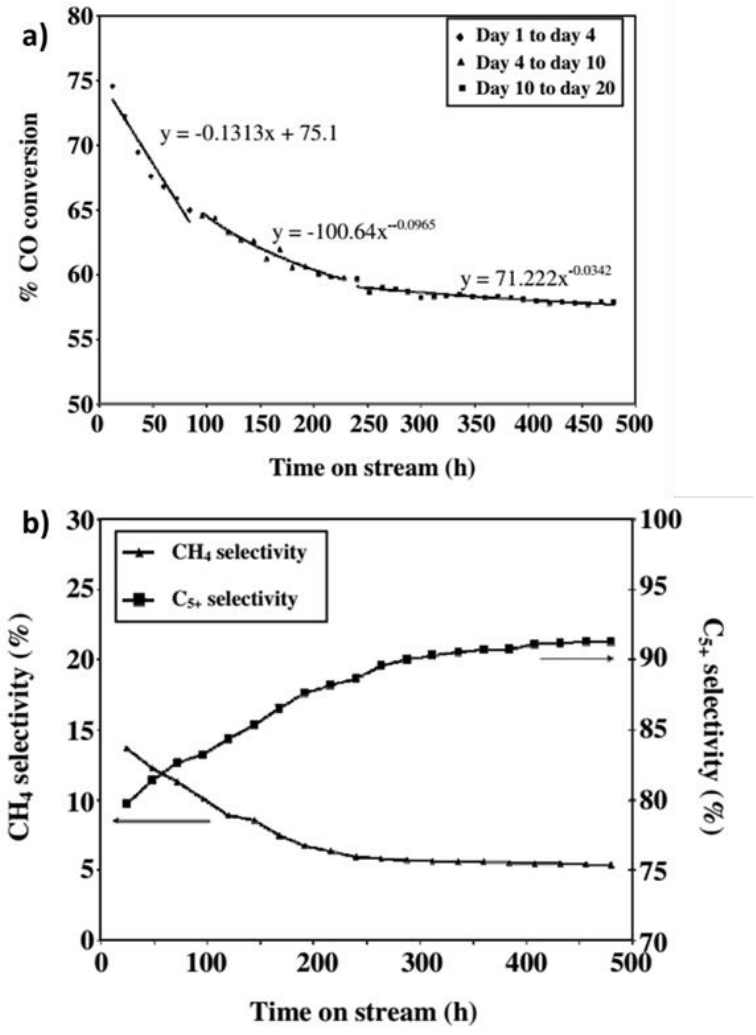

Figure 15. a) %CO Conversion and b) Product selectivity variations with time on stream (T = 220 °C, P = 20 bar, H_2/CO = 2). Reprinted with permission from Ref [146].

The first deactivation step was ascribed to the re-oxidation of Co particles due to the high water partial pressure at high CO conversions. Moreover, the deactivation observed in steps 2 and 3 was assigned to the sintering of Co particles located outside and inside CNT_{ox}, respectively. The slow deactivation rate attributed to Co particles located inside CNT_{ox}, could be related to the electronic and steric effects of the CNT_{ox} channels that inhibited Co sintering. This behavior was confirmed by TEM results of the spent catalyst, which showed that Co particle size inside the CNT_{ox} was still small (4-11nm) while those attached to the outer surface strongly increased (40 nm). They also observed that S_{C5+} increased during the 480 h of FTS and the opposite trend was observed for CH_4 selectivity (Figure 15b). This was assigned to the Co particle size effects since it is known that larger Co particles formed by sintering during FT reaction enhance S_{C5+} and decrease CH_4 production. Thus, the conclusions were that Co sintering and oxidation of Co particles by water were the main contributors to deactivation of Co/CNT_{ox} catalyst. It is important to note that this study was based on *ex-situ* characterizations. Bezemer *et al.* [144] investigated the effect of water on the deactivation of Co/CNF catalysts using *in-situ* Mössbauer spectroscopy carried out at 200-220°C and at 20 bar using different H_2O/H_2 ratios (1-30). No change in the size of cobalt species (very small superparamagnetic and larger Co particles) was found whatever the H_2O/H_2 ratios used. In contrast oxidation of very small superparamagnetic and some larger Co particles were observed in the absence of hydrogen flow. Furthermore, oxidation of Co particles provoked by water partial pressure in the absence of hydrogen was found as the main contributor to deactivation of Co/CNF catalyst.

In another study by Wolf *et al.* [147] the oxidation and sintering of the Co metallic phase of a Co/C catalyst were studied under FTS conditions using *in-situ* magnetometry. In comparison to the study conducted by Bezemer *et al.* [144] the originality of this work comes from the combination of P_{H2O}/P_{H2} ratios and CO partial pressure effects on the oxidation and sintering of Co. The *in-situ* measurements were performed at 220 °C, P_{H2O}/P_{H2} ratios (0.15 to 50), syngas (H_2/CO = 2.1, GHSV = 12000 mL g^{-1} h^{-1}), and P_{CO} of 0, 68 and 340 mbar. At P_{H2O}/P_{H2} ratios of 10 and 220 °C, a decrease in magnetization was observed due to the partial oxidation of the smaller crystallites, due to the hydrothermal sintering provoked by water pressure, leading to a loss in specific surface area (Figure 16a) [147]. The rapid loss in magnetization (3.5 %) due to the oxidation of cobalt was observed with increasing CO partial pressure (Figure 16a, b).

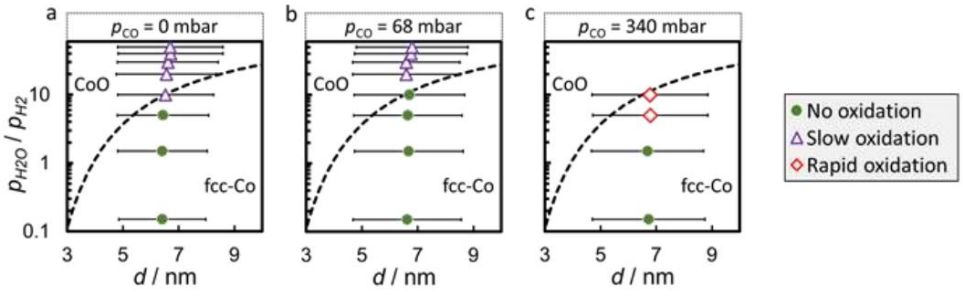

Figure 16. Volume mean crystallite sizes of superparamagnetic Co with standard deviations during exposure to H_2O-rich atmospheres: (a) in the absence of CO, (b) in the presence of 68 mbar CO, and (c) 340 mbar of CO. The sizes were obtained from magnetic measurements and the data points are superimposed on the oxidation equilibrium of *fcc*-Co to CoO by H_2O at 220 °C (dashed). Reprinted with permission from Ref [147]. Copyright 2018 American Chemical Society.

This is due to the fact that the increase in the CO partial pressure further increases the concentration of O* on the Co crystallite surface, while its regeneration might still be hindered due to the presence of water. This contributes to an enhanced catalyst deactivation.

Borg *et al*. [148] studied the effect of water on the activity, selectivity and deactivation of Co/CNF_{ox} catalysts in FTS. For that, three Co/CNF_{ox} catalysts were prepared by IWI and WI methods using two different CNF_{ox} namely, $CNF_{ox\text{-}F}$ for fishbone CNF_{ox} and $CNF_{ox\text{-}P}$ for platelet CNF. IWI was used to load 20 wt.% of cobalt on $CNF_{ox\text{-}F}$ and $CNF_{ox\text{-}P}$ with aqueous solutions of $Co(NO_3)_2$. On the other hand, 12 wt.% of cobalt was loaded on $CNF_{ox\text{-}P}$ using WI method with a toluene/ethanol solution of $Co(NO_3)_2$. The prepared catalysts were denoted Co/CNF_F-I and Co/$CNF_{ox\text{-}P}$-I (derived from IWI), and Co/$CNF_{ox\text{-}P}$-W (derived from WI). The Co particle size obtained from XRD was 19 nm for Co/$CNF_{ox\text{-}F}$-I, 17 nm for Co/$CNF_{ox\text{-}P}$-I and 8 nm for Co/$CNF_{ox\text{-}P}$-W. The smaller Co particle size obtained over Co/$CNF_{ox\text{-}P}$-W was attributed to the better wetting properties of the toluene/ethanol mixture in comparison to the aqueous solution. In addition, Co particle size over Co/$CNF_{ox\text{-}F}$-I was slightly larger than that on Co/$CNF_{ox\text{-}P}$-I, because, $CNF_{ox\text{-}P}$ provided more edge sites for anchoring of Co particles compared to the $CNF_{ox\text{-}F}$ [148]. The FTS was performed at 210 °C, 20 bar, and H_2/CO =2. 20 and 22 mol% of water were used as a co-feed in order to investigate the effect of water. The highest reaction rate was achieved with Co/$CNF_{ox\text{-}P}$-W catalyst due to the highest dispersion of Co on this catalyst. Regarding the effect of water, the reaction rate increased for all catalysts by increasing the amounts of water. No accurate explanation was advanced for the surprising effect of water on the reaction rate. The catalysts deactivation observed in this study was attributed to Co oxidation and sintering caused by water partial pressure. It was also observed that S_{C5+} increased with increasing water partial pressure. This is because, an increase in the water partial pressure provokes an increase in the Co particle size, which is known to contribute to S_{C5+} improvement [89,148,149].

Several methods invoked in the literature such as i) the introduction of functional groups and defects on the support, ii) the surface modification of metal oxide with carbon, iii) the addition of promoters, iv) the adjustment of catalyst preparation methods, and v) the catalyst pretreatment, could be useful to significantly reduce the catalyst deactivation rate [150]. Thereafter, the influence of surface modification of CNT and catalyst pretreatment on catalyst deactivation will be discussed. It was reported that surface oxygen groups and defects present on the CNT_{ox} surface after acid treatment stabilize Co particles and prevent their sintering [151]. Hemmati *et al.* [152] prepared by IWI cobalt-based catalysts supported on different supports such as γ-Al_2O_3, nano-structured alumina (NS-Al_2O_3), NS-Al_2O_3 covered by CNT_{ox} and γ-Al_2O_3 covered by CNT_{ox}. In addition, La, Mo and Ru were used as promoters. The catalytic performances of the resulting catalysts were evaluated in FTS using a fixed-bed microreactor (T = 230 °C, P = 20 bar, GHSV = 3600 mL g^{-1} h^{-1}, H_2/CO = 2.0). Combined catalytic evaluations and catalyst characterization techniques indicated that NS-Al_2O_3 was better than γ-Al_2O_3 and catalyst performances were improved by CNT_{ox} coating. These results were attributed to the fact that CNT_{ox} weakens the MSI, and thus improves cobalt reducibility. TPR results showed that the cobalt-aluminate phase, which is responsible for the deactivation of alumina-supported Co catalysts, was eliminated or significantly reduced when the alumina surface was covered with CNT_{ox} prior to cobalt impregnation. This, not only improved catalysts activity, but also increased catalyst resistance to deactivation. In a recent study, Hong *et al.* [153] improved the reducibility and stability of Co/TiO_2 catalyst by tuning MSI *via* carbon nitride coating. In addition, the presence of a carbon nitride layer on the TiO_2 surface inhibited the encapsulation of Co^0 particle by the TiO_2 support during FTS [153]. The impact of catalyst pretreatment on deactivation in FTS was also evaluated by Aluha *et al.* [79] using plasma synthesized Co/C catalysts. The catalyst was pretreated at 400 °C under different atmospheres including i) H_2 only, ii) CO only, and iii) CO followed by H_2. The deactivation

observed in this work could not be attributed to Co sintering since the Co particle size of the spent catalysts was similar to the one of the fresh ones. The deactivation was more pronounced when the catalyst was pretreated in H_2. This was due to Co re-oxidation and surface reconstruction by the increased H_2O vapor pressure under FTS conditions. The pretreatment under pure CO favored carburization, which did not seem to generate active species for FTS. On the other hand, the successive catalyst reduction in CO and H_2 lowered H_2O production, enhanced WGS activity that enriched the H_2 stream, and made the catalyst more H_2O tolerant.

Van Deelen *et al.* [154] examined the effect of surface oxidation of the CNT support in FTS. CoO/CNT and CoO/CNT_{ox} catalysts were prepared *via* a colloidal technique to attach 6 nm CoO nanocrystals on CNT and CNT_{ox}. Co particles having mean diameters of 5.9 nm on CNT and 6.7 nm for CNT_{ox} were obtained. The amount of metallic Co^0 was higher in CoO/CNT (8.8 wt.%) than in the CoO/CNT_{ox} catalyst (6.1 wt.%). This suggested that oxidation of CNT reduces the formation of the Co^0 [154]. In FTS (T = 220 °C, P = 20 bar, H_2/CO = 2, and GHSV = 5950-8900 mL g^{-1} h^{-1}), the CoO/CNT exhibited better activity, S_{C5+} and stability than the CoO/CNT_{ox} one, because the CNT provides more Co^0 than the CNT_{ox} support. Furthermore, the high deactivation rate observed over CoO/CNT_{ox} was attributed to the deposition of carbonaceous species favored by the defects/oxygen surface groups present on the surface of CNT_{ox} [154].

Taghavi *et al.* [155] compared cobalt catalysts supported on graphene nanosheets (GNS) and N-doped graphene nanosheets (N-GNS) in terms of activity, selectivity and stability in FTS. The Co/GNS and Co/N-GNS catalysts were prepared by IWI method with 15 wt.% of cobalt. The highest Co dispersion and reducibility were obtained over the Co/N-GNS catalyst because N-dopants act as anchoring sites for Co particles, preventing agglomeration, and leading to smaller Co particle size. Moreover, the extent of reduction degree of Co/N-GNS catalyst was assigned to the Co confinement effect and hydrogen spillover that was favored by N-dopants. In FTS (T = 220 °C, P = 18 bar, H_2/CO = 2 GHSV = 5143 mL g^{-1} h^{-1}), the CO conversion was higher for Co/N-GNS (74.5%) compared to Co/GNS catalyst (70.6%).This was attributed to the increased reduction degree and dispersion of Co induced by the functional groups. The spent Co/N-GNS exhibited low Co sintering due to the functional groups, which prevented Co agglomeration. At the same time, the Co/N-GNS catalyst showed a lower S_{C5+} and higher CH_4 selectivity, because of the combined effect of hydrogen spillover and smaller Co particle size, which are beneficial for the termination reactions to paraffins [155]. The first deactivation step was more pronounced for the Co/N-GNS than that for the Co/GNS. This was ascribed to the higher water partial pressure produced during FTS, which induced re-oxidation and sintering of smaller Co particle on Co/N-GNS. This behavior was less pronounced in the Co/GNS catalyst due to the hydrophobic character of GNS, which reduces the water deposition on the catalyst surface and prevents the re-oxidation of Co particles. The second deactivation was more pronounced for the Co/GNS catalyst than that for the Co/N-GNS, since the N-dopant present on the surface of the N-GNS support prevents sintering, and thus catalyst deactivation. After regeneration at 400 °C of the used catalysts, the loss of activity was about 3.1% for the Co/GNS and 0.6% for the Co/N-GNS. Since the activity loss due to the Co sintering is irreversible, the catalyst deactivation was only attributed to the catalyst re-oxidation. This explanation is consistent because Co/GNS with higher Co sintering has a faster deactivation rate.

To conclude this first section dealing with reactivity, we have shown that activity, S_{C5+}, but also stability of the catalyst can be improved depending on the type of the carbon support and surface modifications. Additionally, activity and S_{C5+} can also be improved by changing the reaction conditions during FTS. Generally, the type of carbon support, density of surface functional groups (oxygen or nitrogen groups) or defects allow controlling the Co particle size

and catalyst stability. The optimal Co particle size for a high TOF and S_{C5+} is generally in the range of 6-10 nm or > 10 nm for carbon supports without channels such as CNF, GNS, CS, and AC. Furthermore, the presence of a functional groups or defects provokes a decrease of the Co particle size, thus leading to the improvement of the selectivity in CH_4 *via* hydrogen spillover. The general tendency of the Co particle size effect cannot be directly applied in the case of the CNT_{ox} supported cobalt catalyst, due to confinement effects that can be more important than the Co particle size effect. The confinement effects are more pronounced at high Co filling yields inside the CNT_{ox} channel. For this reason, the optimal Co particle size for CNT_{ox} corresponds to those that can be contained in the CNT_{ox} channel and most of the time the maximum Co particle size is in the range of 3-7 nm, due to the channel diameter. In contrast, those deposited outside the CNT_{ox} (> 7 nm) are less active and selective in FTS, due to the absence of confinement effects. To guarantee better catalytic performance in FTS, it is thus important to control MSI, Co particle size, as well as reducibility during catalyst preparation and activation.

3. Catalyst elaboration

The main goal of this section is to present how various parameters during catalyst elaborations can be used as a handle in order to influence the physicochemical properties of fresh Co/C catalysts. As discussed in the previous section, Co particle size is one of the key parameters to control in FTS, and many elaboration parameters are evaluated on their efficiency over the size and size distribution control of the resulting Co nanoparticles. However, the optimal Co particle size in FTS for Co/C catalysts strongly depends on the type of carbon support and its functionalization. Various methods of preparing catalysts with controlled Co particle size have been reported in the literature. However, it is difficult to associate the characteristics of a catalyst just to the preparation method because, several parameters such as the type of carbon support, the type of dopants, the density of the functional groups and the surface modification are also involved. For this reason, we will limit the discussion to the description of the different methods employed in the literature, the characterization, and the FTS performance in order to link the properties of the catalyst to the catalytic activity and selectivity.

We will first present in detail different methods to reach the optimal Co particle size for CNF, AC, GNS or CS (6-10 nm or > 10nm) and for CNT_{ox} (3-7 nm) or for CNT (7 > nm). The impact of parameters such as the activation atmosphere and temperature on the properties of the catalysts will also be discussed. Co reducibility and catalyst deactivation represent a big challenge during catalyst preparation; the addition of promoters such as Pt, Ru or Mn, Cr may be useful to overcome to these problems.

3.1 Preparation methods

The physicochemical properties of a catalyst are particularly influenced by the catalyst preparation. Thus, various methods for preparing carbon supported cobalt-based catalysts for FTS with a range Co particle size have been reported in the literature as shown in Table 4. The existence of many methods of catalyst preparation [156], enables to tune to a certain extent the metal loading and dispersion, thus, influencing the FTS performances (Table 4). However, the preparation of catalysts with a well-defined crystalline structure, Co particle size and shape remain challenging. In this section, we will focus on the different preparation methods of Co/C catalysts for FTS. The main advantages and drawbacks of each method will also be discussed.

Table 4. Carbon-supported cobalt catalysts prepared by different techniques and corresponding FTS performances.

Catalysts	Co loading (%)	Preparation method	Co size (nm)	Reaction conditions	CO (%)	Activity/TOF	S_{C5+} (%)	Ref.
Co/CNF	40	Plasma Precipitation IWI	12 22 37	GHSV = 6000 mL g^{-1} h^{-1} 30 bar, 230 °C	20 6.2 6.4	- - -	30 - 60	[157]
Co/CNT*ox*	16 18	PFP IWI	4.1 7.5	GHSV = 1066 mL g^{-1} h^{-1} 10 bar, 220 °C	80 65	- -	70 45	[158]
Co/CNT*ox*	15	Sol-gel IWI	7.2 5.6	GHSV = 90000 mL g^{-1} h^{-1} 220 °C	52 45	- -	88 83	[134]
Co-Ru/CNT*ox*	15	Microemulsion IWI	6 8	20 bar, 220 °C	75.1 59.1	0.372[a] 0.291[a]	87.6 92.4	[159]
Co/CNT*ox*	10	SEA	5-7	20 bar, 240 °C	16-59	-	19-59	[126]
Co/CNT*ox*	15	WI	9-10	GHSV = 2400 mL g^{-1} h^{-1} 20 bar, 230 °C	48-54	0.241-0.269[b]	52-62	[63]
Co/CNF*ox*	0.8 11	IA HDP	6 27	1 bar, 220 °C	2 2	2.3[c] 9.6[c]	23 -	[89]
Co/CNT*ox*	15	IWI Microemulsion	12 8-10	GHSV = 2400 NmL/min 20 bar, 220 °C	75 85	37[d] 27-28[d]	72 60-69	[92]
Co/N-CS	1-2	CVD	13	GHSV = 1200 mL g^{-1} h^{-1} 8 bar, 230 °C	-	0.05-0.14[e]	-	[160]
Co/CNT*ox*	10	Microemulsion IWI	4-8 9	20 bar, 220 °C	62 54	0.4[f] 0.35[f]	92 86	[133]
Co/CNT*ox*	9	Colloidal	6	GHSV = 5970 mL g^{-1} h^{-1} 20 bar, 220 °C	15	122[g]	82	[90]
Co/AC*ox*	20	IWI	2.2	GHSV = 6750 mL g^{-1} h^{-1} 20 bar, 230 °C	60	200[g]	77.7	[161]
Co/AC*ox*	15	IWI	-	20 bar, 220 °C	12.6	-	17.9	[78]

[a],[b],[f] In g_{HC} g_{cat}^{-1} h^{-1}. [d] In 10^3 s^{-1}. [e] In mol_{CO} g^{-1} h^{-1}. [c, g] In 10^{-3} s^{-1}. IWI= incipient wetness impregnation; WI = wet impregnation; CVD = chemical vapor deposition; HDP = homogeneous deposition precipitation; PFP = photo-Fenton-process; SEA = strong electrostatic adsorption; IA = ion adsorption; TOF = turn over frequency; and GHSV = gas hourly space velocity.

3.1.1 Impregnation methods

The impregnation method is the most commonly used for the synthesis of supported cobalt catalysts. This is due to its simple implementation and low waste streams in comparison to other techniques [156]. This method does not require complicated or expensive equipment, and metal gradients across the whole catalyst grain from eggshell to a uniform distribution can be obtained [156]. Two main impregnation methods have to be distinguished, namely wet impregnation (WI), whereby an excess amount of solvent is used and incipient wetness impregnation (IWI) or dry impregnation, in which an amount of solvent to just fill the pore volume of the support is used [156]. Common precursors include inorganic metal salts, such as metal sulfates, chlorides, nitrates, or acetates, and metal complexes such as metal acetylacetonates [156]. The most commonly used solvent for inorganic salt is water because of the high solubility of many precursors, whereas organic solvents are mainly used for metal complexes insoluble in water [156]. Generally, these methods involve three steps: (1) contacting the support with the impregnating solution for a certain period of time, (2) drying the support to remove the solvent, and (3) activating the catalyst by calcination, reduction or other appropriate treatments [162].

3.1.1.1 Wet impregnation

Here the volume of the impregnation solution is greater than the total pore volume and therefore a filtration step is usually performed for catalysts of low loading. If high metal loadings (> 10 wt.%) are targeted, which is usually the case of FTS, multistep impregnation can be performed. This often leads to catalysts with large particle size or broad particle size distribution since the majority of the metal precursor is present in the solution outside the pores of the support [27]. Additionally, during solvent evaporation, metal-precursors often deposit on the outer surface of support resulting in the formation of large crystals [27]. Pour *et al*. [63] prepared Co/CNT catalysts with different sonication time for FTS using WI method. The Co loading target was at 15 wt % on purified and functionalized CNT, using cobalt nitrate as precursor. All catalysts resulting from different sonication times present Co particle size around 10 nm (Figure 17a, b, c), which is slightly larger compared to the one obtained by IWI, (around 8 nm, Figure 17d) [133]. The lower FTS rate ($g_{HC}\ g_{cat}^{-1}\ h^{-1}$) of the catalysts prepared by WI compared to that of the catalyst prepared by IWI (Figure 17e) was attributed to the larger Co particle size located outside CNT_{ox}, which are known to be less active than those located inside the tubes due to confinement effects. This is one of the reasons why WI is generally less used than IWI for the preparation of Co/CNT_{ox} catalysts.

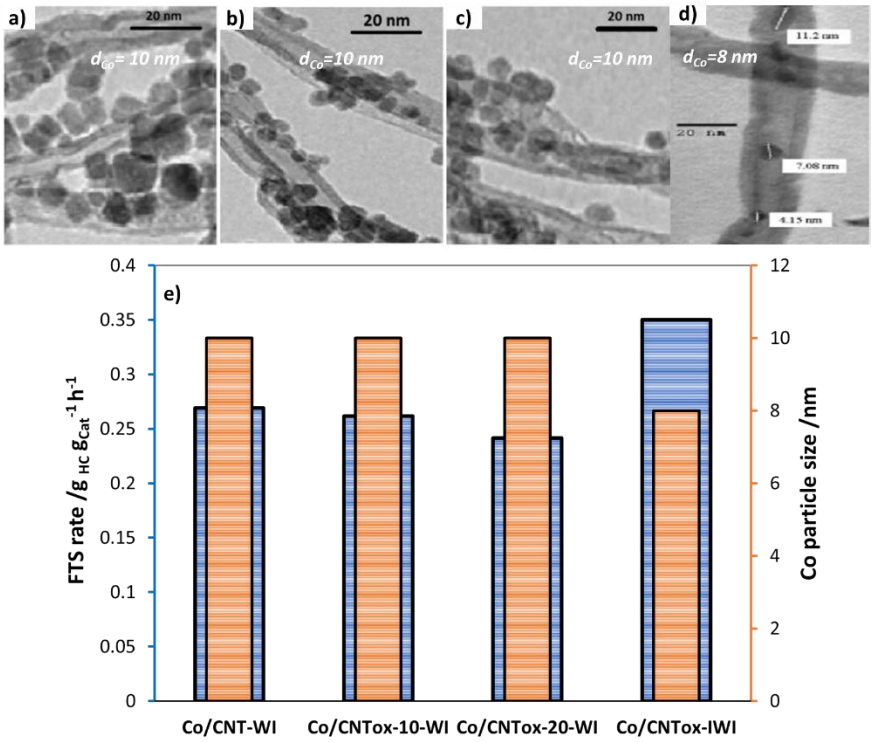

Figure 17. TEM images and particles size for calcined catalysts supported on: a) purified CNT catalyst: Co/CNT-WI; b) functionalized CNT (CNT_{ox}) sonicated by means of a pulsing technique (10 s-on/10 s-off for five cycles): Co/CNT_{ox}-10-WI; c) functionalized CNT sonicated by means of a pulsing technique (20 s-on/20 s-off for five cycles): Co/CNT_{ox}-20-WI. Reprinted with permission from Ref [63].Copyright 2018 American Chemical Society. d) catalyst prepared by IWI. Reprinted with permission from Ref [133]. Copyright 2010 Elsevier. e) Comparison of average Co particle size and FTS rate (g_{HC} g_{cat}^{-1} h^{-1}) for the catalysts prepared by XI (Co/CNT-WI, Co/CNT_{ox}-10-WI, Co/CNT_{ox}-20-WI)[63], and incipient wetness impregnation (Co/CNT_{ox}-IWI) [133].

3.1.1.2 Incipient wetness impregnation

The pore volume of the dried support is determined prior to the impregnation. Then, a solution of metal precursor is prepared according to the pore volume and the targeted metal loading. It is possible that the targeted metal loading cannot be reached by only one impregnation if the pore volume of the support is not high enough. The prepared solution of metal precursor is then added dropwise to the dried support. The solution is spontaneously drawn into the pores by capillary suction [163].Ideally, at the end of the impregnation, the support is completely wet, albeit without solution excess. Then, the mixture is dried before activation by calcination and/or reduction takes place. Because of its simplicity, IWI is one of the most commonly used techniques for depositing metals on carbon supports [27]. Due to the close contact between the metal precursor and the support, IWI generally results in small particle size with narrow particle size distribution [77]. Eschemann *et al*. [106] reported the preparation of supported cobalt catalysts (9 wt% Co) on untreated CNT (Figure 18a) and CNT_{ox} (Figure 18b) by IWI with solutions of cobalt nitrate in water, ethanol, or 1-propanol. They observed that whatever the impregnating solvent, the Co particle size was between 4-5 nm on CNT and CNT_{ox} (Figure 18c, d, e, f); however, clustering was observed for water-impregnated catalysts (Figure 18c). The small size can be explained by a better wettability between the organic solvents and the support, which allow producing catalysts with small particle size. On the other hand, for the catalysts prepared using 1-propanol as a solvent, the Co particle size was slightly higher for Co/CNT_{ox}-PrOH (Figure 18f) than that for Co/CNT-PrOH catalysts (Figure 18e).This result is

not in accordance with the literature since CNT_{ox} should offer more anchoring sites for Co particles *via* surface oxygen groups. The *in*-situ XRD studies revealed that *hcp*-Co was present only in the Co/CNT-PrOH catalyst. The high FTS activity observed for the Co/CNT-PrOH was attributed to the presence of *hcp*-Co phase [106]. The impregnation method could be employed for the preparation of Co/C catalysts with small Co particle sizes, since it is well known that catalysts presenting small Co particle sizes favor the occurrence of the hydrogen spillover, which is beneficial for improving catalytic activity [139].

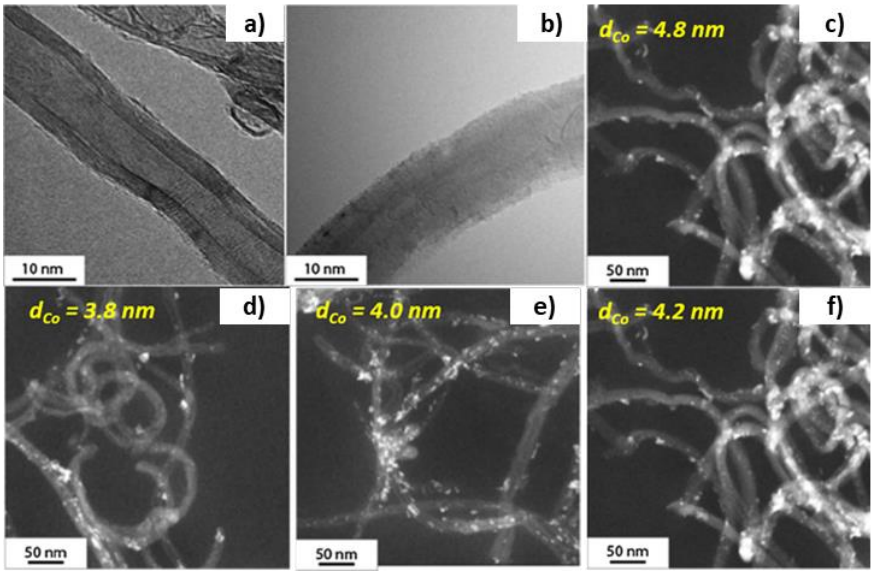

Figure 18. Representative STEM-HAADF of CNT and Co/CNT catalysts: a) untreated CNT; b) CNT_{ox}); c) Co/CNT-H_2O; d) Co/CNT-EtOH; e) Co/CNT-PrOH; and f) Co/CNT_{ox}-PrOH. Reprinted with permission from Ref [106]. Copyright 2015 Elsevier.

3.1.2 Coprecipitation

In this method, the solution containing a salt of the active metal (nitrates, chlorides, or sulfates) and the support are mixed so that nucleation and growth of the active phase on the support are obtained in a single step [156]. Additionally, one or more metals can be precipitated together with the support [163]. The method is technically feasible for the synthesis of solid catalysts with relatively homogeneous particle size distribution and high metal loadings. It is often considered to be more difficult than impregnation and indeed, it requires an accurate control of the conditions, and hence the use of sophisticated equipment. However, a benefit of coprecipitation over impregnation is the high attainable metal loading. There are two general approaches: i) constant-pH coprecipitation; and ii) varying pH coprecipitation to the desired end point [164]. The former provides the best control over the precipitation procedure, because local fluctuation induced by varying pH can cause heterogeneous growth of the active phase [156,164]. Zhang *et al.* [165] prepared unsupported CoCu bimetallic nanoparticles (denoted Co_3Cu_1), and a CNT_{ox} supported Co_3Cu_1 catalyst (11%Co_3Cu_1/CNT_{ox}) using constant-pH coprecipitation method from the corresponding nitrate salts. CNT_{ox} was used as support and the catalysts were tested in CO/CO_2 hydrogenation to alcohols (reaction conditions: T = 300 °C P = 50 bar, $V(H_2)/V(CO)/V(N_2)$ = 45/45/10 and GHSV = 7 200 mL h^{-1} g^{-1}). Under the same conditions, CO conversion reached 27.1 and 13.7 % with 11%Co_3Cu_1/CNT_{ox} and Co_3Cu_1, respectively. This is explained by the higher active metal surface area of 11%Co_3Cu_1/CNT_{ox} (1.21 times) compared to that of Co_3Cu_1 since it is well known that supported metal catalyst

offers more active sites than the unsupported one [16]. Additionally, a lower apparent activation energy of CO hydrogenation was measured for the 11%Co_3Cu_1/CNT_{ox} catalyst (10.7 kcal mol^{-1}) compared to the Co_3Cu_1 catalyst (12.2 kcal mol^{-1}) [165]. The same group also used the coprecipitation technique to prepare a series of $Co_3Cu_1/x\%CNT_{ox}$ catalysts (x% = mass percentage of CNT_{ox}) for higher alcohol synthesis from syngas [166]. CNT_{ox} content was first optimized using a Co/Cu molar ratio fixed at 3/1. Under similar conditions, CO conversion over the prepared catalysts was as follows: $Co_3Cu_1/11.2\%CNT_{ox}$ > $Co_3Cu_1/9.2\%CNT_{ox}$ ≥ $Co_3Cu_1/16.0\%CNT_{ox}$ > $Co_3Cu_1/0.0\%CNT_{ox}$ [166]. Incorporation of an appropriate amount of CNT_{ox} not only increased the catalyst activity for CO conversion, but also strongly improved its selectivity toward alcohol formation [166,167]. Then, the Co/Cu molar ratio was also optimized, and the catalyst with the Co/Cu molar ratio of 3/1 was the most active for higher alcohol synthesis. So, this is an efficient technique for the preparation of homogeneous supported mono or bimetallic catalysts for CO hydrogenation.

3.1.3 Homogeneous deposition precipitation

This method concerns the deposition of the active phase on a support from a precursor solution through the slow and homogeneous introduction of a precipitating agent (such as hydroxyl ions) so that to avoid nucleation in the bulk solution [156]. The homogeneous deposition precipitation technique (HDP) has been developed for the preparation of highly loaded and highly-dispersed oxide-supported metal catalysts [27,168]. HDP can be induced by: i) increase of pH; ii) change of valency of the metal ion; or iii) removal of a stabilizing ligand of the metal ion [169]. Bezemer *et al*. [89] prepared 9-11%Co/CNF_{ox} catalysts using cobalt nitrate, acetate, and carbonate as metal precursors. The HDP technique by urea hydrolysis at 90 °C was applied to achieve the required loading by a slow and homogeneous increase of the pH [89]. The resulting catalyst with 9 wt % cobalt displayed Co particle size around 14 nm (Figure 19a), with intermediate dispersion compared to those prepared by IWI (Co loading of 13wt.%, d_{co} = 7.5 nm) and ion adsorption (Co loading of 0.8wt.%, d_{Co} = 5.5 nm). In FTS (T = 220 °C, P = 1 bar, H_2/CO= 2), the Co/CNF_{ox} catalyst prepared by HDP method exhibited a S_{C5+} of 50 wt % with a CH_4 selectivity of 22 wt % [89]. In comparison with Co/CNF_{ox} catalysts prepared by IWI and ion adsorption, the high S_{C5+} (50 wt %) observed with the Co/CNF_{ox} catalyst prepared *via* HDP was attributed to the larger Co particle size. In addition, no sintering of the Co particles was observed (Figure 19b). One of the major advantages of this technique is that the Co dispersion can be controlled by varying the pH of the solution during catalyst preparation. The same group prepared Co/CNF_{ox} catalysts with cobalt loading of 15wt.% using $Co(NO_3)_2$ both from an acidic and basic solution *via* HDP [170]. Co/CNF_{ox} catalysts derived from an acidic and basic solution exhibited Co particle size of 25 and 7.9 nm, respectively. In acidic solution, the MSI is reduced due to the low density of oxygen groups, leading to larger Co particle size. In contrast, basic solution favors a higher MSI, which led to a catalyst with good dispersion [170]. HDP technique is thus suitable for the preparation of catalysts combining a high metal loading and dispersion.

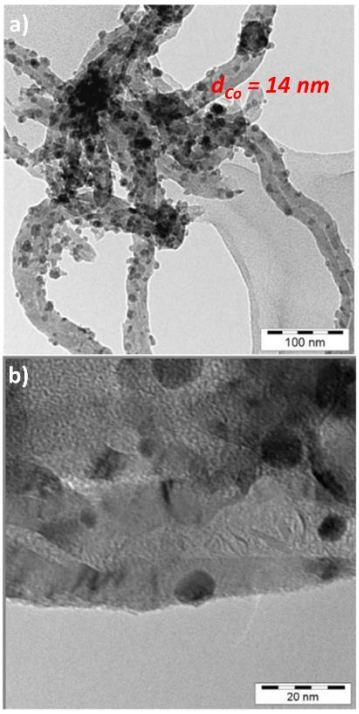

Figure 19. TEM image of a Co/CNF_{ox} catalyst prepared by HDP showing particles with sizes of around 14 nm distributed over the fibers. a) TEM image of the fresh catalyst after reduction and passivation; and b) TEM image of the spent catalyst (1 bar, 220 °C, 48 h) indicating the absence of sintering. Reprinted with permission from Ref [89]. Copyright 2006 American Chemical Society.

3.1.4 Microemulsion technique

The microemulsion technique involves the use of water, oil and an amphiphile (surfactant) [171]. Aromatic organic solvents as tetrahydrofuran are most often used to destabilize the solution favoring the sedimentation of the metal particles [171]. At high oil concentration, the discontinuous phase is transformed into a structure of small water droplets within a continuous oil phase (reverse micelles) when the surfactant is added (Figure 20) [133]. There are two routes for catalyst preparation using microemulsion technique: i) mixing two microemulsions, one containing the precursor and the other the precipitating agent; and ii) adding the precipitating agent directly to the microemulsion containing the metal precursor [171]. Then, the resulting solutions derived from either route are properly mixed with the support in order to obtain a homogeneous distribution of metal particles onto the support [171]. This technique enables the control of metal particle size with narrow particle size distribution, regardless of the metal content [133]. For a better control of catalyst particle size during the preparation, numerous parameters such as: i) size of the water droplets, ii) surfactant concentration, and iii) nature of the precipitating agent (reducing agent) should be taken into account [171]. However, the major difficulty of this technique lies in the elimination of the surfactant during the washing step, which can inhibit the catalytic performance in FTS. In order to overcome this problem, catalyst can be calcined at an appropriate temperature.

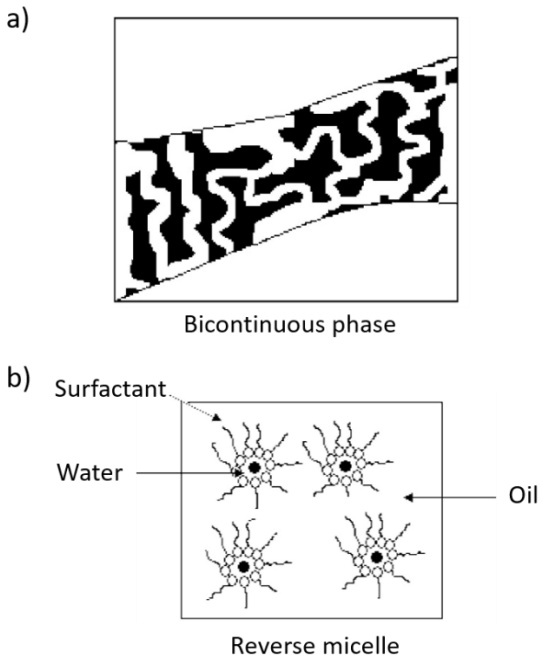

Figure 20. Microemulsion structure at a given concentration of surfactant: a) water-in-oil phase; and b) formation of cobalt particles (black dots) within the reversed micelles with the addition of surfactant. Reprinted with permission from Ref [133]. Copyright 2010 Elsevier.

This method has been used for the preparation of Co/CNT_{ox} [133,172,173], and CoRu/CNT_{ox} [159]. Trepanier *et al.* [133] obtained very narrow particle size distributions of various sizes (3-10 nm). Particle size is proportional to the water-to-surfactant ratio (3-10) used during catalyst preparation [133]. Additionally, the most abundant Co particle size in this case was in the range of 2-3 nm. At the same Co loading of 10 wt.%, the Co particle size obtained from IWI method was around 10 nm. In FTS (T = 220 °C, P = 20 bar, and H_2/CO = 2), the catalysts prepared by the microemulsion technique were found to be more active (+15 % of CO conversion) than the catalyst prepared by IWI. This was explained by the confinement effect of the small Co particles located inside CNT_{ox} and this was more pronounced for the catalysts prepared *via* the microemulsion technique.

Pour *et al.* [102] prepared five 15%Co/CNT_{ox} catalysts *via* the microemulsion and IWI methods in order to examine a possible intrinsic particle size effect in FTS. To achieve a series of catalysts displaying different Co particle sizes in the microemulsion system, they varied the water-to-surfactant molar ratio (W/S) from 2 to 12. The resulting Co particle size was between 4-10 nm *via* the microemulsion method and 12 nm *via* the IWI. These catalysts were investigated in FTS reaction at T = 220-235 °C, P = 20 bar, H_2/CO = 2 and GHSV = 2400-12000 mL g^{-1} h^{-1}. The activity (mol g_{cat}^{-1} h^{-1}) increased with the decrease of the Co particle size [102]. Moreover, the optimal particle size was found at 7.6 nm. The high activity of the small Co particle is related to the high fractions of *hcp*-Co phase [47]. Additionally, the apparent activation energy increased from 89 to 98 kJ mol^{-1} when Co particle size increased from 4.8 to 12.4 nm [102]. Microemulsion is thus a suitable method for controlling Co particle size for FTS.

3.1.5 Sol-gel synthesis

This method involves in the first step the formation of stable colloidal solutions (‘‘sol’’), followed by the anisotropic condensation of colloidal particles (micelles) producing polymeric chains with entrapped solution of condensation by-products, resulting in the formation of a ‘‘lyo- or hydrogel’’ or ‘‘monolith’’ when no external solvent is used [163]. For supported catalysts preparation, the inorganic precursor immobilized in the sol-gel is mixed with the support followed by decomposition of the precursor during the heat treatment [163]. The sol-gel method is commonly used for the preparation of supported catalysts on metal-oxides (*eg*.TiO_2, Al_2O_3, SiO_2) [174] or on carbon materials for FTS [134,175]. This technique has advantage to allow controlling and adjusting the surface, the porosity, and the particle size of catalysts. Karimi *et al*. [134] have used sol-gel and IWI routes to prepare Co/CNT_{ox} catalyst for FTS. For the sol-gel route, three molar ratios of metal ion (cobalt nitrate) to citric acid (1, 5, and 10) have been used and the resulting catalysts were denoted C1, C2 and C3, respectively. The catalyst prepared by IWI was named C4. TEM analysis showed that the mean Co particle size was 5, 7, 9 and 10 for C1, C2, C3 and C4, respectively (Figure 21). That is, the mean Co particle size of the catalysts prepared by the sol-gel route increased with the metal ion to citric acid ratio (complexing agent). This was explained by the fact that the complexing agent prevents agglomeration of Co particles and enhances the metal dispersion. Under the same FTS conditions (T = 220°C, P = 25 bar, H_2/CO = 2, GHSV = 90000 mL g^{-1} h^{-1}), the catalysts prepared by the sol-gel technique showed higher FTS rate (0.71 g_{HC} g_{cat}^{-1} h^{-1}), higher S_{C5+} (increased by 7%) and lower S_{CH4} (decreased 4%) compared to that prepared by IWI [134]. This was attributed to an increase of the confinement effect for small Co particles located inside the CNT_{ox} channel (Figure 21) in the case of catalysts prepared by sol-gel technique, which improves the Co dispersion and reducibility.

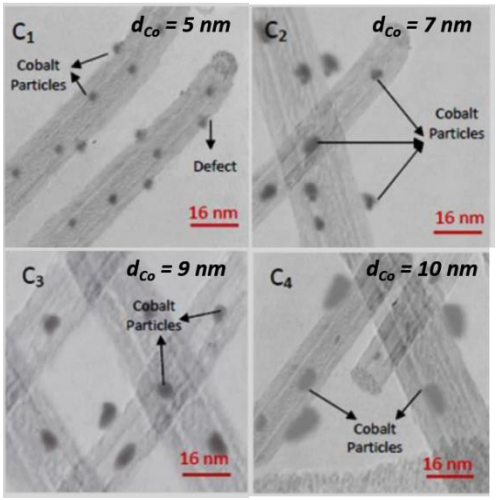

Figure 21. TEM images of the calcined catalysts using the sol-gel route (C1-C3) and IWI route C4. Reprinted with permission from Ref [134].Copyright 2012 Springer Nature.

3.1.6 Plasma synthesis

This synthesis method is based on the decomposition of a metal−oil suspension using plasma to produce supported catalysts in a carbon matrix (Co/C or Fe/C catalysts) [75,157,176] or oxide matrix such as Ni/Al_2O_3 [177]. This method has the remarkable advantage of producing core-shell structures, in which the carbon shell can protect the nanometric metallic core (Co or Fe) from coming into contact with air [157]. The particle size of the as-prepared catalysts strongly depends on the cooling rate of products at the plasma reactor exit [176]. Low cooling

rate favors the formation of small particles [178]. The preparation of monometallic (Co/C) and bimetallic (Co-Fe/C) catalysts by plasma synthesis was reported by Aluha *et al*. [179]. The average particle size of Co/C (Figure 22a) seemed to be slightly larger than that of bimetallic catalysts (Figure 22b, c) containing different Co and Fe loadings. In another study conducted by the same group [157], three catalyst elaboration methods were used: plasma synthesis, WI, and precipitation to prepare 40%Co/C catalysts for FTS (T = 230 °C, P =30 bar, H_2/CO = 1.88 GHSV = 6 000 mL g^{-1} h^{-1}). The catalyst prepared by the plasma method (d_{Co} = 12 nm) displayed a relatively higher CO conversion in FTS (*ca*. 30 %) compared to those prepared by impregnation (*ca*. 3 %, d_{Co} = 37 nm) and precipitation (11 %, d_{Co} = 22 nm). This result was attributed to the higher Co dispersion of the catalyst prepared by plasma synthesis.

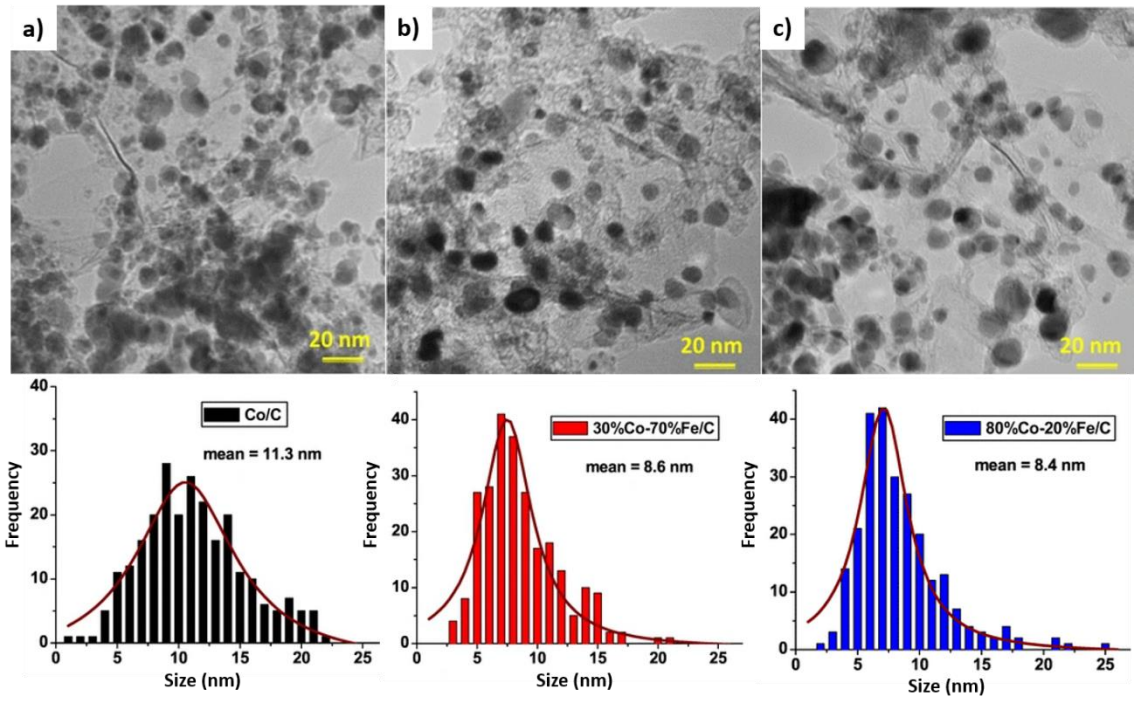

Figure 22. TEM micrographs and particle size distribution of plasma synthesized catalysts. a) Co/C; b) 30%Co-70%Fe/C; and c) 80%Co-20%Fe/C samples. Reprinted with permission from Ref [179]. Copyright 2018 Springer Nature.

3.1.7 Colloidal synthesis

Colloidal synthesis provides unique opportunities to control the size, shape, and composition of nanoparticles in the liquid phase [156]. In this technique, a metal precursor is reduced chemically or electrochemically [169]. The preparation of carbon-supported catalysts by this technique consists in directly adding the solid support to a suspension of metallic nanoparticles in solution. Metal nanoparticles are preferentially adsorbed in pores having commensurable diameter. In fact, the interaction of nanoparticles with pore walls is stronger than with flat surfaces [169]. In order to avoid aggregation, coalescence, and growth, ligands present in the solution play an essential role in stabilizing the nanoparticles [156]. The main challenge in catalyst preparation by this method is ligands removal, which hamper the accessibility of reactants to the metal surface and thereby limit catalytic activity, especially in FTS [90,180]. In this context, van Deelen *et al*. [90] investigated the effect of oxidative treatments (Figure 23a) on the deposition of cobalt nanocrystals (Co-*NC*) or (CoO-*NC*) onto CNT and subsequent

ligand removal. First, Co-*NC* (ε-cobalt) with a cubic shape were synthesized using $Co_2(CO)_8$ as metal precursor and oleic acid as stabilizer. CoO-*NC* were then obtained by air-exposure of the Co-*NC* at ambient conditions during subsequent washing steps. CoO-*NC* had a narrow particle size distribution centered between 6-7 nm and a roughly spherical shape (Figure 22b). Both Co-*NC* and CoO–*NC* were deposited *via* colloidal suspension onto CNT through mixing in toluene at 200 °C (Figure 23d, e).

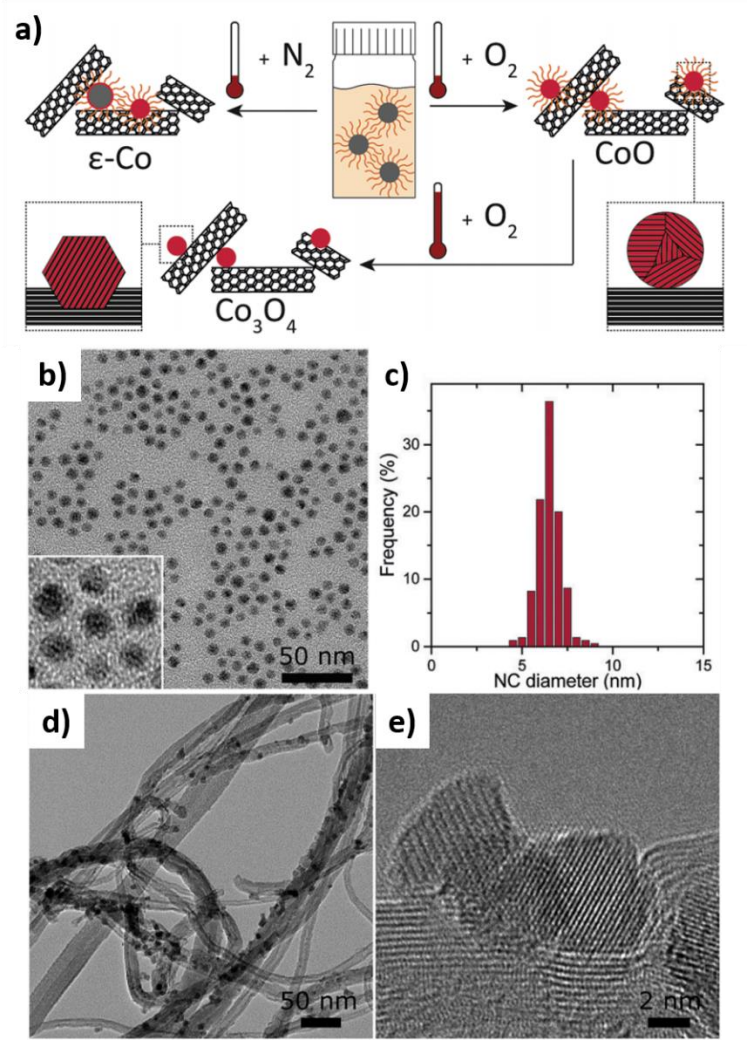

Figure 23. a) Schematic overview of the oxidative treatments applied to the Co nanocrystals (NC). a) TEM of CoO-NC with a higher magnification inset; and c) size distribution of CoO-NC with a surface- averaged particle diameter of 6.8 nm. Overview of NC supported on CNT: d) TEM and e) HR-TEM of the CoO-*NC*/CNT catalyst treated at 250 °C. Reproduced by permission from Ref [90]. Copyright 2018 Royal Society of Chemistry.

After deposition on CNT, the resulting catalysts are denoted Co-*NC*/CNT and untreated CoO-*NC*/CNT. Co-*NC* were agglomerated (d_{Co} = 7-60 nm), probably due to magnetic interactions between the NC, while the CoO-*NC* were well dispersed (d_{Co} = 5.7 nm). For ligand removal, the untreated CoO-*NC*/CNT catalyst was heated under 20 vol% O_2/N_2 at 250 °C. This treatment did not affect the particle size (d_{Co} = 5.9 nm) and size-distribution of CoO-*NC*/CNT, but some clustering of CoO-*NC* on the CNT was also observed. In FTS (T = 220 °C, P = 20 bar, H_2/CO = 2 v/v), the CoO-*NC*/CNT catalyst thermally treated at high-temperature was significantly less active than untreated CoO-*NC*/CNT catalyst. The lower activity observed on

the CoO-*NC*/CNT catalyst treated at high-temperature oxidation was ascribed to the sintering of the CoO nanoparticles on CoO-*NC*/CNT catalyst during the *in*-situ reduction and/or FTS. For the untreated CoO-NC/CNT catalyst, the ligands were readily removed during in-situ reduction. Also, the aggregated Co-NC/CNT showed a low activity. So, the preparation via colloidal synthesis followed by a direct in-situ reduction seemed to be an efficient method to prepared well-dispersed Co/C catalysts, with narrow Co particle size distribution. However, the necessary treatments for ligand removal may impact the shape, size and size distribution of the nanoparticles, and consequently their catalytic properties.

3.1.8 Chemical vapor deposition

Chemical vapor deposition (CVD) allows the direct deposition of the active phase onto the catalyst support by means of a reaction between a specific group of the support surface (*eg*. oxygenated groups of functionalized carbon materials) and the vapor of a suitable metallic precursor [181,182]. Generally, organometallic complexes are needed to ensure high volatility of the precursor [27]. Kuang *et al*. [183] used this method to deposit cobalt onto carbon spheres (6.1%Co/C-CVD) using [$Co(acac)_2$] as a precursor. CoO/C catalysts were also prepared by IWI (5.2%Co/C-IWI) and ultrasonic impregnation (5.7%Co/C-UI) using cobalt nitrate hexahydrate dissolved in ethanol. The CVD approach led to the formation of uniformly-dispersed CoO particles (CoO/C-CVD, d_{Co} = 21 nm, Figure 24a) while the IWI (CoO/C-IWI, d_{Co} = 17 nm, Figure 24b) and UI (CoO/C-UI, d_{Co} = 22 nm, Figure 24c) led to an agglomeration of CoO particles on the support. In FTS (T = 230 °C, P =10 bar, H_2/CO = 2, GHSV = 2000 mL h^{-1} g^{-1}), the catalytic performance of CoO/C-CVD was significantly better (TOF = 4.2 10^{-3} s^{-1}, S_{C5+} = 81.9 %) than that of CoO/C-IWI (TOF = 1.1 10^{-3} s^{-1}, S_{C5+} = 59.5 %) and CoO/C-UI (TOF = 1.4 10^{-3} s^{-1}, S_{C5+} = 59.5 %). This result was assigned to the good dispersion of the CoO particles on the support surface achieved by the CVD technique. A similar CVD technique was employed by Feizbakhsh *et al*. [184] to prepare 15%Co/CNT (d_{Co} = 14 nm) and 15%Co/GNS catalysts (GNS = graphene nanosheet) (d_{Co} = 10 nm) that showed high stability under FTS conditions (T = 220°C, P = 18 bar, H_2/CO = 2).

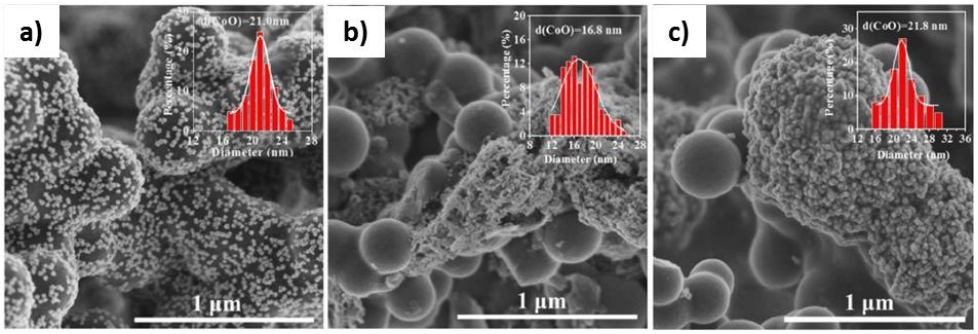

Figure 24. SEM images of cobalt catalysts prepared by different methods: a) CoO/C-CVD; b) CoO/C-IWI; and c) CoO/C-UI. Reprinted with permission from Ref [183]. Copyright 2019 Elsevier.

The CVD technique was also used to prepare 0.2%Pt−10%Co/CS catalysts on carbon spheres using cobalt and platinum acetylacetonates as metal precursors [185]. This method allowed obtaining smaller Co particles (d_{Co} = 5 nm) compared to IWI method (d_{Co} = 11 nm) for the same metal loadings. Under the same conditions in FTS (T = 220 °C, P = 20 bar, H_2/CO = 2, GHSV

= 1500 mL g^{-1} h^{-1}), the catalysts prepared by CVD showed higher CO conversion (26.5%) than the one prepared by IWI (7.4%) due to the improved dispersion of Co particles.

3.1.9 Miscellaneous methods

We have shown up to now the most common methods for the preparation of supported cobalt catalysts for FTS. Less conventional methods have also been described in the literature and the most relevant will be presented in this section.

3.1.9.1 Chemical reduction method

In this method, the inorganic precursor is reduced in the presence of a reducing agent such as $NaBH_4$ to form the nanoparticles on the surface of the support [186]. This method can be performed in one or two steps in order to deposit mono or bimetallic particles, respectively. Shariati *et al.* [186] compared the preparation of 10% Co/CNT_{ox} by WI and chemical reduction method from cobalt chloride and $NaBH_4$ as reducing agent. The reduction of cobalt chloride in the presence of H_2 derived from the decomposition of $NaBH_4$ affords directly the cobalt particles onto the CNT_{ox} support at 180 °C (Figure 25). Afterwards, Ru particles were deposited onto Co/CNT_{ox} catalyst following the same procedure using ruthenium chloride and N_2H_4 as a reducing agent (Figure 25). In FTS (20 bar, 220 °C, H_2/CO = 2, GHSV = 1400 mL g^{-1} h^{-1}), the catalyst prepared by chemical reduction (d_{Co} = 6.5 nm) performed slightly better (conversion = 36%, S_{C5+} = 46%) than the one prepared by WI (d_{Co} = 8.9 nm, conversion = 32%, S_{C5+} = 42%). Because chemical reduction method reduces the cobalt particles cluster and enhances the confinement of Co particles inside the CNT_{ox}.

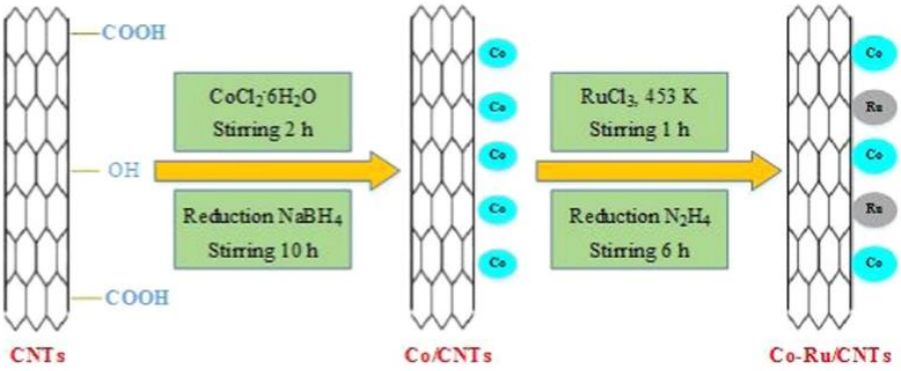

Figure 25. The schematic illustration of the preparation method of Co-Ru/CNT nanocatalyst. Reprinted with permission from Ref [186]. Copyright 2019 Elsevier.

3.1.9.2 Photo- Fenton process

The photo-Fenton process is a new synthesis route for exploiting the properties of CNT in FTS [158]. This method involves the generation of OH* radicals *via* a complex reaction sequence comprising activation of hydrogen peroxide (H_2O_2) by ferrous (Fe^{2+}) ions (*Eqs11*) [187], oxidation of CNT by the OH* radical, and deposition of metal particles (Figure 26).[158]

$$Fe^{2+} + H_2O_2 \rightarrow Fe^{3+} + HO^* + OH^- \quad (Eq.11)$$

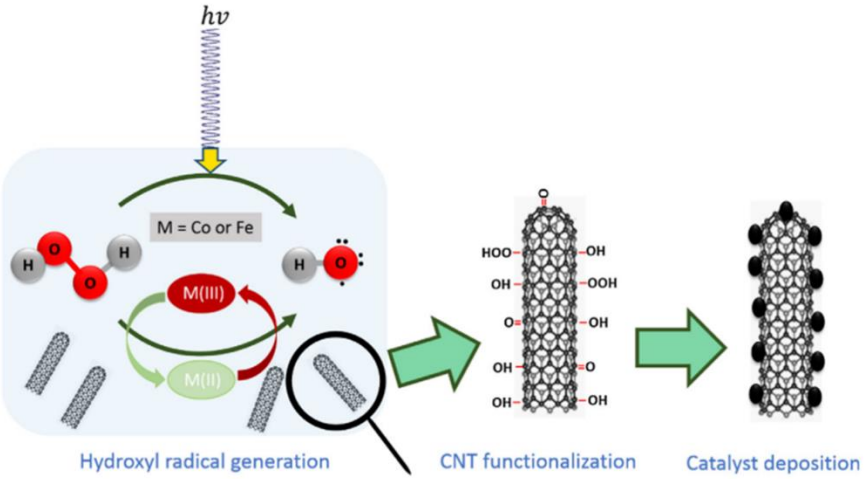

Figure 26. Schematic illustration of modified photo-Fenton process for CNT oxidation and catalyst deposition. Reprinted with permission from Ref [158]. Copyright 2018 Elsevier.

Almkhelfe *et al.* [158] have compared 15%Co/CNT_{ox} catalysts prepared by the photo-Fenton process and by IWI in the FTS reaction. The photo-Fenton based approach consisted in two main steps. The first step corresponded to the functionalization of the CNT *via* reaction of H_2O_2 under stirring at 60 °C. Then, the total amount of metal precursor ($Co(OH)_2$) mixed with H_2O_2 was separated in four batches, which were added successively over a period of four days. After the addition of each batch, the mixture was exposed to UV illumination (wavelength, λ= 300 nm). After filtration, the resulting powder was dried at 150 °C to yield the catalyst (Co/CNT_{ox}-Fenton). The Co particle size on these catalysts was relatively small (d_{Co} < 10 nm), highly uniform, and well dispersed on the CNT_{ox} surface. On the other hand, the catalyst prepared by IWI (Co/CNT_{ox}-IWI) contained larger Co particles (d_{Co} > 10 nm), which in addition were agglomerated. The narrow distribution and well-dispersed Co particles of Co/CNT_{ox}-Fenton was ascribed to the absence of post-synthesis treatments, such as drying and calcination, which often leads to sintering and strong interactions with the catalyst support [24,158]. TPR data showed a remarkable improvement in the dispersion of Co particles in the photo-Fenton process. The Co/CNT_{ox}-Fenton catalysts showed higher CO conversion (*ca.* 80%) and S_{C5+} (*ca.* 70%) than the Co/CNT_{ox}-IWI catalysts under FTS conditions (T = 200 °C, P = 10 bar, H_2/ CO = 2 and GHSV = 1066 mL g^{-1} h^{-1}). This was attributed to the green and less aggressive environment of the photo-Fenton process, which not only preserves the structural integrity of CNT, but also avoids the calcination step which causes Co particles sintering [158].

3.1.9.3 Hydrothermal process

This method consists in immobilizing a metallic precursor on a porous material followed by crystallization and *in* situ deposition of metallic particles during a heat treatment [163,188]. This technique is efficient for the synthesis of inorganic materials with different morphologies [189]. This approach was explored for the preparation of a support for mono [190,191] or bimetallic [192] catalysts for FTS. Wang *et al.* [191] have thus synthesized Co/NGA catalysts (NGA = 3D nitrogen-doped graphene aerogel). This method involves the simultaneous formation of NGA and immobilization of cobalt species [191]. In this study three Co/NGA catalysts with different cobalt loading (2.7%, 5.4%, and 13.9%) were prepared using cobalt acetylacetonate as precursor. The preparation method consisted in dispersing GO (graphene oxide) in deionized water under sonication. Then, an amount of urea was added in the mixture during 20 min,

followed by heat treatment at 100 °C for 1h, in an autoclave. The cobalt precursor and ethylene glycol were mixed with the GO suspension and the whole mixture was let under sonication for 30 min. Subsequently, the resulting suspension was transferred once more to the autoclave and treated hydrothermally at 180 °C for 12 h to obtain Co/NGA catalysts. Raman analyses showed that the I_D/I_G value increased with the increase of cobalt loading, which indicates that a high Co^{2+} concentration was beneficial for the self-assembly cross-linking during the formation of the three-dimensional (3D) NGA [191]. FTIR analysis also confirmed that the Co^{2+} concentration influenced the cross-linking of graphene during the construction of 3D NGA and affected the catalyst structure. XRD patterns of the fresh catalysts evidenced the characteristic peaks of the *fcc*-Co phase. The Co particle size decreased with the increase of cobalt loading as follows: 11.25 nm for 2.7%Co/NGA; 6.25 nm for 5.4%Co/NGA; and 5.25 nm for 13.9%Co/NGA. In general, the Co particle size increases with cobalt loading [193]. The observed trend was explained by the fact that at higher Co loading, most of the Co^{2+} species were linked to graphene edges or defects thus leading to Co particles with higher dispersion [191]. Under the same conditions of FTS (T = 250°C, P = 10 bar, H_2/CO = 2), the cobalt-time-yield increased with time-on-stream. This was attributed to the transformation of a large portion of the *fcc*-Co into *hcp*-Co phase during FTS reaction (Figure 27). In addition, 2.7%Co/NGA with larger Co particle size exhibited higher cobalt time yield than the other catalysts, due to the improved mass transfer of reactants to cobalt active sites [191].

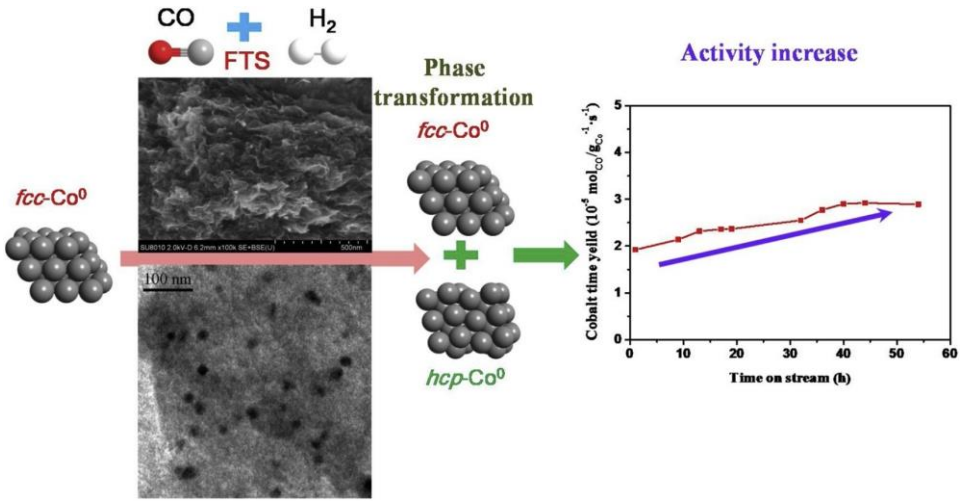

Figure 27. Effect of cobalt phase transformation on activity in FTS. Reprinted with permission from Ref [191]. Copyright 2019 Elsevier.

3.1.9.4 Metal-organic framework based catalysts for FTS

Metal-organic frameworks (MOF) are porous coordination polymers composed of metal ions or clusters and bridging organic linkers. They are established as a relatively new class of crystalline porous materials with high surface area, structural diversity, and tunability, which attracts great interest for a variety of applications, including heterogeneous catalysis [194]. These materials not only combine the benefits of both organic and inorganic components but also usually exhibit properties that exceed the sum of those of their components [195]. In comparison with conventional materials, MOF present a number of advantages such as adjustable framework structure, hybrid composition, defined and diverse crystal structures, and confined micro-environments [195]. Thanks to the carbon present in the organic linkers, MOFs can serve as excellent templates for carbon/metal-based porous materials by means of

pyrolysis. Three essential features of MOF (metal nodes, organic linkers and internal pore space) provide a large number of catalytic sites: i) functionalized metal nodes or coordinatively unsaturated-metal sites (CUS), ii) functional and modified linkers, and iii) catalytically active guest species incorporated into the cavities (Figure 28) [195].

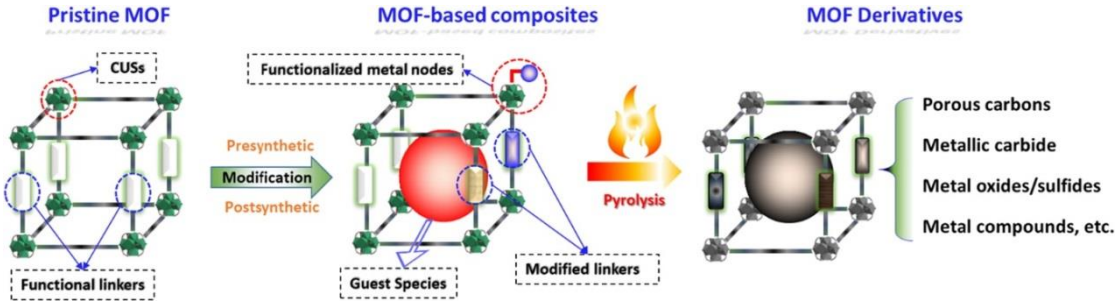

Figure 28. Schematic representation of the catalytic site locations on/in different types of MOF-based catalysts. Reprinted with permission from Ref [195]. Copyright 2019 Elsevier.

Luo *et al.* [99] investigated the effect of the Co particle size for FTS using MOF-based catalysts. To prepare Co/C catalysts with various Co particle sizes, the pyrolysis of well-structured MOF ZIF-67 was performed at different temperatures. Depending on the temperature used, different phenomena occurred during the pyrolysis including the collapse of the framework, the decomposition of the organic ligand, the reduction of Co^{2+} by released reducing gases (*eg.* CO, H_2), as well as the nucleation and growth of Co particles [99]. The main process for the formation of Co/C catalysts derived from ZIF-67 is illustrated in Figure 29a.

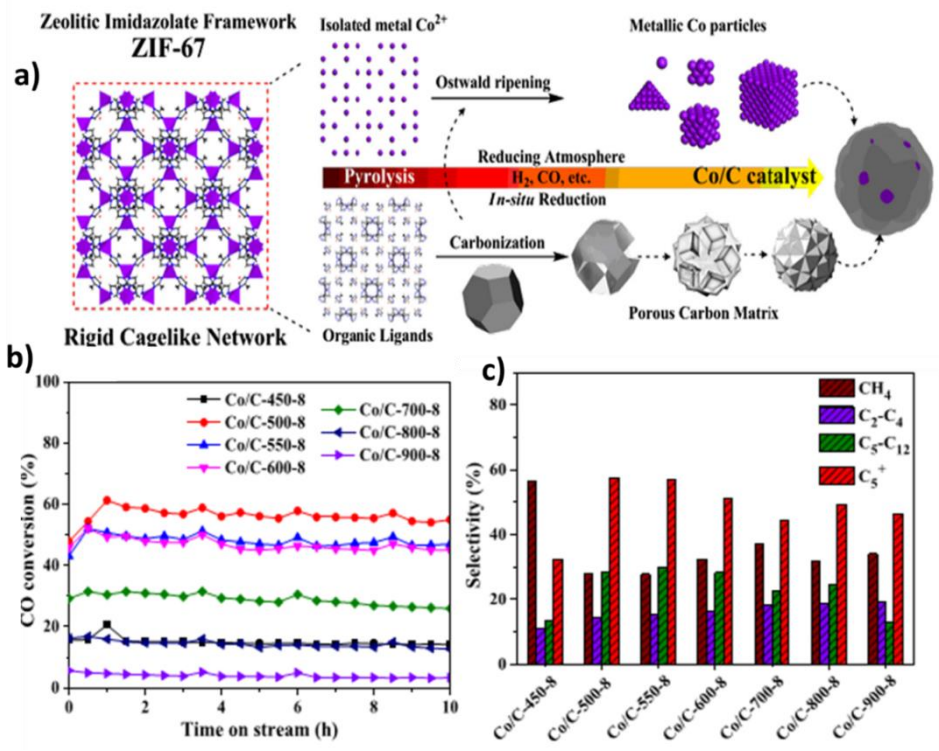

Figure 29. a) Illustrative representation for the one-step synthesis of metallic Co particles confined in porous carbon matrix *via* pyrolyzing ZIF-67; b) FTS results over Co/C catalysts under the conditions of m_{cat} = 0.4 g, T = 235 °C, 1.0 MPa, H_2/CO = 2, and GHSV = 5550 mL g^{-1} h^{-1}(CO conversion as a function of TOS); and c) selectivity of different products at a TOS of 10 h. Reprinted with permission from Ref [99]**.** Copyright 2019 Elsevier.

By increasing the pyrolysis temperature from 500 to 900 °C, the average Co particles size increased from 9.7 to 120 nm, indicating a significant impact of the pyrolysis temperature on the Co particle size. Changing the pyrolysis duration had much less impact on the Co dispersion and on the reduction of Co species [99]. The results of the catalytic performance in FTS (T = 235 °C, P = 10 bar, H_2/CO = 2, and GHSV = 5550 mL g^{-1} h^{-1}) showed that CO conversion first increased and then decreased with the increase of the pyrolysis temperature from 450 to 900 °C, and the maximum CO conversion (*ca*. 57 %) was obtained over Co/C-500-8 (500 °C pyrolysis temperature, 8 h pyrolysis time, Figure 29b). Moreover, this catalyst also showed the highest selectivity in S_{C5+} (*ca.* 58%) and the lowest S_{CH4} (*ca.* 28%) (Figure 29c). These results were assigned to the Co particle size effect. The high S_{CH4} obtained over catalysts pyrolyzed at lower temperature (eg. Co/C-450-8) was due to the incomplete decomposition of the pristine ZIF-67. The presence of a carbon shell, pyridinic/graphitic N, and cobalt oxides over Co/C catalysts after heat-treatment influences the hydrogen adsorption and modifies the S_{CH4}.

In another work, Zhang *et al.* [196] studied the impact of the reducing atmosphere, reaction temperature and time, using the Co-MOF approach on the formation of Co particles, Co-species reduction, and nucleation and crystal growth steps. The Co/C catalyst prepared in an atmosphere of 2% C_2H_2 in helium led to smaller Co particle size, and higher reduction degree in comparison with the Co/C catalyst prepared in pure helium. Furthermore, the catalyst prepared under C_2H_2/He exhibited high performance in FTS and low sintering of Co particles. This was because the carbon shell formed during CVD in acetylene and Ar atmosphere can effectively inhibit the cobalt particles from migration and agglomeration during the FTS [197]. This result is consistent with the one described by Ning *et al*. [197].

The reported examples of Co/C catalysts synthesized using the Co-MOF method for FTS are summarized in Table 5. To prepare well-dispersed Co catalysts by this approach, pyrolysis temperature between 500-600 °C in C_2H_2/He or Ar atmosphere should be used. Moreover, the addition of promoters as Pt or Nb into the parent MOF significantly increases the catalytic activity [198,199]. MOF materials seem to be well-suited for the CO transformation not only because of their structural diversity, functionality and tunability, but also because they can be used as supports or sacrificial precursors to create highly controllable MOF-derived catalysts [195].

Table 5. Catalytic performance of Co-MOF for FTS reported in the literature.

MOF	Metal precursors	T^a °C	Catalyst	d_{Co} nm	P bar	T °C	GHSV mL g_{cat}^{-1} h^{-1}	X_{CO} %	Activity	Product selectivity (%)		
										CH_4	C5+	Ref
MOF-71	$Co(NO_3)_2.6H_2O$	600	Co/C	12.3[b]	30	300	ND	ND	3.5[d]	ND	ND	[200]
ZIF-67	$Co(NO_3)_2.6H_2O$	600	0CTAB-Co/C	10.5[b]	20	230	6.75[c]	35.7	2.0[e]	26	63	[201]
ZIF-67	$Co(NO_3)_2.6H_2O$	600	2CTAB-Co/C	10.6[b]	20	230	6.75[c]	34.2	1.9[e]	23	65	[201]
ZIF-67	$Co(NO_3)_2.6H_2O$	600	4CTAB-Co/C	10.0[b]	20	230	6.75[c]	36.2	2.0[e]	27	62	[201]
ZIF-67	$Co(NO_3)_2.6H_2O$	600	8CTAB-Co/C	9.91[b]	20	230	6.75[c]	40.1	2.2[e]	26	63	[201]
ZIF-67	$Co(NO_3)_2.6H_2O$	600	16CTAB-Co/C	10.7[b]	20	230	6.75[c]	30.7	1.8[e]	24	65	[201]
ZIF-67	$Co(NO_3)_2.6H_2O$	450	Co/C-450-8	ND	10	235	5550	18.0	ND	58	3	[99]
ZIF-67	$Co(NO_3)_2.6H_2O$	500	Co/C-500-8	9.70[b]	10	235	5550	60.0	ND	27	59	[99]
ZIF-67	$Co(NO_3)_2.6H_2O$	550	Co/C-550-8	11.9[b]	10	235	5550	50.0	ND	27	58	[99]
ZIF-67	$Co(NO_3)_2.6H_2O$	600	Co/C-600-8	17.9[b]	10	235	5550	50.0	ND	32	55	[99]
ZIF-67	$Co(NO_3)_2.6H_2O$	700	Co/C-700-8	28.9[b]	10	235	5550	30.0	ND	35	42	[99]
ZIF-67	$Co(NO_3)_2.6H_2O$	800	Co/C-800-8	82.1[b]	10	235	5550	18.0	ND	30	50	[99]
ZIF-67	$Co(NO_3)_2.6H_2O$	900	Co/C-900-8	120.0[b]	10	235	5550	5.0	ND	32	48	[99]
Co-BDC	$Co(CH_3COO)_2{\cdot}4H_2O$	550	Co@C-C_2H_2	14.6[b]	30	220	3000	10.5	ND	83	15	[197]
Co-BDC	$Co(CH_3COO)_2{\cdot}4H_2O$	550	Co@C-Ar	16.9[b]	30	220	3000	6.2	ND	66	22	[197]
Co−MOF	$Co_2(dhtp)(H_2O)_2{\cdot}xH_2O$	400	Co@C-400	3.2[b]	30	260	8000	12.6	4.4[e]	27	52	[196]
Co−MOF	$Co_2(dhtp)(H_2O)_2{\cdot}xH_2O$	450	Co@C-450	4.5[b]	30	260	60000	18.6	31.2[e]	22	58	[196]
Co−MOF	$Co_2(dhtp)(H_2O)_2{\cdot}xH_2O$	500	Co@C-500	2.8[b]	30	260	60000	14.4	25.4[e]	13	75	[196]
Co−MOF	$Co_2(dhtp)(H_2O)_2{\cdot}xH_2O$	550	Co@C-550	4.7[b]	30	260	50000	16.8	18.6[e]	12	78	[196]
Co−MOF	$Co_2(dhtp)(H_2O)_2{\cdot}xH_2O$	600	Co@C-600	6.2[b]	30	260	20000	13.2	8.9[e]	10	82	[196]
ZIF-67	$Co(NO_3)_2.6H_2O$	550	Co@NC-550	ND	30	230	24000	10.0	ND	22	31	[202]
Co-MOF-74	$Co(NO_3)_2.6H_2O$	550	Co@C-550	ND	30	230	24000	30.0	ND	20	65	[202]
$M_2(bdc)_2$ (dabco)	$CoCl_2.6H_2O$	ND	Pt@Co/C	ND	10	250	ND	35.0	ND	70	6	[199]
MOF-1	$CoCl_2.6H_2O$	500	Co-MOF-1/C	ND	10	320	3600	65.1	ND	13	47	[203]
MOF-2	$CoCl_2.6H_2O$	500	Co-MOF-2/C	ND	10	320	3600	73.7	ND	13	54	[203]
CPO-27(Co)	$Co(NO_3)_2.6H_2O$	500	NbOx-Co@C	ND	1	220	28000	3.1	0.51[e]	42	36	[198]
CPO-27(Co)	$Co(NO_3)_2.6H_2O$	500	Co@C	ND	1	220	28000	1.1	0.18[e]	41	36	[198]
OMC	$Co(NO_3)_2.6H_2O$	600	CoNPs@OMC	ND	20	250	10	30.2	ND	15	81	[204]
TEOS	$Co(NO_3)_2.6H_2O$	600	Co@SiO_2@C	34[b]	20	230	4500	62.2	ND	21	62	[205]

[a]Pyrolysis temperature. [b]Co particle size determined from TEM observations. [c]in L. h^{-1} g^{-1} .[d]10^{-4} mol g_{cat}^{-1} .[e]10^{-5} mol_{CO} g_{Co}^{-1} s^{-1}.

A comparative summary of the catalyst preparation methods reviewed in this section is presented on Table 6. Among the studies listed in the literature, the IWI method is by far the most popular in comparison with other methods for the preparation of Co/C catalysts (Figure 30).These methods allow producing Co/C catalysts for FTS that present significant loadings (typically between 10-20 wt.%) on various carbon supports. It is important to note that the metal particle size can be modulated, for a similar loading, by changing the preparation method. Thus, in the case of CNT that have been particularly used, the particle size has been modulated between ~ 3 nm and ~ 12 nm for a 15%wt.% cobalt loading.

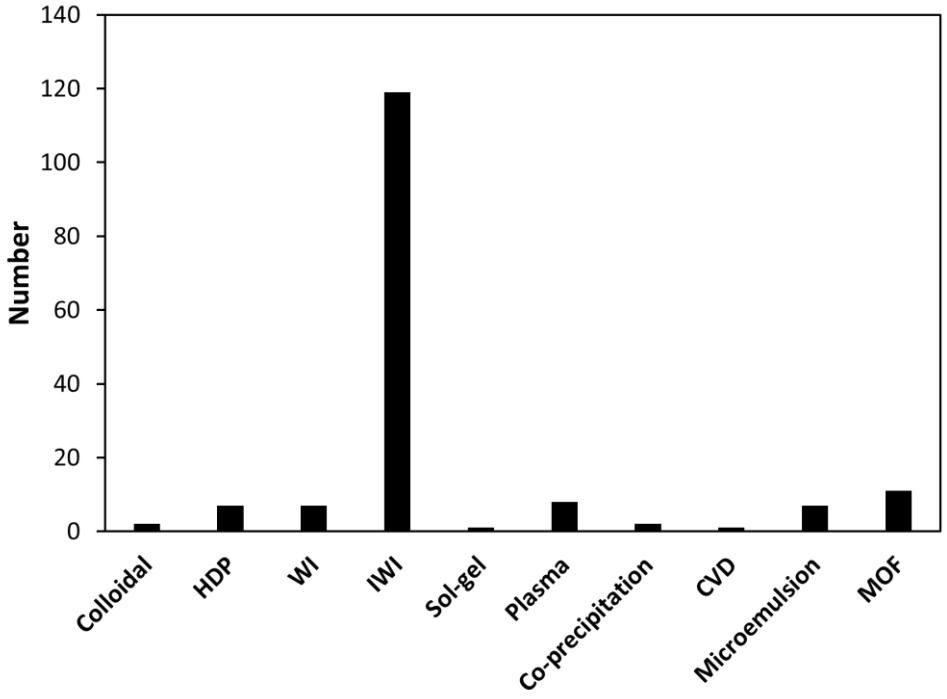

Figure 30. Number of article published for the different methods of preparation for Co/C catalysts from 1986 to 2019.

Table 6. The mains advantages and drawbacks of preparation methods for Co/C catalysts.

Preparation techniques	Advantages	Drawbacks	Ref.
WI	• Relatively fast and inexpensive method • Easy to prepare a layer of active phase on the catalyst's surface	• Multistep method (limited if chemical reduction is used) • Difficult to prepare highly loaded catalysts in one cycle • Easy agglomeration of particles in solution • Metal-precursors often deposit on the outer surface of the support particles • Loss of metal-precursors during the filtration step	[27,186, 206]
IWI	• Relatively fast and inexpensive method • Small particle size and narrow particle distribution • No need to filter • Close contact between precursor and support is achieved	• Multistep method • The maximum loading is limited by the solubility of the precursors in the impregnation solution	[27,206]
Coprecipitation	• High metal loadings can be achieved in one step • Bimetallic particles and support may be deposited in a single process • Small particle sizes can be achieved	• Washing steps are necessary to remove residual ions (nitrates,sodium,potassium)	[156,163]
HDP	• Good reproducibility • High metal loadings can be achieved • High metal dispersions at high metal loadings • Uniform distribution of the active component over the support	• Multi-step method	[27]
Microemulsion	• Good control of particle size • Narrow particle size distribution • High metal dispersions at high metal loadings	• Surfactant removal • Particle growth during heat treatment to remove the surfactants	[133]
Sol-gel	• Enables to control a narrow particle size distribution • High metal loadings can be achieved	• Multi-step method	[134]
Plasma	• Single-step method • Highly distributed active species • Shortened preparation time	• Energy consumption	[157,207,208]
Colloidal	• Excellent control over the size, shape, and composition of Co particles • Highly distributed active species	• Expensive metallic precursors • Ligands, limit accessibility of the metal surface for reactants Ligand removal • Particle growth during heat treatment	[90]
CVD	• High dispersion of the active phase • One-step method • Narrow size distribution of particles	• Toxic/expensive metallic precursor	[27,183]
Chemical reduction method	• Narrow size distribution of particles • High filling yield of Co particles inside CNT_{ox} channel • Avoid pore blockage of support by Co particles	• Multi-step method • Generates a lot of waste	[186]

Photo-Fenton process	• The calcination step is not necessary • Preserves the integrity of the CNT_{ox} support • Highly dispersed Co particles can be prepared	• Several reagents are involved • Multi-step method	[158]
Hydrothermal process	• Enables to prepare mono and bimetallic catalysts	• Multi-step method	[191]
MOFs based catalysts for FTS	• Inhibits the sintering or aggregation of Co particles	• Multi-step method • Energy consumption	[99]

The above section showed how the Co particle size, dispersion or reducibility can be tuned in order to obtain supported catalyst with the best FTS performances. The availability of an arsenal of methods makes it possible to prepare a supported Co catalyst with a wider range of Co particle size (d_{Co} = 2-180 nm) depending on the type of support and metal loading. Depending on the preparation method employed, metal precursors will interact differently from one carbon support to another, thus leading to the Co particles with different sizes, because the surface chemistry, which controls both the final particle size of the catalyst and the MSI is different. Consequently, it is important to properly address each type of carbon support for the catalyst preparation using the proper techniques.

IWI, microemulsion, photo-Fenton process, sol-gel, and colloidal methods are suitable to reach an optimal Co particle size < 7 nm on the CNT_{ox} with narrow distribution for FTS. In fact, Co particle size < 7 nm implies that most of the particles are confined inside CNT_{ox}, which reduces the MSI and affords good dispersion and stability to the FTS catalysts. However, after catalyst preparation using colloidal and microemulsion methods some organic compounds such as ligands or surfactants remain on the surface of metallic particles, which blocks the active sites and significantly reduces catalytic activity. Removal of surfactant or ligands requires post-treatment at high temperature, which in most of cases leads to the sintering of the Co particles, thus decreasing the catalyst activity. It has to be noted that Co particle size < 7 nm on the CNT_{ox} can be also obtained from photo-Fenton process, and sol-gel methods; however the catalyst preparation using these techniques is performed in several steps. For that reason, the one-step IWI method, remains the best approach for preparing catalysts presenting the Co particles size in the range of 3-7 nm with narrow distribution. Concerning Co/CNF_{ox}, or Co/C, the optimal Co size with the best FTS performances can be obtained using HPD, MOFs approach, IWI, and plasma technique. Generally, the Co particles size > 10 nm supported on the CNF_{ox} or C support can be obtained from these methods, which according to Bezemer et *al.* [89] leads to the improvement of TOF and S_{C5+}.

Apart from the preparation techniques, the physicochemical properties of carbon-supported cobalt catalyst also depend on several parameters such as the type of carbon support, the surface modification/functionalization, the nature of the solvent, the nature of the Co precursors, the cobalt loading, and the activation conditions. In order to rationalize the catalytic performances in the FTS, it is important to present the different contributions of each of these parameters and this will be the subject of the next section.

3.2 Effect of the type of carbon support

Carbon supports having different nanostructures that are commonly used include, CNF [144,209–212], CNT [127,213], AC [97], carbon sphere (CS) [91,211], mesoporous carbon (CMK) [107,214–216], or graphene nanosheets (GNS) [155,217,218]. The nature of the carbon support has impacts on MSI, mass and heat transfer, stability, and mechanical and thermal resistance [219]. Thus, the choice of a carbon support having appropriate physicochemical properties is critical to obtain an efficient catalyst, in particular for the control of metal particle size and reduction degree [97]. For example, CNF present graphene layers with an angle > 0° with respect to the central axis, while the graphene layers of CNT are aligned to the central axis, leading to different surface properties [125,220]. Another major difference between CNT and CNF consists in the lack of hollow cavity for the latter [125]. These structural differences between CNT and CNF significantly impact the properties of the resulting catalysts. It was reported that 12%Co/CNF_{ox}-*p* (platelet type) tested in FTS (T = 210 °C, P = 20 bar, H_2/CO =

2, GHSV = 2900 mL g^{-1} h^{-1}) showed a 2.5-fold increase of the initial activity compared to 12%Co/CNF_{ox}-*f* (fishbone-type) [209]. This was attributed to the higher Co dispersion in 12%Co/CNF_{ox}-*p* catalyst due to the higher specific surface area of CNF_{ox}-*p* (155 m^2 g^{-1}) as compared to CNF_{ox}-*f* (89 m^2 g^{-1}). Xiong *et al.* [220] have studied the influence of different structures of CNF, CNT and carbon micro-coils (CMC) (Figure 31a, d, g) on the size, dispersion and reducibility of cobalt particles. The three supports were functionalized with HNO_3 and 15wt.% of Co was impregnated using IWI [220]. XPS and Raman analyses revealed that CMC_{ox} presented both sp^2 and sp^3-bonded carbon atoms (the latter are characteristic for non-graphitic carbon materials), whereas CNT_{ox} and CNF_{ox} present mainly sp^2-bonded carbon. The density of surface acidic groups of these supports was as follows: CMC_{ox} (2.111 mmol g^{-1}) > CNT_{ox} (1.175 mmol g^{-1}) > CNF_{ox} (0.600 mmol g^{-1}). This was explained by the hybridisation of sp^2 and sp^3-carbon atoms of CMC_{ox} during the HNO_3 treatment [220]. TEM evidenced also the impact of the nature of carbon supports on the Co particle size: 6.4 nm for Co/CNT_{ox}, 5.6 nm for Co/CNF_{ox} and 4 nm for Co/CMC_{ox} (Figure 31b,c,e,f,h,i). Co/CMC_{ox} had also the lowest reduction degree, followed by Co/CNT_{ox}, then by Co/CNF_{ox}. This reducibility tendency was ascribed to the effect of Co particle size, due to various degrees of interaction between the cobalt and the support, which results from the different density of surface functional acid groups. The higher CO conversion and S_{C5+} obtained in FTS (T = 225 °C, P = 8 bar, H_2/CO= 2, GHSV = 3840 mL g^{-1} h^{-1}) for Co/CNT_{ox} were due to the higher reducibility and an optimal Co dispersion in comparison to Co/CNF_{ox} and Co/CMC_{ox}.

Fu *et al.* [97] highlighted the impact of the crystalline structure of carbon on the catalytic performance. For this purpose, AC and CNT_{ox} supported cobalt catalysts were prepared by IWI. In FTS (T = 230 °C, P = 20 bar, H_2/CO = 2, GHSV = 5400 mL g^{-1} h^{-1}) Co/CNT_{ox} showed higher TOF and S_{C5+} than Co/AC. These results are explained by two main reasons. First, CNT_{ox} are more graphitic than AC, which allows a better electronic transfer between cobalt particles and CO molecules, and thus an enhanced CO activation. Second, CNT_{ox} had larger pores than AC, which favored the formation of larger Co particles. These latter favor bridge-type CO adsorption, while small Co particles in Co/AC favor linear-type CO adsorption. C−O bond in bridge-type adsorbed CO is weaker and thus more reactive than in linear-type adsorbed CO. Similar trends was observed by the same group in another study [161]. Once again, among CMK (ordered mesoporous carbon), CNT_{ox} and AC supports, CNT_{ox} was found as the best support for cobalt catalyst in FTS, thanks to its highest graphitization degree, which facilitates the electron transfer between cobalt particles and CO molecules.

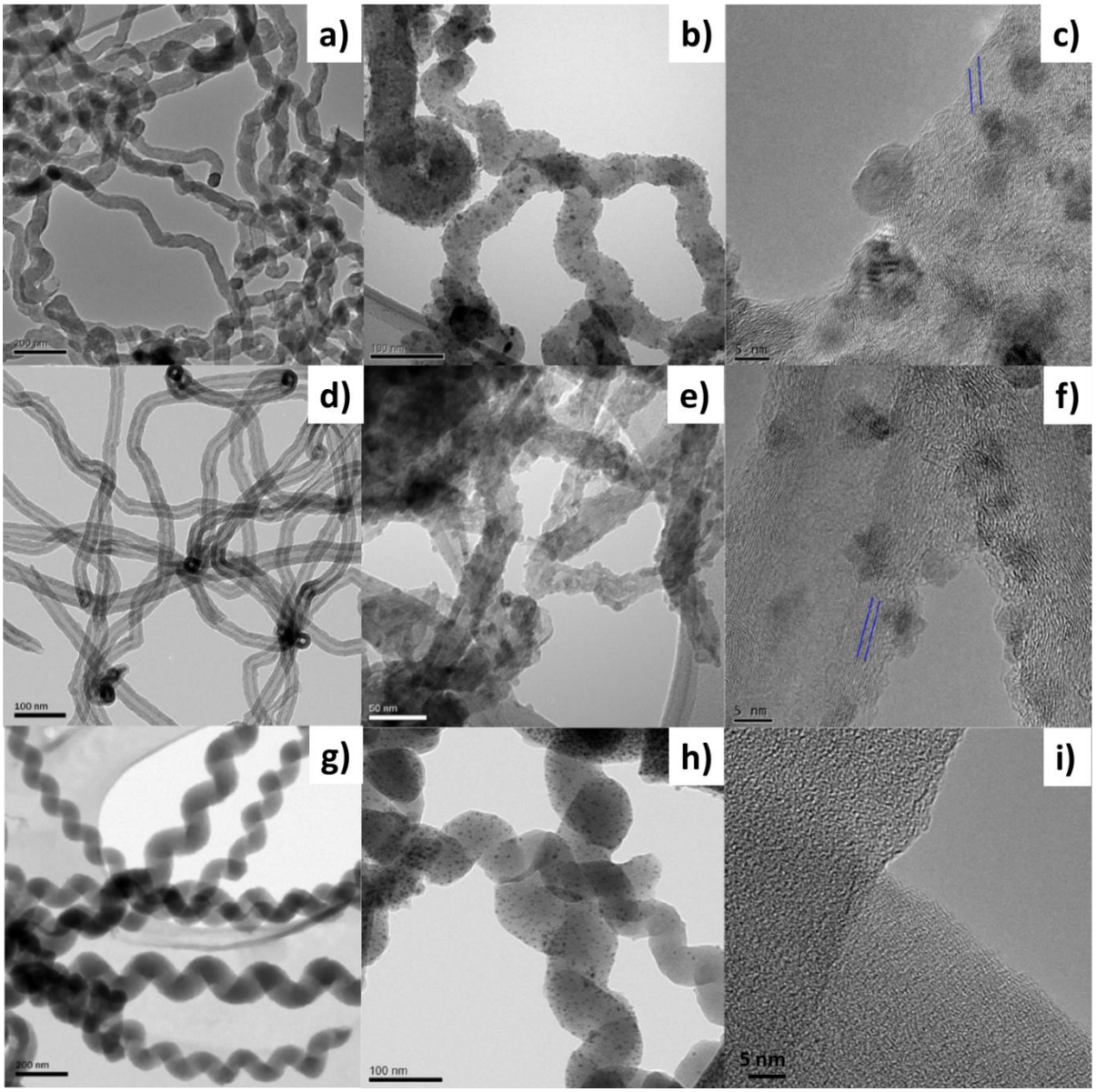

Figure 31. TEM images of raw shaped carbon materials and passivated Co catalysts: a) CNF_{ox} ; b) and c) Co/CNF_{ox}; d) CNT_{ox} ; e) and f) Co/CNT_{ox}; g) CMC_{ox} ; h) and i) Co/CMC_{ox}. Reprinted with permission from Ref [220]. Copyright 2013 Elsevier.

On Co/CNF catalysts, it was also observed that support crystallinity and pore size have an influence on the metal dispersion and, as a consequence, on the product selectivity and catalyst deactivation [212]. The crystallinity of the support played an important role in catalyst deactivation, being the most crystalline support the most resistant from the deactivation point of view. In FTS (T = 250 °C, P = 20 bar, H_2/CO = 2, and WHSV = 3000 mL g^{-1} h^{-1}), catalysts with medium pore diameter led to higher catalytic activity, but higher selectivity to CH_4 and CO_2 as compared to catalyst with higher pore diameter. On the other hand, catalysts with higher pore diameter, presented the highest S_{C5+}, and a low catalytic activity. Karimi *et al.* [218] investigated the effect of morphology and structure of GNS and CNT on the Co catalyst performance. In FTS (T = 220 °C, P = 18 bar, H_2/CO = 2, GHSV = 4500 mL g^{-1} h^{-1}), higher activity, S_{C5+} and stability were obtained over Co/GNS. This was attributed to the fact that GNS generated a higher density of active sites and provided better electrical conductivity than CNT.

Additionally, a higher density of functional groups and defects in Co/GNS contributes to a decrease of Co sintering [218].

From this analysis, it appears that the structure of carbon supports is one of the parameters which influence the physicochemical properties of catalysts. The type of carbon support and their morphology depend on the CVD synthesis conditions (Table 7). The carbon supports differ from each other by the arrangement of graphene layers, which are formed during the synthesis. Thus, parameters such as textural properties, defects, crystallinity, and density of oxygen groups will be dependent on the structure of the carbon supports. Several carbon supports exhibiting different morphologies such as CNT, CNF, FM, AC, CMC, CS, GNS, CNS and CMK have been reported in the literature for the preparation of Co/C catalysts for FTS. The advantages and drawbacks concerning the use of these supports on the Co/C catalysts properties are presented in the Table 7. According to their specific surface, these supports can be categorized into three classes.

The first class deals with carbon supports presenting a low specific surface (< 20 $m^2 g^{-1}$): the supports like CS (2.6 $m^2 g^{-1}$), CNS (4 $m^2 g^{-1}$), and CMC (14.3 $m^2 g^{-1}$) belong to this class. The CS are composed of random curling graphitic flakes with a size of 1-10 nm and exhibit low surface areas [91], which leads to Co/C catalysts with large Co particle sizes. The structure of CNS consists of a conglomeration of spherical bodies [211]. Their unclosed graphitic layers composed of open edges and dangling bonds, which are highly reactive during nitric acid treatment, decrease the Co particle size, and favor a strong MSI. The CMC are amorphous and their structure looks like a polymer-like carbon material [220]. The amorphous structure of CMC makes them unstable under FTS conditions.

The second class is composed of carbon supports with intermediate surface area such as CNT_{ox} (80-500 $m^2 g^{-1}$), CNF_{ox} (50-250 $m^2 g^{-1}$), and FM_{ox} (~200 $m^2 g^{-1}$). All these supports present graphitic structure with different arrangement of the graphene layers. The surface of FM_{ox} and CNF_{ox} present graphene edges, and the angle between the graphene layers and the axis of this objects are 90° and 26 ° for FM_{ox} and CNF_{ox}, respectively [139]. FM_{ox} with an angle of 90° present high level of reactive defects and oxygen content. Consequently, FM_{ox} favors strong MSI as compared to CNF_{ox} and CNT_{ox} supports. Under the FTS conditions, FM_{ox} and CNF_{ox} afford good stability to the catalysts due to the presence of edges, whereas the catalyst deactivation is more pronounced for catalysts based on CNT_{ox} due to the absence of graphene edges, which contribute to avoid Co sintering.

The third class is composed of AC_{ox} (1897 $m^2 g^{-1}$), CMK_{ox} (1051 $m^2 g^{-1}$), and GNS_{ox} (848 $m^2 g^{-1}$) supports, which exhibit high surface area. The mains advantages of AC_{ox} and CMK_{ox} supports is their high specific surface area, which is known contribute to improve Co dispersion, but their poor crystalline structure inhibits the electron transfer between CO and cobalt particle, and then reduces the catalytic activity in FTS [161]. The use of GNS_{ox} support improves the dispersion and stability of Co due the high specific surface and its high number of defects.

Carbon supports such as GNS_{ox}, CNT_{ox}, FM_{ox}, and CNF_{ox} offer attractive way to prepare Co/C catalysts, and their morphology can be tuned by several treatments (nitric acid treatment, thermal treatment etc…) in order to optimize the catalyst performances in FTS.

Table 7. The advantages and drawbacks of the different morphology of carbon supports on the Co/C catalysts properties.

Catalysts	BET surface ($m^2\ g^{-1}$)	I_D/I_G	NP size (nm)	Advantages	Drawbacks	Ref.
Co/CNT$_{ox}$	79.1	-	3.9	• CNT$_{ox}$ present high BET surface. • CNT$_{ox}$ internal diameter is beneficial for controlling particle size. • CNT$_{ox}$ allow avoiding the intraparticle mass transfer due to the presence of the internal channel. • CS are produced without catalyst. • No purification is needed after the synthesis of CS. • CS present the edges of the graphitic flakes, which are suitable for stabilizing particles during FTS.	• CS$_{ox}$ lead to catalysts with large particle sizes due to its low BET surface. • The absence of graphene edges from the CNT$_{ox}$ surface improves the catalyst deactivation.	[91,139,160]
Co/CS$_{ox}$	2.6	-	14.2			
Co/CNT$_{ox}$	220	1.54	4.3	• CNT$_{ox}$ and FM$_{ox}$ supports present high BET surface and high level of defects. • FM$_{ox}$ presents a high density of oxygen groups due to the presence of reactive edges. • The combination of high oxygen content and high level of defect in the FM$_{ox}$ and CNT$_{ox}$ allows decreasing the particle size and promotes the hydrogen spillover. • The presence of the edges on the FM$_{ox}$ and CNF$_{ox}$ inhibits the catalyst deactivation.	• High density of oxygen groups on FM$_{ox}$ support promotes bimodal distribution of the particle sizes. • FM$_{ox}$ favors a strong MSI and decreases the catalyst reducibility. • FM$_{ox}$ allows preparing cobalt based catalysts with high CH_4 selectivity due to the hydrogen spillover. • The low BET surface of the CNF$_{ox}$ leads to catalyst with larger Co size.	[139]
Co/CNF$_{ox}$	71	1.31	15.1			
Co/FM$_{ox}$	173	1.48	7.5 and 28.1			
Co/CNF$_{ox}$-1	130	-	36.4	• An increase in the temperature during the synthesis of the CNF$_{ox}$ decreases the pore volume and resultes in more graphitic materials (CNF$_{ox}$-1). • High graphitic support (CNF$_{ox}$-1) leads to the catalyst with the weaker MSI. • CNF$_{ox}$-3 support with a low graphitic character allows preparing highly dispersed catalyst due to the high pore volume. • The Co catalyst derived to CNF$_{ox}$-3 support presents high CO activity and high S_{C5+}. • The most crystalline supports (CNF$_{ox}$-1 and CNF$_{ox}$-2) resist to the catalyst deactivation.	• The catalysts derived from the most crystalline supports are more selective into CH_4 due to their low pore volume. • CNF$_{ox}$-3 with a low graphitic character do not stabilizes the Co particles.	[212]
Co/CNF$_{ox}$-2	164	-	32.8			
Co/CNF$_{ox}$-3	144	-	13.9			
CoFe/CNF$_{ox}$	234	1.00	18.2	• The crystalline graphitic carbon in CNS$_{ox}$ affords good stability to the catalyst. • The high reactivity of conglomerates of spherules in CNS induces the deposition of small and well dispersed particles.	• The chemical reactivity of the surface of CNS$_{ox}$ leads to a strong MSI.	[211]
CoFe/CNS$_{ox}$	4	0.50	6.6			
Co/CNT$_{ox}$	497	1.03	8.6	• GNS$_{ox}$ presents a significant degree of disorder and defect site. • High BET surface and density of functional groups in GNS$_{ox}$ induce a decrease in the particle size. • GNS$_{ox}$ support enhances the catalyst reducibility caused by the hydrogen spillover. • High level of defect in GNS$_{ox}$ allows avoiding the Co sintering.	• CNT$_{ox}$ promotes de sintering of Co particles due to absence of edges in their structure.	[218]
Co/GNS$_{ox}$	848	1.18	7.8			

Co/CNT$_{ox}$ **Co/AC** **Co/CMK$_{ox}$**	217 1897 1051	- - -	4.9 2.2 3.0	• CNT$_{ox}$ and CMK$_{ox}$ present large pore diameter. • The Co particles are well dispersed inside the tube of the CNT$_{ox}$ or pores of the CMK$_{ox}$ support. • AC$_{ox}$ present high BET surface and its use results in a catalyst with small particle sizes. • CMK$_{ox}$ affords better stability to the catalyst causes by its ordered pore structure and its high BET surface • High level of crystalline structure and the presence of the channel in the CNT$_{ox}$ facilitate the Co reducibility.	• AC$_{ox}$ and CMK$_{ox}$ have a poor crystalline structure.	[161]
Co/CNT$_{ox}$ **Co/CNF$_{ox}$** **Co/CMC$_{ox}$**	79,1 50,8 14,3	0.6 0.6 -	6.4 5.6 4	• The graphite-like CNT$_{ox}$ and CNF$_{ox}$ present high thermal stability under N_2. • The intermediate BET surface of CNF and their graphitic structure leads to weak MSI.	• CMC$_{ox}$ are unstable under N_2 because they are non-graphitic carbon materials.	[220]

3.3 Effects of surface modification of carbon support

The catalytic performances of carbon supported metal catalysts in terms of activity and selectivity highly depend on carbon surface properties [63]. Indeed, in comparison with unsupported catalysts, catalytic performances of Co/C catalyst can be enhanced by tuning MSI. The MSI allows controlling several characteristics of the final catalyst such as particle size, charge transfer, reducibility, and crystallinity [221,222]. It is possible to regulate metal-carbon support interactions using various surface modification techniques including: i) acid treatment [63,96,127,172,173,209,223,224]**,** ii) nitrogen-doping [20,98,131]**,** iii) thermal treatment [126,225,226]**,** or iv) modification by metal oxides [78,222,227–230]**.** In the following section, the effect of support surface modification on physicochemical properties and FT catalytic performances of Co/C catalyst will be discussed.

3.3.1 Surface modification of carbon by acid treatment

Among the carbon materials, the ones with a graphitic structure like CNF, CNT, and graphene are the most commonly used as catalyst supports in FTS [217,231,232]. However, their inherent hydrophobic properties and their poor surface reactivity can limit their application as catalyst support, due to a poor interaction with the metallic precursor during catalyst preparation [221]. In order to increase their hydrophilicity *via* the introduction of oxygen-containing groups (hydroxyl, carbonyl, and predominantly carboxyl), and to create reactive structural defects, the functionalization by wet chemical oxidation with mineral acids is generally used. Acid treatment can also successfully remove ashes and inorganic compounds in char or activated carbon supports [233], and metallic impurities in CNT [234]. In addition, acid treatment also removes amorphous carbon and breaks CNT into shorter subsections [20]. The surface oxygen groups and defects introduced after this treatment allow anchoring of the Co precursor/particles on the surface of the support and contribute to high metal dispersion [20,209]. However, for CNT_{ox}, a significant amount of the functional groups decomposes during catalyst preparation and activation stages, and only a quarter of the initial oxygen remains on the support surface by the time the FTS starts [235]. The functionalization of CNT which is often performed with nitric acid, but also with H_2O_2, generally result in a narrow Co particle size distribution and a confinement in the inner cavity of the tubes (Figure 32) [63,121,236]. Indeed, Co particles were detected solely outside pristine CNT after an impregnation process [236], because internal channels of pristine CNT were closed, consequently the Co particles could not penetrate inside CNT [236]. Chernyak *et al.* [96] compared Co-catalysts supported on untreated and CNT_{ox} in terms of Co particles size, and FTS activity and selectivity. CNT_{ox} had higher specific surface area, higher oxygen content and larger number of surface defects compared to untreated CNT. Thus, Co/CNT_{ox} showed smaller Co mean particle size (d_{Co} = 4 nm) than that of Co/CNT (d_{Co} = 8 nm). Also, Co particle size distribution was narrower on CNT_{ox} than on untreated CNT [96]. In FTS (T = 190 °C, P = 1 bar, H_2/CO = 2, GHSV = 2200 mL g^{-1} h^{-1}), Co/CNT_{ox} exhibited higher CO conversion and S_{C5+} than Co/CNT. This was attributed to the increase in Co dispersion, the encapsulation of Co inside CNT_{ox} channels and the cutting of CNT_{ox}, which are known to enhance internal mass transfer for reactants and products [20,96]. Additionally, it is known that Co confinement inside CNT_{ox} channel improves reducibility of catalyst and enhances FTS performances [173].

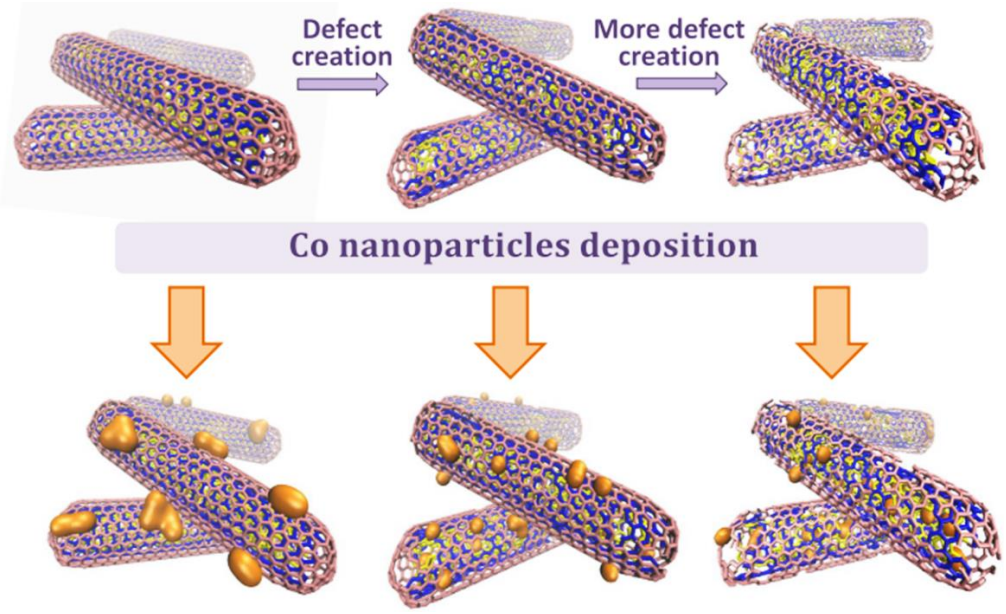

Figure 32. Co particle deposition inside or outside multi-walled CNT *via* support functionalization. Reprinted with permission from Ref [236]. Copyright 2018 Elsevier.

The density of the functional groups on the carbon support after acid treatment not only depends on the type of carbon support but also on the oxidation conditions such as acid concentration, treatment time, and treatment temperature. These parameters can have a significant impact on the FTS performance of the catalyst in terms of activity, selectivity, and stability. Below the impact of these parameters for the preparation of the functionalized Co/C_{ox} catalysts for FTS is presented.

3.3.1.1 Influence of HNO_3 acid concentration

Vosoughi *et al.* [127] investigated the functionalization of pristine CNT with different HNO_3 concentrations, and its impact on textural properties, metal dispersion, crystallite size, defect generation, and reducibility of 15%Co/CNT_{ox}. After treating pristine CNT with different HNO_3 concentrations (35, 50, and 70 wt. %), 15%Co/CNT_{ox} catalysts were prepared by IWI. The surface area and I_D/I_G ratio of CNT_{ox} increased with the nitric acid concentration (Figure 33a). At the same time the Co particle size decreased when the nitric acid concentration increased (Figure 33a). The differences observed in I_D/I_G ratio and Co particle size were attributed to the effect of tube fragmentation, surface defects, and opening of tube tips during the acid treatment, which favor a decreasing in the Co particle size [127]. The 15%Co/CNT_{ox}-70 catalyst, which was prepared on the support treated with 70wt.% HNO_3 solution, presented higher cobalt dispersion (20%) and higher reduction degree than 15%Co/CNT_{ox}-35, which was prepared on the support treated with 35wt.% HNO_3 solution. This was ascribed to the uniform distribution of cobalt oxide particles, which resulted from the high density of defective sites on CNT_{ox}-70 support [127,237]. In FTS (T = 220 °C, P = 2 bar, H_2/CO = 2, and GHSV = 3000 mL g^{-1} h^{-1}), the 15%Co/CNT_{ox}-70 catalyst showed the best CO conversion (30.1 %), the lowest chain growth probabilities (α equal to 0.75), but the lowest S_{C5+} (81.2%), and the highest S_{CH4} (9.5%) (Figure 33b, c). The best CO conversion of this catalyst was attributed to its highest cobalt dispersion and reducibility. Its lowest S_{C5+} can be due to enhancement of the hydrogen spillover after treatment with strong acid concentrations [237]. In another work conducted by

Yang *et al.* [107] on the oxidizing pretreatment mediated auto-reduction behavior of cobalt particles, it was reported that on ordered mesoporous carbon, the average Co particle size gradually decreased (from 25.3 nm to 12.9 nm) by increasing the nitric acid concentration during support functionalization. Consequently, the auto-reduction of cobalt oxide on the carbon supports was improved, which allowed improving catalytic activity.

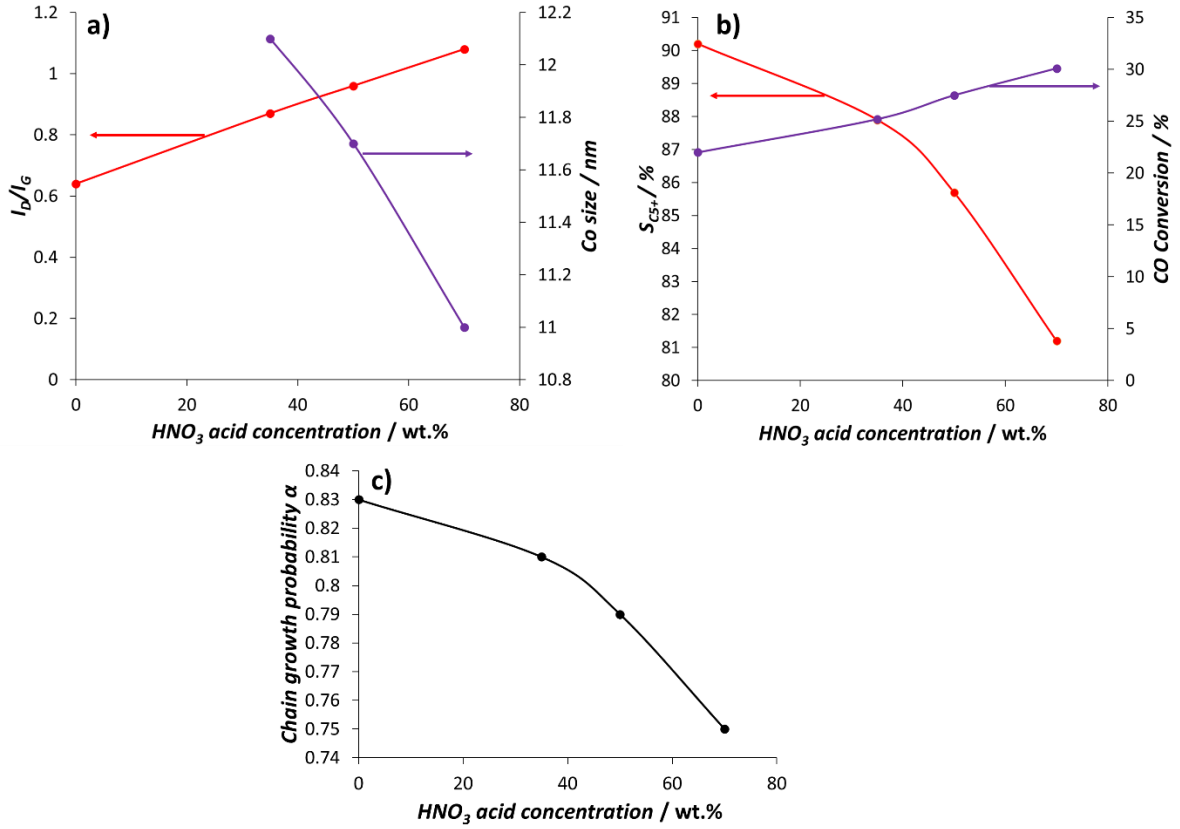

Figure 33. Influence of HNO_3 acid concentration on the Co/CNT_{ox} properties of catalysts and FTS performances. a) influence of HNO_3 acid concentration on the I_D/I_G ratio and Co particle sizes ; b) influence of HNO_3 acid concentration on CO conversion and S_{C5+} (T = 220°C, P = 20 bar, H_2/CO = 2 ; GHSV = 3000 mL g^{-1} h^{-1}) ; and c) influence of HNO_3 acid concentration on the chain growth probability α obtained at the same FTS conditions [127].

3.3.1.2 Influence of HNO_3 treatment temperature

Trépanier *et al.* [128] studied Co catalysts supported on untreated CNT, and oxidized CNT with concentrated HNO_3 at 25 °C (cold oxidation, CNT_{ox}-25) and 100 °C (hot oxidation, CNT_{ox}-100). The I_D/I_G ratio increased with HNO_3 treatment and upon increasing treatment temperature (Figure 34a).This can be explained by the fact that an increase in temperature during the HNO_3 treatment increases the density of functional groups and provokes a higher number defects on CNT. As a consequence of the number of nucleation sites, the Co particle size decreased with an increase of the HNO_3 treatment temperature as follows: Co/CNT > Co/CNT_{ox}-25 > Co/CNT_{ox}-100 (Figure 34a) [128]. The reducibility of the catalysts increased by 10 and 50 % by cold and hot oxidation, respectively, as compared to untreated CNT (Figure 34b). Most of the cobalt particles were homogenously distributed inside the tubes of treated CNT supports [128]. Consequently, in FTS (T = 220 °C, P = 20 bar, H_2/CO = 2, GHSV = 3600 mL g^{-1} h^{-1}), the activity of the catalysts prepared on treated supports increased by 36 and 114% by cold and hot oxidation, respectively, in comparison to the catalyst prepared on the untreated CNT support (Figure 34b). In addition, the CO conversion for Co catalyst supported on untreated

CNT drops rapidly from 37.2% to 22% (41% of loss) during 48h, while for Co/CNT_{ox}-100 catalyst was about 8%. This means that functional groups contribute to stabilize the Co particles during FTS. On the other hand, the S_{C5+} decreased and selectivity in CH_4 increased when the HNO_3 treatment temperature increase from 0 to 100 °C (Figure 34c). This was attributed to the acidic functional groups, which favor the occurrence of the H-spillover and enhance the termination reaction to paraffin [128,139].

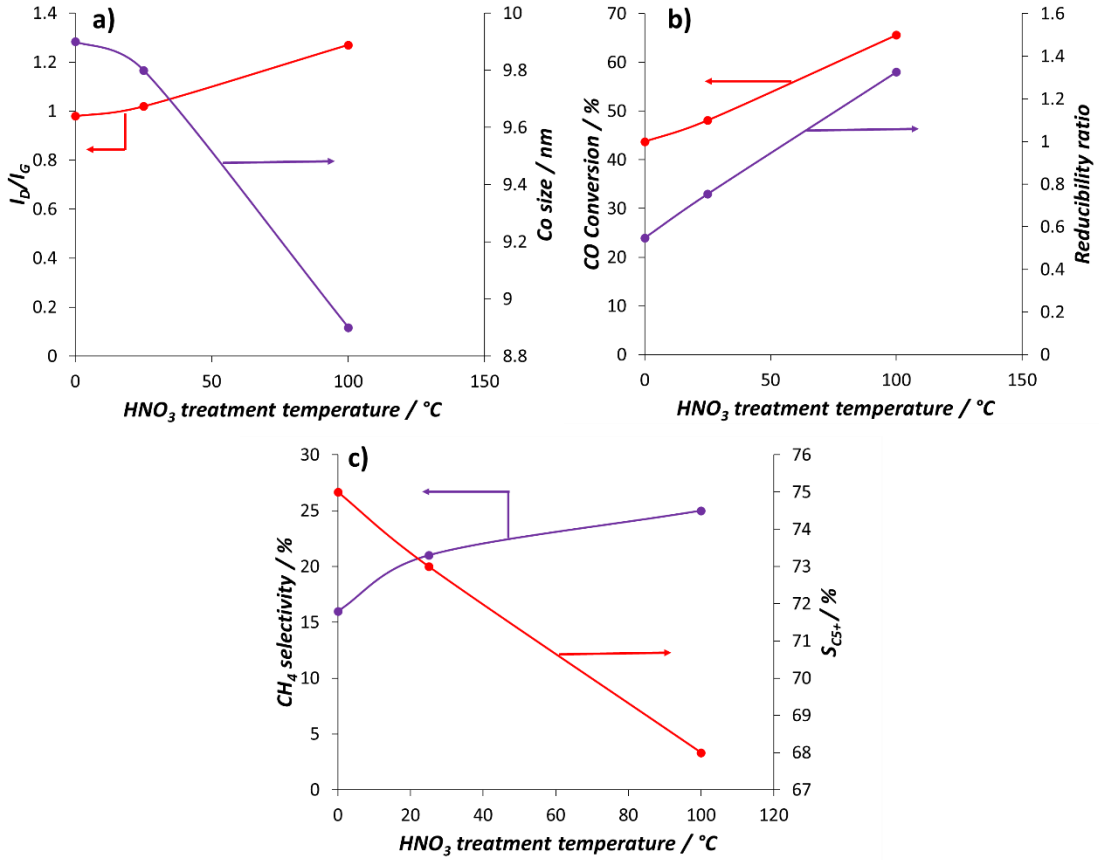

Figure 34. Influence of HNO_3 treatment temperature on the Co/CNT_{ox} properties of catalysts and FTS performances. a) influence of the HNO_3 treatment temperature on the I_D/I_G ratio and Co particle sizes ; b) influence of HNO_3 treatment temperature on the reducibility ratio and CO conversion (T = 220°C, P = 20 bar, H_2/CO = 2 ; GHSV = 3600 mL g^{-1} h^{-1}) ; and c) influence of HNO_3 treatment temperature on the CH_4 selectivity and S_{C5+} obtained at the same FTS conditions [128].

3.3.1.3 Influence of HNO_3 treatment duration

The Figure 35a,b and c are related to the work carried out by Chernyak et *al*. [96] on the influence of HNO_3 treatment time on the FTS performances of the Co catalysts supported on oxidized CNT_{ox} in comparison with Co catalysts supported on untreated CNT. Five catalysts were prepared by IWI using as a support CNT treated during different times with HNO_3 acid and the resulting catalysts were labelled Co/CNT (untreated CNT), Co/CNT_{ox}-1 (1h treatment), Co/CNT_{ox}-3 (3 h treatment), Co/CNT_{ox}-9 (9h treatment), and Co/CNT_{ox}-15 (15h treatment).The defects and oxygen content increased with oxidation time and stabilized from 9h on (Figure 35a). This shows that longer oxidation times increase simultaneously the degradation, fragmentation, and the density of functional groups on the CNT_{ox} [96]. The Co particle size

decreased as follows: Co/CNT > Co/CNT$_{ox}$-1 > Co/CNT$_{ox}$-3 = Co/CNT$_{ox}$-9 > Co/CNT$_{ox}$-15 (Figure 35a). This decrease in Co particle size was due to the effect of functional groups and defects present on the CNT surface. Interestingly, the Co particle sizes were close enough for Co/CNT$_{ox}$-3, Co/CNT$_{ox}$-9, and Co/CNT$_{ox}$-15 catalysts because the number of defects and the density of functional groups vary very little between 3 and 15 h. This causes a slight variation in the size of the Co particles. Figure 35b shows the influence of treatment time of the CO conversion and Co sintering parameter during FTS. CO conversion increased with treatment time and a decrease was observed from 9h to 15h. This was attributed to the increase in Co dispersion and confinement of Co inside CNT channels [96]. Furthermore, the decrease of conversion observed between 9 and 15h was due to the damage of the CNT during HNO_3 treatment. The Co sintering parameter decreased when treatment time increased up to 9h and then increased (Figure 35b). This means that the functional groups and defects stabilized the Co particles during FTS. In addition, the Co sintering was more important for Co/CNT$_{ox}$-15 catalyst than Co/CNT$_{ox}$-3 and Co/CNT$_{ox}$-9 catalysts. This was attributed to the strong degradation of CNT during long acid treatment which leads to the loss of specific surface area and to aggregation of Co particles [96]. The S_{C5+} decreased and CH_4 selectivity increased up to 3h and then became constant (Figure 35c).

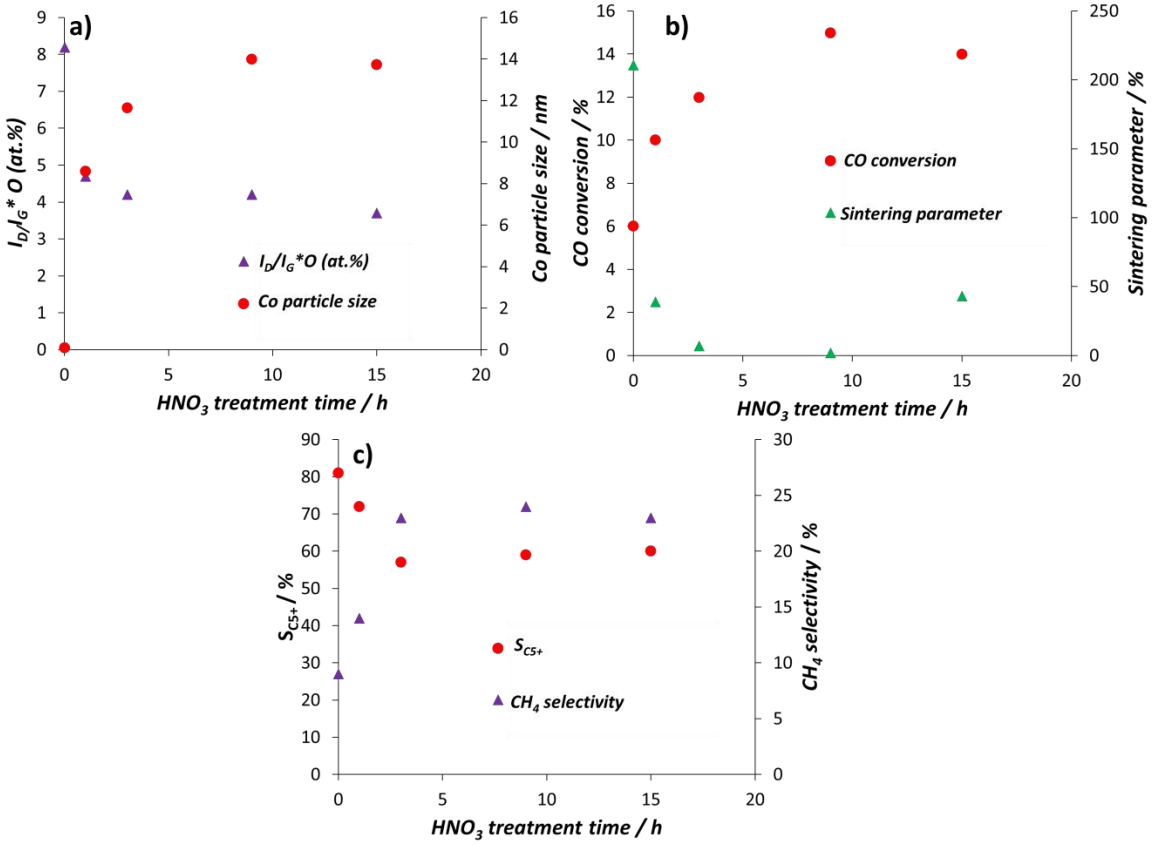

Figure 35. Influence of HNO_3 treatment time on the Co/CNT$_{ox}$ properties of catalysts and FTS performances. a) influence of the HNO_3 treatment time on the I_D/I_G*O (at.%) and on the Co particle size; b) influence of HNO_3 treatment time on the CO conversion and sintering parameter (calculated based on Co particle size before and after test) , and c) influence of HNO_3 treatment time on the CH_4 selectivity and S_{C5+} (T = 190 °C, P = 1 bar, H_2/CO = 2 , GHSV = 2200 mL g^{-1} h^{-1}) [96].

The decreased in S_{C5+} with treatment time could be attributed to the H-spillover effect, which inhibits the growth of long-chain hydrocarbons and favors termination reactions.

However, other studies reported that acid treatment of the carbon supports led to a negative impact on the FTS activity. Van Deelen *et al.* [154] compared cobalt catalysts prepared by the colloidal approach on untreated CNT and on CNT_{ox} treated by concentrated HNO_3 at 80°C. During TPR (heating to 800 °C under 5%H_2/Ar), the cobalt oxide particles on CNT were completely reduced into metallic cobalt, while only 46% of cobalt oxide particles could be reduced on CNT_{ox}. This was explained by strong MSI in the case of the CNT_{ox} support. Consequently, Co/CNT_{ox} showed lower FTS activity (TOF 35% less) than Co/CNT in FTS under the same conditions (T = 220 °C, P = 20 bar, H_2/CO = 2, GHSV = 5950-8900 mL g^{-1} h^{-1}). Similar results were obtained by Eschemann *et al*. [106] who compared the catalytic performances of cobalt catalysts (9wt.%Co) prepared on pristine CNT and CNT_{ox} supports treated by HNO_3. Using cobalt nitrate in ethanol and IWI method, the fresh catalysts presented similar particle size (~ 4 nm) as well as similar degree of reduction. In FTS (T = 220 °C, P = 20 bar, H_2/CO = 2, GHSV = 2000 mL g^{-1} h^{-1}), the Co/CNT catalyst outperformed the Co/CNT_{ox} catalysts in terms of both activity and S_{C5+}. This was explained by the presence of *hcp*-Co on the untreated CNT support surface, which was not the case for CNT_{ox}. However, Co/CNT_{ox} catalysts showed better stability than Co/CNT [106]. The effect of functional groups on FTS selectivity was studied by Chernyak *et al*. [235] over CNT supported cobalt catalysts. For that, WI method was used to prepare 15%Co/CNT (pristine CNT) and 15%Co/CNT_{ox} catalysts. In FTS (T = 190 °C, P = 1 bar, GHSV = 2000 mL g^{-1} h^{-1}), 15%Co/CNT showed significantly higher S_{C5+} (ca. 80.5%) than that of 15%Co/CNT_{ox} (ca.59.3%). This was ascribed to the Co particle size effect, which is larger over 15%Co/CNT (d_{Co} = 26.5 nm) in comparison to 15%Co/CNT_{ox} (d_{Co} = 3.6 nm). In fact, dynamic vapor sorption experiments using water and hexane as polar and non-polar sensor molecules evidenced only a negligible effect of the functional groups of the supports on their adsorption properties [235].

Based on the results presented above it appears that the effect of the treatment time on the FTS performance of the catalyst is less important as compared to the acid concentration and acid treatment temperature (Figure 33, 34 and 35), since the change in HNO_3 concentration or treatment temperature causes a drastic change in catalyst performance during FTS. Acid treatment leads to an increase of the number of functional groups and defect sites on CNT support, consequently, enhances Co dispersion, reducibility, stability, and confinement of Co inside CNT_{ox}, which are beneficial for improving the catalytic activity of Co catalyst supported on CNT_{ox} as compared to Co/CNT catalysts. However, the S_{C5+} decreases with oxygen content and defects *via* hydrogen spillover mechanism. To improve at the same time activity and S_{C5+} on the Co/CNT_{ox}, it is important to control the density of functional groups and the number of defects during acid treatment. In order to suppress hydrogen spillover on the Co/CNT_{ox} catalyst, *hcp*-Co on the untreated CNT support showed better activity and S_{C5+} as compared to Co/CNT_{ox}. The major challenge here is to prepare the Co/CNT catalysts presenting only *hcp*-Co phase.

3.3.2 Surface modification of carbon by nitrogen-doping

In order to improve Co dispersion on carbon supports, recent studies evidenced that the introduction of nitrogen functional groups on/in the carbon materials can alter the electronic structure and thus improve Co dispersion [20,131,238]. More specifically, this doping: (i) increases the local basicity and/or the local electron density of the carbon support; (ii) modifies the nucleation and growth kinetics during metal particle deposition, favoring the formation of small particles and therefore increases Co dispersion; (iii) increases the MSI, which can lead to improved catalyst stability during the reaction, and (iv) modifies the electronic structure of catalyst particles and can consequently enhance the FTS performances [20,160,239–241]. The influence of nitrogen functional groups on the physicochemical properties of Co/C

catalysts was studied by Fu *et al.* [131] The FTS activity and the S_{C5+} of cobalt catalysts prepared on N-doped oxidized CNT (Co/N-CNT_{ox}) were compared with those prepared on undoped oxidized CNT (Co/CNT_{ox}). After HNO_3 treatment, the bamboo-like structure of the N-CNT disappeared, and defect density seemed to be increased on the surface of these supports. TEM analyses revealed that Co particles in Co/N-CNT_{ox} (d_{Co} = 5.4 nm) were distributed more uniformly than those in Co/CNT_{ox} (d_{Co} = 16.2 nm). The presence of N-functional groups contributed to the increase of surface defects density, and to the hydrophilicity and wettability of the N-CNT_{ox} support. This facilitated the access of solvated and charged ions onto the N-CNT surface, and thus led to an increase of Co dispersion. Additionally, most of Co particles in Co/N-CNT_{ox} were located inside the cavities of N-CNT_{ox} supports. The FTS results (T = 230 °C, P = 20 bar, H_2/CO = 2, WHSV = 6750 mL g^{-1} h^{-1}) showed that Co/N-CNT_{ox} exhibited higher CO conversion (74.3 %) and slightly-lower S_{C5+} (S_{C5+} = 80.0%) than those obtained with Co/CNT_{ox} (CO% = 56.6 and S_{C5+} = 83.3 %). These results are ascribed to the Co particle size effect. The same group reported in another study that a N-CNT_{ox} support treated by HNO_3 acid led to smaller Co particles than untreated N-CNT [20]. However, it was also reported that increasing acid treatment time could increase Co particle size and decrease cobalt reducibility, due to the high density of functional groups [20]. Fraga et *al.* [242] demonstrated for carbon supported Pt catalysts that an increase in the oxygen content provokes an increase in the surface negative charge and a decrease in the number of initial nuclei, which induces a decreased in the Pt dispersion. A similar trend was found by Li et *al.* [243] for the preparation of activated carbon supported palladium catalysts. In FTS (T = 230 °C, P = 20 bar, H_2/CO = 2, GHSV = 7500 mL g^{-1} h^{-1}), the Co catalyst prepared on acid treated N-CNT_{ox} was more active but less selective to C_{5+} than the Co catalyst prepared on untreated N-CNT. This was associated to the confinement effect of Co particles, which is favored by the acid treatment of N-CNT_{ox} support [244].

The deactivation of cobalt-based catalysts is a challenging problem in FTS. Tuning catalyst structure can improve catalyst stability. Taghavi *et al.* [155] studied the effects of nitrogen functional groups on N-doped graphene nanosheets (N-GNS) = on the activity, selectivity and stability of Co/N-GNS in FTS using a fixed-bed microreactor. An increase of sp^3 defect sites was observed by Raman spectroscopy, after nitrogen doping. Furthermore, the Co particles were well-dispersed on N-GNS surface with a size within the 4-11 nm range, while a broader particle size distribution was observed for Co/GNS (3-15 nm). In addition, anchoring or defect sites created by the presence of nitrogen functional groups reinforce MSI [240], and prevent Co particle agglomeration and sintering. In FTS (T = 220 °C, P = 18 bar, H_2/CO = 2, GHSV = 5143 mL g^{-1} h^{-1}), the Co/N-GNS catalyst exhibited better activity, stability and lower particle growth rate than Co/GNS, which was explained by the improvement of Co species reducibility by nitrogen functional groups [155].

During the N-doping of carbon materials, various types of N-containing groups can be created such as pyridinic-N, pyrrolic-N and graphitic-N. It was reported that the electronic transfer between N-containing groups and the surface of metallic particles may affect the activity and selectivity in FTS [245]. Cheng *et al.* [245] studied the influence of the type of N-containing groups over carbon spheres (N-CS) in FTS. N-CS materials were obtained *via* the carbonization of polydopamine nanospheres at different temperatures (500, 600, 700 and 800 °C) under a N_2 flow. Co/N-CS catalysts were prepared with a Co loading of 3 wt.% from cobalt acetate by ultrasonically-assisted IWI. The authors found that the N content in N-CS supports, obtained by XPS, decreased from 9.5 to 6.7 wt.% with the increase of the carbonization temperature from 500 to 800 °C. The I_D/I_G values decreased from 1.03 for N-CS-500 to 0.80 for N-CS-800, which further indicated that the graphitization degree of the N-CS increased with the carbonization temperature. The schematic illustration of the N-doping is shown in Figure 36a. The authors also found from elemental analyses that the N-pyrrolic (Figure 36b) was

higher in N-CS-500 (6.2 %) and Co/N-CS-500 (4.0 %) in comparison to the others samples. Interestingly, cobalt dispersion in the reduced Co/N-CS catalysts decreased from 14.8 to 10.1% with the increase of carbonization temperature from 500 to 800 °C. This was explained by the low density of N-pyrrolic groups at high carbonization temperature and knowing that N-pyrrolic groups are more favorable for Co dispersion than N-pyridinic groups and N-graphitic groups. As evidenced by CO-TPD, the amount of desorbed CO increased with the increase of N-pyrrolic groups' content. This suggests that N-pyrrolic groups are more favorable to generate active sites for CO adsorption than N-pyridinic and N-graphitic groups (Figure 36c).Furthermore, when the adsorbed CO dissociated, it generates more CH_2 species to stimulate chain growth [245]. Consequently, in FTS (T = 220 °C, P = 20 bar, H_2/CO = 2), increasing N-pyrrolic groups' content in Co/N-CS catalysts allowed enhancing the catalytic activity and the S_{C5+} (Figure 36d).

In another study, it was also shown that on N-doped graphene nanoflakes (N-GNF), the resistance to Co sintering during catalyst reduction was lower for the support predominantly containing amide groups localized at the edges of graphene layers than for the ones containing pyridones and pyridines/pyrrols/graphitic nitrogen groups [231].It was reported that the pyridine-like sites near carbon vacancies affect the electronic state of cobalt and contribute to the auto-reduction of cobalt oxide of Co_3O_4/N-CNF catalysts used for the oxidation of carbon monoxide [108,160,246]. The FTS catalytic tests (T = 240 °C, P = 20 bar,H_2/CO= 2, GHSV = 6000 mL g^{-1} h^{-1}) showed that the catalysts prepared on oxidized GNF and N-GNF had the highest activity, as a result of their highest contents of functional groups (O or N), leading to the best Co dispersion and stabilization. However, these catalysts showed low S_{C5+}, which was assigned to the narrow pore size < 1 nm in the pore structure of oxidized GNF and N-GNF, which hindered CO diffusion and increased H_2 diffusion, consequently, limiting the formation of long-chain hydrocarbons [231].

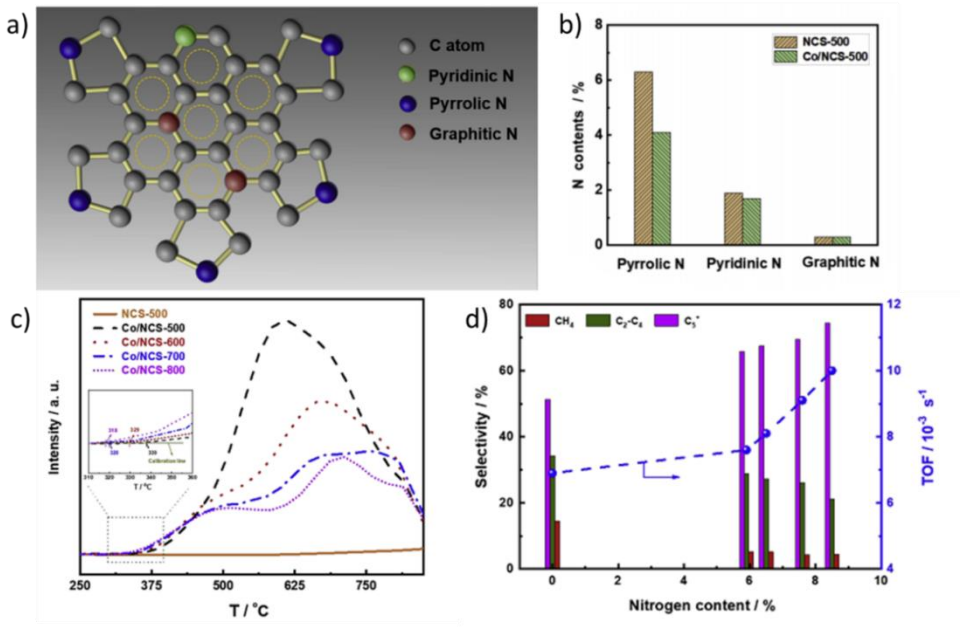

Figure 36. a) Schematic illustration of the N dopants; b) N dopants molar content in the N-CS supports and Co/N-CS-500 catalysts; c) CO-TPD/MS profiles of the reduced Co/N-CS catalysts and the N-CS-500 support; and d) catalytic performances of the catalysts according to the N contents. Reprinted with permission from Ref [245]. Copyright 2019 Elsevier.

The combination of functional groups such as O or N in the carbon structure decreases the MSI, enhances the Co reducibility and dispersion, and affords good stability to the Co particles [231]. However, the excess of oxygen groups on the N-doped oxidized carbon support

improves the CH_4 selectivity *via* the occurrence of the H-spillover [231]. Two strategies can be used in order to improve the S_{C5+}, while keeping a reasonable catalytic activity during FTS. First, doping the carbon structure only with N groups especially N-pyrrolic groups, which are known to generate more active sites, consequently, enhances activity and S_{C5+} [245]. The second strategy consists in controlling the amount of oxygen groups after acid treatment *via* the de-functionalization of the surface of carbon support by thermal treatment. The main advantages of this strategy are that it makes it possible to control the Co particle size and the MSI of the catalyst both by reducing the density of functional groups on the carbon support and by extending the degree of graphitization, which enhance the S_{C5+}. The latter will be discussed in detail in the following section.

3.3.3 Surface mofication of carbon by thermal treatment

The surface properties of carbon materials can be modified by thermal treatment which can, in turn, impact Co dispersion and reducibility. Akbarzadeh *et al.* [126,247] reported that thermal treatment of CNT following an acid refluxing step could enhance Co dispersion and avoid sintering and deactivation of active sites during the FTS. For CNT_{ox} support, the thermal pre-treatment at high temperature led to surface de-functionalization by decomposition of surface oxygen groups (-C=O, -COOH, -OH) as shown on Figure 37. The Co particles were thus encapsulated in CNT_{ox} channels and this tendency was increased by increasing the temperature of the thermal pretreatment [126]. About 70% of cobalt oxide particles were deposited in the inner walls of CNT, which were pretreated at 900 °C, compared to only 10% in the case of untreated CNT_{ox} [126]. The catalytic performances were evaluated with Co catalysts prepared with CNT_{ox}, which were thermally pretreated at different temperatures. CO conversion and S_{CH4} reached 16.4% and 18.6%, respectively over the catalyst prepared on the untreated CNT_{ox}. For the catalyst prepared on the pretreated supports, CO conversion increased up to 58.7%, and S_{CH4} decreased to 9.5% when the pretreatment temperature increased from 600 to 900°C[126]. In another study, Xing et *al*. [226] prepared 10%Co/CNT catalysts by IWI method using open CNT_{ox}, and the same CNT thermally treated Co/CNT-x (x = 400, 650, 900 °C). The resulting catalysts presented an average particle size around 4 nm. However, in the case of Co/CNT-x, the Co particles were more confined in the CNT channel as compared to the CNT_{ox}. The highest CO conversion (92.8%) and selectivity in CH_4 (23.5%) were achieved with Co/CNT_{ox} catalyst (without thermal treatment of CNT after HNO_3 functionalization). This result can be attributed to the hydrogen spillover induced by the higher concentration of oxygen-containing groups formed on the surface of CNT_{ox} [139], consequently enhanced CO conversion and selectivity in CH_4 were obtained compared with that of Co/CNT-x catalysts. Thus, the thermal pretreatment following the acid treatment of CNT is a promising technique for carbon surface modification. It contributes to the control of MSI and enhances the reducibility of cobalt oxide particles thanks to confinement effect.

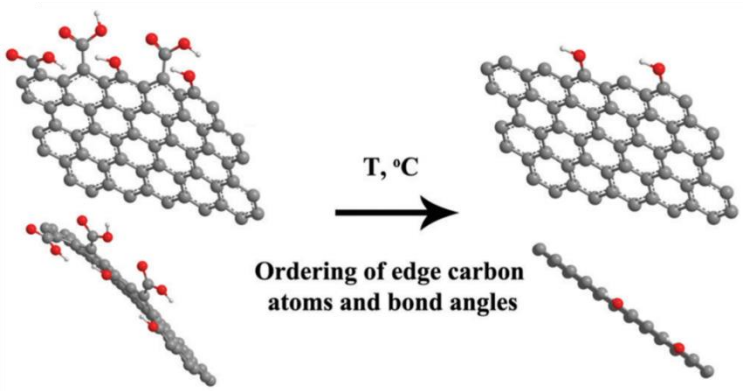

Figure 37. Transformation of CNT edges after thermal annealing at 370 °C. Reproduced by permission from Ref [248]. Copyright 2017 Royal Society of Chemistry.

Zhao *et al.* [216] studied the influence of the graphitization degree of mesoporous carbon (MC) on the structure and performance of cobalt catalysts. MC supports with different graphitization degrees were prepared *via* the pyrolysis of furfuryl alcohol with SBA-16 (mesoporous silica) at different temperature (800, 1100 and 1300 °C). Then, Co/MC catalysts were prepared with a cobalt loading of 20 wt% *via* IWI. Raman analyses revealed that the I_D/I_G ratio decreased with the increase of carbonization temperature, indicating an increase of graphitization degree. The average Co particle size for all samples determined by TEM was almost the same (d_{Co} ≈ 6 nm). The reducibility of catalysts increased with the extent of graphitization and the optimal value was achieved for Co/MC-1300. This suggested that the graphitization of the support decreases MSI, and consequently enhances Co reducibility. In FTS (T = 220 °C, P = 10 bar, H_2/CO = 2 , GHSV = 2300 mL g^{-1} h^{-1}), Co/MC-1300 catalyst showed a significant increases of CO conversion (49.7%), which is about 2.5 times that of Co/MC-800. This result was explained by the enhancement of Co reducibility when increasing the pyrolysis temperature. The S_{C5+} followed a similar trend, which was attributed to the average pore size following the next trend: Co/MC-1300 > Co/MC-1100 > Co/MC-800, and the graphitization degree. Both increased with the carbonization temperature of the support, which favor mass transfer of syngas and products [216]. Other studies have confirmed that the carbon support crystallinity clearly influenced the MSI, the metal reducibility, and the metal particle size [212]. Generally, the carbon support crystallinity can be controlled during the catalytic growth of the support, by selecting appropriate growth reaction conditions, *i.e*. temperature, catalytic metal, type of carbon source, and carrier gas [212]. Diaz *et al.* [212] studied the impact of the CNF support crystallinity in FTS. Different CNF were prepared *via* the catalytic decomposition of ethylene over a Ni/SiO_2 catalyst at 750, 600 and 450 °C, and the resulting supports were named CNF-750, CNF-600 and CNF-450, respectively. Cobalt catalysts were then prepared by IWI, with a metal loading of *ca.*13 wt.%. XRD analysis showed that the graphitic character (L_c and d_{002}) of the supports, which is related to the interlayer spacing (d_{002}), and the average crystalline size (L_c) of graphene sheets, increased in the following order: CNF-450 (L_c = 9 nm) < CNF-600 (L_c = 11.7 nm) < CNF-750 (L_c = 15.8 nm). Thus, increasing the support synthesis temperature allowed increasing the graphitization degree. Consequently, the average Co particle size increased with support crystallinity as follows: CNF-450 (13.9 nm) < CNF-600 (32.8 nm) < CNF-750 (36.4 nm). The opposite behavior was observed with the support pore radius, which decreased with synthesis temperature. In FTS (T = 250 °C, P = 20 bar, $H_2/CO/N_2$ = 6/3/1, GHSV = 3000 mL g^{-1} h^{-1}), the CO conversion and the catalyst stability also increased with the increase of the support crystallinity, because crystallinity decreases the MSI, which leads to improved Co reducibility[216]. In addition, Co/CNF-450 showed intense Co particle sintering, as a consequence of the low crystallinity of the CNF-450 support. These studies evidenced

that the properties of carbon supported cobalt catalysts can be tuned by controlling the crystallinity/graphitization degree of the carbon supports.

3.3.4 Surface modification of oxides with carbon and of carbon supports with oxides

Catalyst reducibility is one of the key factors affecting the FTS. For the metal-supported catalysts, it is well known that the MSI is directly related to the reducibility, particle size, and dispersion of the metal [222]. In FTS, the Co^0 active phase is generally supported on oxides such as SiO_2, Al_2O_3, TiO_2, or MgO [249]. A drawback of these supports is their strong interaction with cobalt, which makes the reduction step difficult. To avoid this, the use of carbon materials as a coating of the oxides' surface is appealing. Indeed, carbon-based materials are relatively stable at high temperature, and are able to weaken the MSI and to increase the specific surface area. This can significantly enhance the catalytic performances in FTS [222,229]. Jiang *et al*. [222] studied MSI regulation by impregnating $Co(NO_3)_2$ on silica coated with different amounts of amorphous carbon. Carbon coating was carried out *via* carbonizing glucose under Ar and the resulting catalysts were named 10%Co/xC-SiO_2 (x = carbon content in wt.%) varying from 0.1 to 1.5. In comparison to the catalyst prepared on the uncoated support (10%Co/SiO_2), 10%Co/xC-SiO_2 catalysts showed smaller Co particle size and higher Co dispersion [222]. The highest Co dispersion was obtained with the catalyst presenting the highest amount of amorphous carbon (10%Co/1.5C-SiO_2). The small Co_3O_4 particle size observed for 10%Co/xC-SiO_2 catalysts was attributed to the small pore size induced by the carbon coating. In addition, MSI between Co^0 and the carbon-coated silica supports decreased by increasing the carbon content. Consequently, a high CO conversion and low S_{C5+} (< 70%) was achieved for 10%Co/1.5C-SiO_2. This high CO conversion can be rationalized by the high reduction degree of this catalyst, while its small particles could explain the low S_{C5+} [222]. Moreover, the selectivity of the Co/xC-SiO_2 catalysts toward light hydrocarbons increased by increasing the carbon content, because the diffusivity of H_2 in micropores of carbon materials is more favored than that of CO [45]. A similar study was conducted by other groups using a series of Co/xC-SiO_2 and CoPt/xC-SiO_2 catalysts, with and without promoter, respectively [230]. The unpromoted and promoted catalysts were prepared by IWI with $Co(NO_3)_2$ and ($Pt(NH_3)_4(NO_3)_2$) as a promoter and the carbon pre-coated silica (5, 10 and 50 wt.% of carbon). Then, the catalysts were calcined in nitrogen and air flow at 450 °C for 4 h. The carbon coating allows producing smaller Co particle size than on the pristine silica. The major enhancement of the catalytic performance observed over catalysts calcined in the air flow was attributed to the small cobalt particle size, and the removal of the carbon layer by the air calcination, since deep encapsulation of cobalt nanoparticles by the carbon layer was pointed as the main reason for low catalytic performances [230].

In another study, hydrothermal carbon-coated TiO_2 was used as a support for FTS [190]. TiO_2 coated by hydrothermal carbon (HTC) layers was first prepared by hydrothermal synthesis. Then, cobalt deposition was performed by the IWI method. It was found that CoO particles were of 8.7 nm on Co/C-TiO_2 and 11.6 nm on Co/TiO_2. This result suggests that the functional groups such as hydroxyls and carboxylates of the HTC surface favored the formation of small CoO particles, and enhanced the dispersion of cobalt species on Co/C-TiO_2 (Figure 38a) [190]. Furthermore, the functional groups on the HTC surface could act as nucleation sites for cobalt oxide crystallization providing optimal nucleation and growth rates. Under FTS reaction conditions (T = 210 °C, P = 10 bar, H_2/CO = 2, GHSV = 2000 mL g^{-1} h^{-1}), the Co/C-TiO_2 catalyst exhibited an activity 2.3 times higher than that of Co/TiO_2 and showed 82.5% selectivity to C_{5+} products (Figure 38b). This was explained assuming that HTC coated on TiO_2 weakened MSI and improved the reducibility of cobalt species. The same group modified the surface of TiO_2

with carbon, alumina, and silica to examine the effect of different surface coating layers on the FTS catalysts [25]. The C-TiO_2 support was prepared *via* hydrothermal method while Al-TiO_2 and Si-TiO_2 were produced by sol-gel method. Then, 15 wt.% of cobalt was loaded on these three supports using the IWI technique. The dispersion of the catalysts followed the order: Co/C-TiO_2 > Co/Al-TiO_2 > Co/TiO_2 > Co/Si-TiO_2. In addition, the Co/C-TiO_2 catalyst exhibited higher reducibility than the other catalysts due to the weaker MSI induced by the presence of HTC layer. In FTS (T = 230 °C, P = 10 bar, H_2/CO = 2, GHSV = 800 mL g^{-1} h^{-1}), the highest CO conversion, CTY, and S_{C5+} was obtained for the Co/C-TiO_2 catalyst. This was attributed to the combination of good dispersion and reducibility of the active phase, which led to improve the FTS performances. It was also found that, the CO conversion was 1.5 times higher over Co/Al-TiO_2 and Co/Si-TiO_2 as compared to Co/TiO_2 catalyst. This was due to the higher dispersion of Co on Co/Al-TiO_2 and higher Co reducibility on Co/Si-TiO_2 catalyst [25].

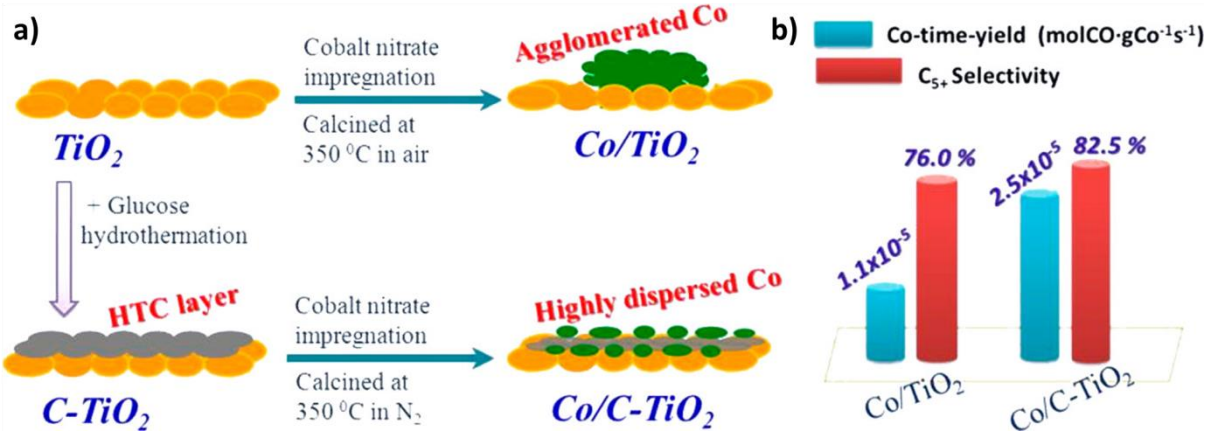

Figure 38. The HTC layers on TiO_2 with enrichment of functional groups (e.g. COOH and COH) that are beneficial for cobalt dispersion. Reprinted with permission from Ref [190]. Copyright 2018 American Chemical Society.

In order to lower the reduction temperature of cobalt species, cobalt catalysts supported on metal oxides are usually promoted by noble metals such as Pt, Ru, and Re [227]. However, noble metals have high cost and to overcome this problem, other promoters could be used. Park *et al.* [227] prepared g-C_3N_4-coated alumina support (CN-Al) for cobalt-based FTS catalyst, where g-C_3N_4 layers block the direct interaction between cobalt and alumina and facilitate the reduction of cobalt species into Co particles (see Figure 39a, b). The dispersion and reducibility of cobalt was much improved in the presence of graphitic carbon nitride (g-C_3N_4). The proposed reduction mechanism of cobalt under an inert gas for Co/CN-Al catalysts is shown in Figure 39c. Under FTS conditions (T = 220 °C, P = 20 bar, H_2/CO = 2,), the cobalt time yield (CTY) of Co/CN-Al was 21.84 μmol_{CO} s^{-1} g_{Co}^{-1}, which is two times higher than that of Co/Al_2O_3 catalyst (10.75 μmol_{CO} s^{-1} g_{Co}^{-1}) (Figure 39d). The enhanced activity of Co/CN-Al was explained by the higher reduction degree of Co.

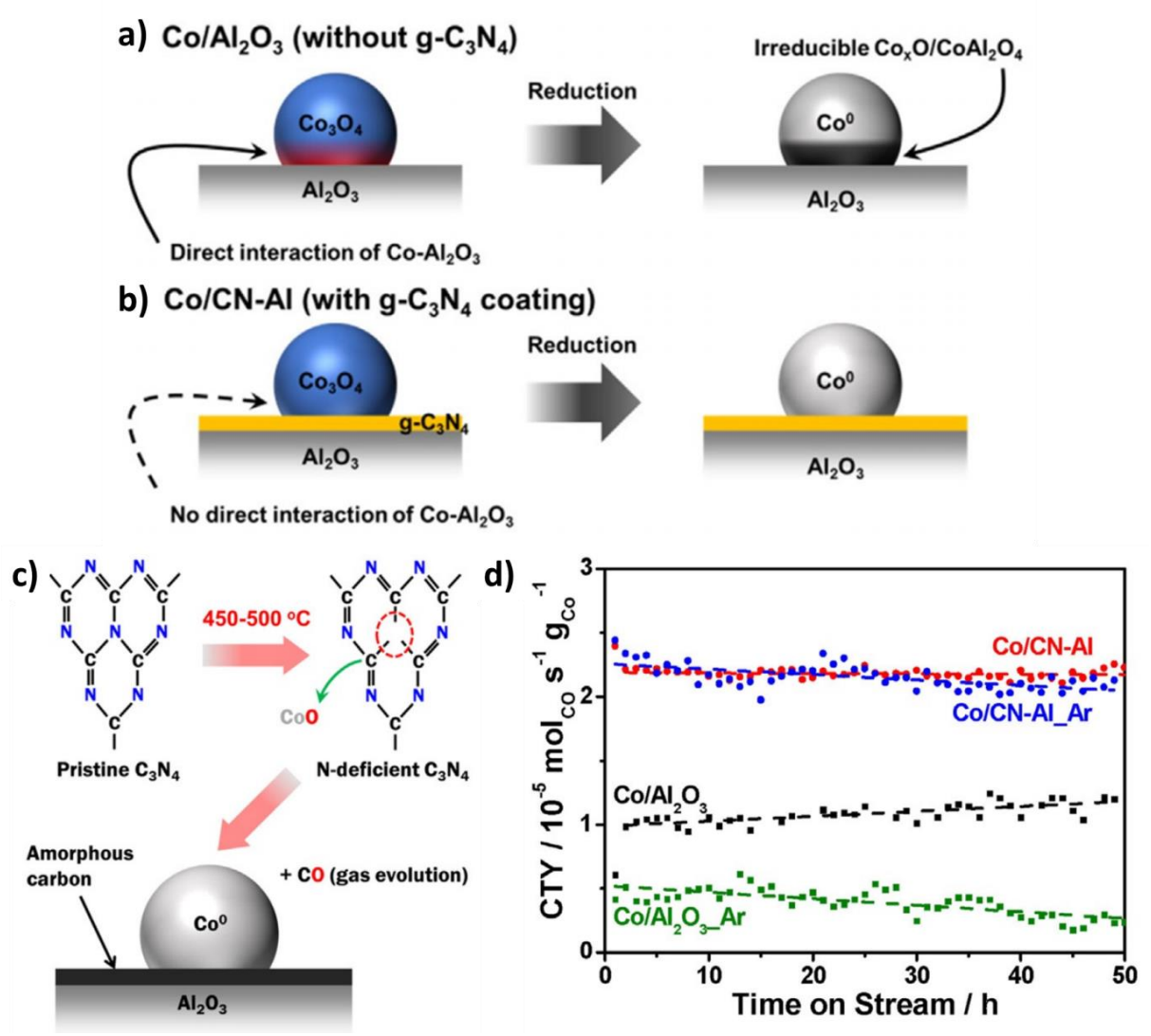

Figure 39. a-b) Effect of the g-C_3N_4-Al_2O_3 support on the reducibility of cobalt species; c) the reduction mechanism of cobalt species under an inert gas flow for Co/CN-Al catalysts; and d) cobalt time yield (CTY, $mol_{CO}\ s^{-1}\ g_{Co}^{-1}$) for the FTS reaction with time on stream. Reaction conditions: 220 °C, 20 bar, $H_2/CO = 2$. Reprinted with permission from Ref [227]. Copyright 2017 John Wiley and Sons.

Developing efficient FTS catalysts *via* strategies that result in stable and optimal cobalt crystalline facets is highly desirable. Thus, a Co@C-SiO_2 catalyst composed of a single Co crystalline core, a coated-carbon layer, and an amorphous silica shell was studied [250] in this context. It was reported that the presence of carbon introduced a moderate MSI, which together with a confinement effect of the silica shell, contributed to protecting and maintaining the optimal Co crystalline facet (10-11) of the Co core [250]. Co@C-SiO_2 and Co@SiO_2 catalysts were prepared by sol-gel method (Figure 40a) [250]. Hexagonal Co_3O_4 nanoplates (p-Co) were first prepared, followed by hydrolysis of tetraethoxysilane (TEOS) on the surface of the PVP-capped p-Co. After pyrolysis at 500 °C under N_2 or calcination in air, Co@C-SiO_2 or Co@SiO_2 were obtained, respectively. Co@C-SiO_2 catalysts maintained a well-defined hexagonal morphology and presented a single crystalline phase dominantly exposing CoO (112) planes after pyrolysis under N_2. For the Co@SiO_2 catalyst, the core was split into many particles (*ca.* 20 nm) with no preference over the facets exposed. The degree of reduction followed the order: Co@SiO_2 (88.8%) < Co@C-SiO_2 (92.5%). The single-crystalline structure (hexagonal Co_3O_4) and high reduction degree of the Co@C-SiO_2 catalyst was assigned to the

presence of carbon, which contributed to reduced MSI and improved reducibility [205,250]. The TOF obtained in FTS (T = 220 °C, P = 20 bar, H_2/CO = 2, GHSV = 1700 mL g_{Co}^{-1} h^{-1}) for the Co@C-SiO_2 catalyst (4.0×10^{-2} s^{-1}) was 10 times higher than that of Co@SiO_2 (0.4×10^{-2} s^{-1}). Additionally, the S_{C5+} was found to be higher in the case of Co@C-SiO_2 catalyst (Figure 40b). This was due to the increase of the reduction degree and to the high amount of bridged-type adsorbed CO on the Co@C-SiO_2 catalyst surface, which is much more active in FTS than the linear-type adsorbed CO [251].

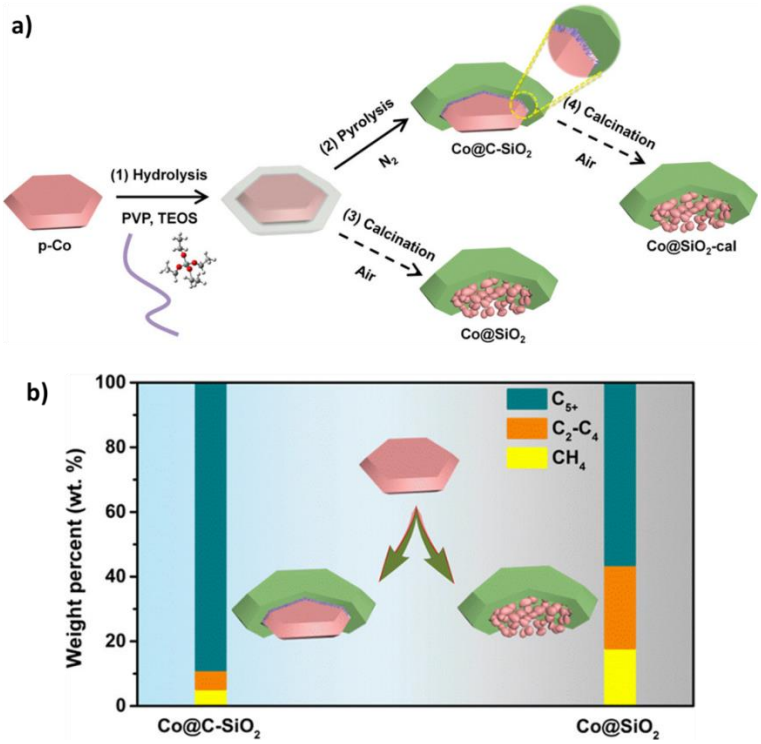

Figure 40. a) (1) TEOS hydrolysis on the surface of p-Co; (2) pyrolysis under nitrogen to form Co@C-SiO_2; (3) calcination in air to form Co@SiO_2; (4) further calcination in air to remove the carbon; and b) comparison of the selectivity of the Co@C-SiO_2 and Co@SiO_2 catalysts. Reprinted with permission from Ref [250]. Copyright 2019 American Chemical Society.

Metal oxide supports generally offer several inherent advantages in FTS such as stability of the Co^0 active phase and narrow pore size distribution, which are known to contribute to the enhancement of the S_{C5+} during CO hydrogenation. However, the strong MSI limits the catalytic performances of oxide supported catalysts. This drawback can be addressed by coating a layer of carbon on the metal-oxide surface with improved catalytic performance. However, oxide coated with high amount of carbon enhances selectivity in CH_4 *via* hydroxyl or carboxylate groups and its small pore size, which favor the enrichment of H_2 at the catalyst center, thus improving the paraffins products. To overcome this problem in some cases, the catalysts properties can be tuned by controlling the amount of carbon coated on the oxides during catalyst preparation. For example, the single-crystal structure with *hcp* phase, which is known to improve both activity and S_{C5+} can grow selectively on the oxide coated with an appropriate amount of carbon. Furthermore, oxides coated with a small amount of carbon are recommended for the improvement of S_{C5+}. The effects of carbon-coated oxides on the catalyst properties and FTS performances are summarized in Table 8.

Table 8. Impact of carbon coating on the physicochemical properties of the catalyst and FTS performance.

Oxide	Carbon material	Catalyst	Effects on catalyst properties and FTS performances	Ref.
SiO_2	AC Graphene Carbon	Co/xC-SiO_2	• Increased BET surface area of SiO_2 • Decreased pore size of SiO_2 • Decreases of the MSI between Co and SiO_2 • Increased Co dispersion and reducibility • Improved CO conversion • Decreased S_{C5+} • Suppressed Co aggregation • Enhanced *hcp-Co* phase	[88,200,222,230,250,252]
SiO_2	Organic molecules	Co/$(CH_3)_3$-SiO_2 Co/COOH-SiO_2	• Increased Co dispersion and reducibility • Improved FTS activity and S_{C5+}	[253–255]
MgO	CNT	Co/CNT-MgO	• Improved S_{C5+} and olefins/paraffins ratio	[78]
Al_2O_3	CNT	Co/CNT-Al_2O_3 Co/C-Al_2O_3	• Enhanced Co dispersion • Modifies the interaction between Co and Al_2O_3 • Increased CO conversion	[78,152,221,227,256,257]
SiO_2	CNT/CF	Co/CNF@CF-SiO_2	• Enhanced thermal conductivity of SiO_2 • Decreased pressure drop • Enhanced CO conversion and S_{C5+} • Improved catalyst stability	[229,258]
TiO_2 Al_2O_3	Pyrolitic carbon CNT	Co/C-TiO_2 Co/TiO_2/CNT- α-Al_2O_3	• Improved Co-active site and reducibility • TiO_2 core enhances the stability of the catalyst • Increased conversion and C5+ hydrocarbon	[190,259]
SiO_2	Pyrolitic carbon	Co/C-Ni/SiO_2	• Mitigates the MSI • Increased FTS activity	[260]

The deactivation of carbon-supported catalysts by thermal Co particle sintering remains a key problem in FTS in fixed-bed reactors (see section 2.6). It generally causes the loss of activity and selectivity toward light hydrocarbons. To overcome this problem, oxides, which offer strong interaction with Co particles [16], can be used to inhibit the thermal sintering of Co particles. Zhu *et al.* [229] developed an *in*-situ sol-gel method to coat a thin layer of SiO_2 onto CNF/CF (carbon felt) surface. The resulting support, CNF/CF@SiO_2 presented several advantages, such as a high specific surface area, low pressure-drop, improved stability, high thermal conductivity, and good mass transfer properties. It was found that the deactivation degree of different catalysts linearly correlated with the Co oxidation potential. Co/CNF/CF@SiO_2 catalyst presented a lower oxidation potential compared to Co/CNF/CF. Consequently, high activity, high S_{C5+} and high stability were obtained with Co/CNF/CF@SiO_2. Furthermore, low pressure drop and excellent thermal conductivity make it attractive for applications in the conversion of biomass, coal, and natural gas to liquids.

The use of oxide supports affords a good stability to the nanoparticles due to the strong MSI, and allows high catalytic performances when noble metals such as Pt or Ru are used as promoters to avoid the formation of mixed compounds. The use of carbon materials is appealing since they offer the advantage of being stable at high temperature under inert atmosphere, do not lead to strong MSI, and have a high surface area, which leads to significantly enhanced activity and selectivity of the catalyst during FTS. In addition, it is not necessary to use noble metals (Pt or Ru) for the reduction of the metal particles when carbon supports are used. The drawbacks of the catalysts supported on carbon supports are the inability to regenerate them in the oxidizing atmosphere (air, oxygen), and their insufficient mechanical strength [230]. A future development and use of hybrid oxide/carbon supports could give the opportunity to combine the advantages of carbon and oxide supports in the same matrix.

3.4 Solvent effect

The solvents used during the catalyst preparation allow not only dissolving the precursor and promoting its contact with the support, but also controlling the final structure of the catalyst. The interaction between the metal precursor present in solution and the support depends on the solvent surface tension, which controls support wettability. The solvents used in conventional impregnation processes have been reported to affect the properties of catalyst in FTS [89,101,106,217]. Thus, Luo *et al*. [217] have demonstrated that a graphene supported cobalt catalyst prepared by IWI in ethanol exhibited higher CO conversion and higher S_{C5+} in FTS (T = 210 °C, P = 25 bar, H_2/CO = 2, GHSV = 500 mL g^{-1} h^{-1}) than a catalyst prepared in water. This is due to the ability of ethanol to suppress aggregation of Co_3O_4, thus increasing the dispersion. A similar study was conducted by Eschemann *et al*. [106] for Co/CNT_{ox} catalysts. Catalysts prepared with water, ethanol and propanol as solvents were compared in terms of cobalt oxide clustering and FT activity. Water led to the formation of larger Co particles compared to organic solvents (Figure 41**a**). Under identical FT conditions (T = 220 °C, P = 20 bar, H_2/CO = 2 v/v, GHSV = 2000 mL g^{-1} h^{-1}), the catalyst prepared by using ethanol as solvent showed the highest initial and final TOF (Figure 41b).

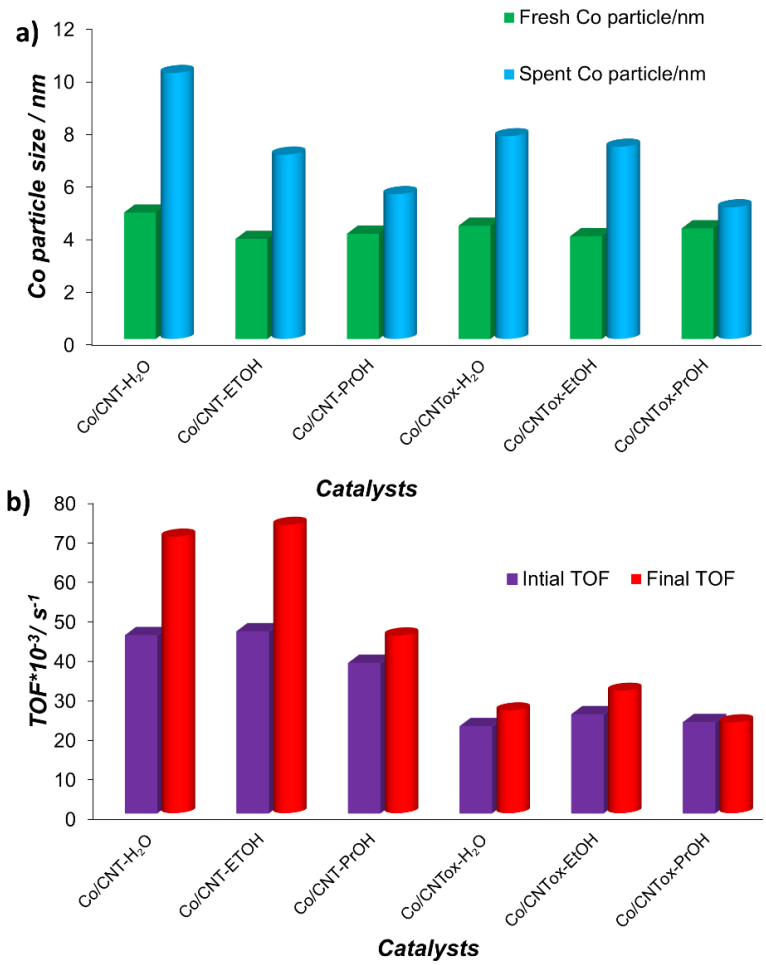

Figure 41. CO particle size and TOF for CNT-supported cobalt catalysts prepared in different solvents, FTS at 20 bar, 220 °C, H_2/CO = 2.0 v/v, GHSV = 2000 h^{-1}. The final TOF and spent Co particle presented here are based on the catalytic performance after 60 h [106].

The trend is the same for cobalt catalysts prepared on untreated CNT and oxidized CNT. These results indicate that the solvent surface tension effect during the drying step has a larger impact than the wetting of the support during the impregnation step [106].

3.5 Effects of cobalt precursors

The decomposition of cobalt precursors is a crucial step in catalyst preparation. A slow decomposition rate favors small Co particle size, high metal dispersion and enhances the catalytic performance in FTS [261]. The nature of the cobalt precursor was found to influence the basicity of the catalysts, the extent of reduction, the metal particle size and distribution on SiC supports [262]. Consequently, different CO conversion, selectivity to S_{C5+}, and chain growth probability during FTS reaction have been reported for different metal precursors [262]. Many Co precursors such as $Co(NO_3)_2$, $Co(CH_3COO)_2$, $CoCl_2$, and $Co(OH)_2$ have been used to prepare Co/C catalysts [262–265]. Bezemer *et al.* [89] and Radstake *et al.* [101] have prepared Co/CNF catalysts with $CoCO_3$ [89], $Co(NO_3)_2$ [89,101] and $Co(CH_3COO)_2$ [89,101], but it is difficult to make a comparison of Co particle size because the catalysts were prepared

with different Co loadings. Xiong et *al*. [91] prepared Co-N/CNT_{ox} and Co-A/CNT_{ox} (15 wt.%) catalysts using cobalt acetate and cobalt nitrate precursors, respectively, *via* the IWI method. Mean Co particle sizes of 3.9 and 4.4 nm were obtained with cobalt nitrate and cobalt acetate precursors, respectively. This effect was attributed to the chemical interactions between the cobalt precursors and the CNT_{ox} support, which probably occurred during precursor decomposition, nucleation and growth of oxide crystallites [91]. In FTS (T = 225 °C, P = 8 bar, H_2/CO = 2, GHSV = 3840 mL g^{-1} h^{-1}), the Co-N/CNT_{ox} catalyst showed slightly higher CO conversion (25.9%) than Co-A/CNT_{ox} (22.6%), because of a higher dispersion of the Co particles in Co-N/CNT_{ox}. However, in another study conducted by Honsho *et al.* [80], Co-based catalysts, prepared on activated carbon and oxidized diamonds as supports from cobalt acetate, were more active than those prepared from cobalt nitrate, which is inconsistent with the findings by Xiong et *al*. [91]. These contradictory results could be related to the nature of the supports used in these studied, which are different from each other. However, the data available in the literature are insufficient to really explain the effect of cobalt precursors in the case of the carbon-supported cobalt catalysts. A summary will be made thereafter on metal oxides (Al_2O_3, TiO_2 and SiO_2) in order to extend our conclusions on the effect of Co precursor in FTS. Fratalocchi *et al.* [266] studied the effect of the cobalt precursor (nitrate or acetate) on the structural and catalytic properties of Co-based catalysts supported on γ-Al_2O_3. In FTS (T= 210 °C, P = 25 bar, H_2/CO = 2, GHSV = 6410 mL g^{-1} h^{-1}), the best catalytic performances were obtained for Pt-promoted and non-promoted cobalt catalysts prepared from cobalt nitrate; this latter led to better Co dispersion than the one prepared from cobalt nitrate [266]. In another study, four different Co precursors, $Co(NO_3)_2$(Co-N), $Co(C_2H_3O_2)_2$ (Co-A), $CoCl_2$ (Co-Cl), and $Co(OH)_2$ (Co-H), were used to prepared 20%Co/SiO_2 catalysts *via* IWI [265]. It was reported that the CO conversion increased in the following order: Co-Cl < Co-A < Co-N < Co-H. The high activity of the catalysts prepared from Co-N and Co-H were attributed to their higher reducibility in comparison with those prepared from Co-A and Co-Cl. Panpranot et *al.* [267] prepared Co/MCM-41 (ordered mesoporous silica) catalysts by the IWI technique using $Co(NO_3)_2$, $CoCl_2$, $Co(CH_3COO)_2$, and $Co(acac)_2$ as precursors. The best FTS performance was achieved with cobalt nitrate supported on MCM-41 [267]. For titania-supported catalysts in FTS (P = 20 bar, H_2/CO = 2, GHSV = 1200 mL g^{-1} h^{-1}), the use of CoC_2O_4, $Co(CH_3COO)_2$ and $Co(acac)_2$ as cobalt precursors resulted in a higher activity compared with the reference catalyst prepared from $Co(NO_3)_2$ [268]. Based on these results we can conclude that there is no simple correlation between the catalyst performances and the Co precursors. The type of the support could strongly influence the decomposition of Co precursors, MSI, and the particle size distribution.

3.6 Effects of cobalt loading

The Co dispersion of a given FTS catalyst can be improved by different methods, including the tuning of the cobalt loading [41]. As Co dispersion greatly impacts the availability of active sites, it is important to optimize Co loading [24,249]. Various works in the literature have shown that regardless of the carbon support (*eg.* CNT or CNF), increasing the cobalt loading causes a remarkable increase of the Co particle size (Figure 42), which is due to the agglomeration of cobalt crystallites [193,225,249,269,270].

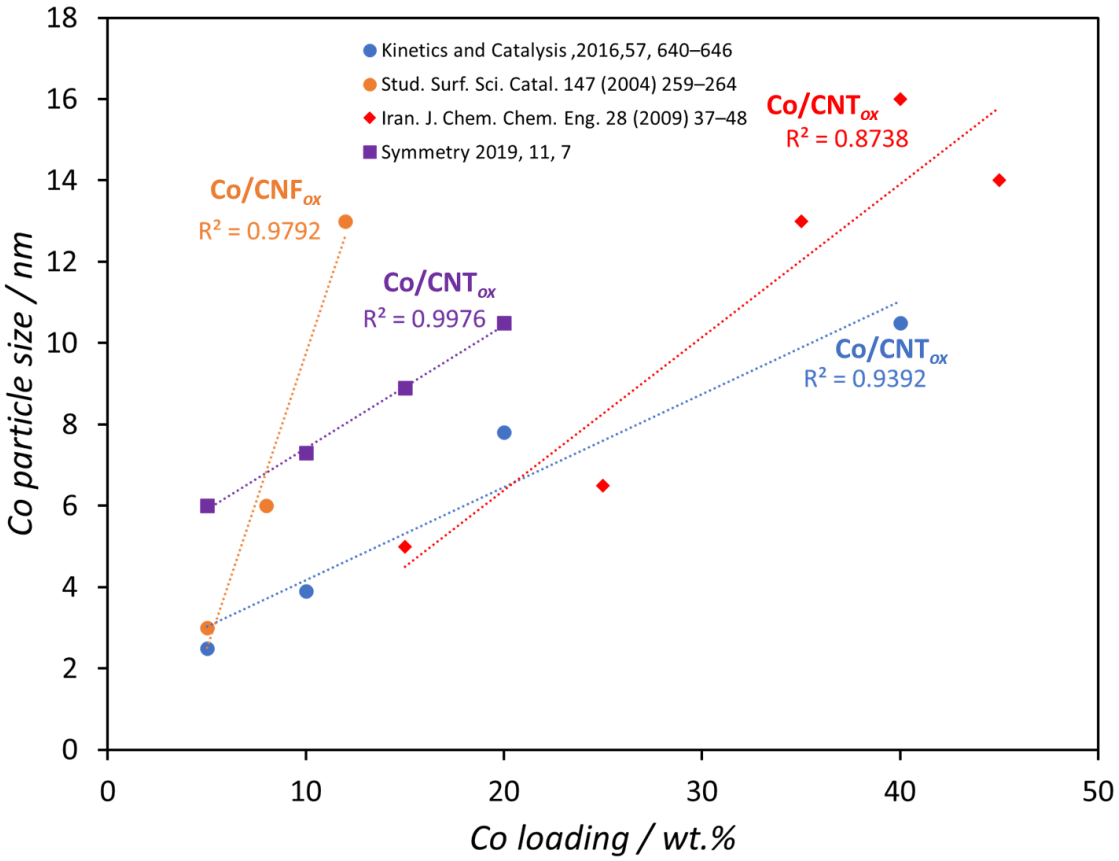

Figure 42. Variation of Co particle size with cobalt loading on CNT_{ox} [193,225,249] and CNF_{ox} [269].

Tavasoli *et al.* [213] investigated the effect of Co loading in FTS by increasing the amount of Co on CNT_{ox} from 15 to 40 wt.% using the WI method. The density of active surface Co^0 sites increased with the Co loading, and the maximum of Co^0 active sites was found at 40 wt.%. Moreover, the reducibility of Co particles increased with Co loading, while the Co dispersion significantly decreased [213]. The improvement of reducibility of large Co particles is due to their weak MSI which led to an increase of the number of Co^0 active sites. This explained the results in FTS using a continuous stirred tank reactor (T = 220 °C, P = 25 bar and H_2/CO = 2), where the reaction rate (in $g_{HC}\ g_{cat}^{-1}\ h^{-1}$) increased with the cobalt loading. Also, increasing the Co loading from 15 to 40 wt.% allowed improving S_{C5+} by 11%. In another study, Akbarzadeh *et al.* [225] used the strong electrostatic adsorption method to prepare Co/CNT_{ox} catalysts with different cobalt loadings. Increasing Co loading from 5 to 20 wt.% led to an increase in Co particle size from 2 to 10 nm [225]. In FTS (T = 240 °C, P = 20 bar, H_2/CO = 2, GHSV = 40000 mL $g^{-1}\ h^{-1}$), the reaction rate (in $g_{HC}\ g_{cat}^{-1}\ h^{-1}$) passed through a maximum at 10 wt.%Co, due to the highest amount of active surface Co^0 sites. However, the optimal Co loading in Co/CNT_{ox} catalysts for maximum FTS activity was found different in the following studies: 25 wt.% by Lv *et al*. [270], and 40 wt.% by Tavasoli *et al*. [249] In fact, the optimal Co loading depends on catalyst preparation methods, support nature, solvent nature, and preparation conditions. Once again, these studies show that there is no simple correlation between the Co loading and the performance of carbon-supported Co catalysts in FTS.

3.7 Effect of catalyst calcination and activation

The pretreatment conditions of cobalt catalysts play a crucial role on their chemical composition, crystallinity, and particle size, which consequently affect their catalytic performances [261,270]. Catalyst pretreatment before FTS is complex and it can be separated into two steps, calcination, and activation, which will be discussed in detail in the following sections.

3.7.1 Effect of calcination temperature

The calcination temperature is a critical parameter in catalyst preparation, which can affect the physicochemical properties of the catalysts [271]. Generally, the calcination allows simultaneously controlling the thermal decomposition of the metal precursor and its transformation into metal-based particles [271]. The effect of the pretreatment of a $CoMnO_x$/C catalyst in FTS was examined by Iqbal *et al*. [272] The catalyst was prepared from $Co(NO_3)_2$ and $Mn(NO_3)_2$ precursors by WI method. It was pretreated in air at 300, 400, 500 and 600 °C. In FTS (T = 240 °C, P = 6 bar, H_2/CO = 1, GHSV = 600 mL g^{-1} h^{-1}), both CO conversion and S_{C5+} increased with the increase of the calcination temperature from 300 to 500 °C, while for the catalyst calcined at 600 °C, the CO conversion (and the S_{CH4}) strongly decreased. The low CO conversion observed at 600 °C was attributed to the damages of the carbon support structure but also to the sintering of Co particles [270]. The high S_{C5+} obtained with the catalyst calcined at 600 °C was ascribed to the Co particle size effect [89]. Similar results were also observed with Co/CNT catalysts calcined in air at 400, 550 and 700 °C [270].

The transformation of Co_3O_4 to metallic Co on CNT_{ox} was observed at temperatures above 500 °C under Ar atmosphere, which corresponds to an auto-reduction [271]. As already stated, surface oxygen functional groups are of great interest for the preparation of Co/C catalysts [150], since they increase the hydrophilicity of carbon surface making it more accessible to the aqueous solution of the metal precursor during impregnation. According to Keyser *et al.* [150], the temperature at which the oxygen surface functional groups decompose plays an important role on catalytic performances. The influence of calcination temperature (no calcination, 300 and 600 °C) in an Ar atmosphere on Co particle size of Co/CNF_{ox} catalysts was studied [150]. It was found that the O_{1s}/C_{1s} ratio decreased by increasing the calcination temperature in the following order: CNF_{ox} (0.48) < CNF_{ox}-300 (0.25) < CNF_{ox}-600 (0.10). This was in accordance with a decrease of the density of carboxylic and carbonyl groups by increasing the calcination temperature. After the impregnation process, a shift of the aromatic stretching band at 1600 cm^{-1} to lower wavenumbers was observed by FTIR, which confirms the electrostatic attraction between negatively-charged surface oxygen functional groups and cobalt species during the catalyst preparation. On the other hand, the calcination at 300 and 600 °C enhanced the MSI. Furthermore, the amount of cobalt carbide was higher in Co/CNF_{ox}-600 than that in Co/CNF_{ox}-300. This is due to the decomposition of the majority of the surface oxygen functional groups at 600 °C, leading to the transfer of the oxygen atoms from cobalt oxides to the support, which is in turn oxidized. Consequently, a decrease in the number of active sites on the carbon surface was observed. The FTS results showed that the catalyst calcined at 600 °C was about six times less active than the other samples. This was attributed to the formation of Co_2C at high calcination temperature, thus decreasing the number of cobalt active sites.

3.7.2 Effect of calcination atmosphere

Before the catalytic test, catalyst calcination can be typically carried out under air or inert atmosphere (argon, nitrogen) for the thermal decomposition of metal precursors [270]. It was demonstrated by TGA that the weight loss of CNT_{ox} was not significant under Ar up to 650 °C, whereas, under air, it started at 500 °C [271]. In the case of 20%Co/CNT_{ox}, the decomposition temperature of CNT under air started at 230 °C, because cobalt species catalyze oxidation reactions. It was reported that 20%Co/CNT_{ox} calcined under Ar at 200 °C and reduced under H_2 at 400 °C showed better catalytic performance in FTS than the same catalyst calcined under air (Table 9) [271]. In another study, the FTS performances were similar for samples calcined either under N_2 or air at temperature below 550 °C [270]. This is probably due to the fact that the CNT structure is unchanged under N_2 or under air at low calcination temperature. However, in order to avoid carbon support degradation and to improve FTS performances, calcination under an inert environment (Ar or N_2) is recommended [106,128].

Table 9. The FTS performances of Co/CNT catalysts produced from cobalt nitrate and calcined in different atmospheres [271].

Catalyst	Calcination	CO conversion (%)	Product selectivity (%)		Ref
			CH_4	C5+	
20%Co/CNT_{ox}	Air at 200 °C	91	13	85	[271,273]
	Ar at 200 °C	95	14	84	[271,273]
15%Co/CNT	Air at 400 °C	25	19	70	[270]
	Ar at 400 °C	25	19	70	[270]

3.7.3 Effect of activation conditions

The final Co particle size, Co exposed facets and carbon structure stability strongly depend on activation conditions, which consequently affect the surface reactivity of the catalyst. Xiong *et al*. [160] reported the activation of cobalt oxide supported on N-doped carbon spheres (N-CS) under different environments (H_2 and Ar). Thus, a classical reduction at 480 °C under H_2 was compared with a thermal treatment under Ar (carboreduction). It was demonstrated that Co_3O_4 supported on N-CS could be auto-reduced to Co^0 upon heating under Ar, thus leading to smaller Co particle size (d_{Co} = 11 nm) compared to the catalyst reduced under H_2 (d_{Co} > 50 nm) (Figure 43a). FTS performances (T = 230 °C, P = 8 bar, H_2/CO = 2, GHSV = 1200 mL g^{-1} h^{-1}) were evaluated for 2.3%Co/N-CS catalysts activated under H_2 or Ar. The results showed similar S_{C5+} and higher CO conversion for the catalyst activated under Ar, as compared to the catalyst heated under high-purity H_2, suggesting that H_2 reduction can be avoided (Figure 43b). This is explained by the higher Co dispersion of the catalyst pretreated under Ar than that of the catalyst pretreated under H_2 (Figure 43a) [160,274]. Similar results were obtained for 1.1% Co/CS (Table 10).

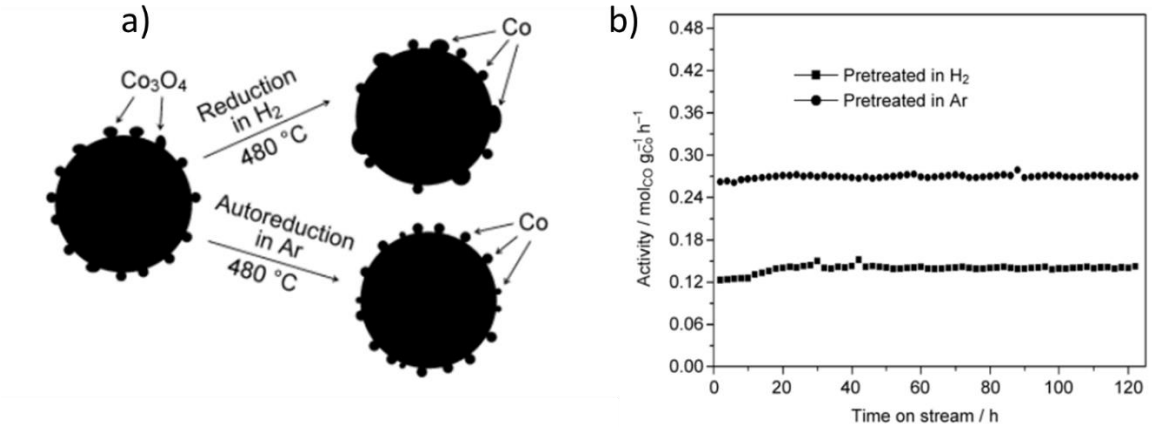

Figure 43. a) Scheme of the cobalt catalysts reduced in different atmospheres; and b) activity as a function of time for FTS over 2.3%Co/N-CS pretreated under Ar or H_2. Reprinted with permission from Ref [160]. Copyright 2010 John Wiley and Sons.

Similar results were also obtained by Yang *et al.* [107] It was reported that cobalt oxide particles, auto-reduced by a mesoporous carbon support, exhibited higher activity than the ones activated under H_2, thanks to the formation of smaller Co particles under inert atmosphere. A reduction reaction mechanism of CoO (Figure 44) was proposed to account for the particle size difference. First, during the hydrogen-reduction process, oxygen atoms in the outermost layer of the Co particles are released from the lattice and combine with hydrogen to form water (*Route 1*, hydrogen reduction process). When the reduction is performed by the carbon material, oxygen atoms located at the interface between the cobalt oxide and the carbon support preferentially interact with carbon atoms to release CO. Subsequently, the oppositely oriented diffusion of oxygen atoms from the top to the bottom of the particles would remove all the oxygen atoms as indicated by the blue arrows in *Route 2* (auto-reduction process). Well-dispersed Co particles are obtained under an inert environment due to the rapid diffusion of oxygen atoms that induces the migration of cobalt atoms on the carbon surface at high temperature, which act as heterogeneous sites for the rearrangement of cobalt atoms [107]. By changing the atmosphere of the catalyst activation to N_2, it was found that Co/CNT_{ox} can be auto-reduced by the support at *ca*. 480 °C. This catalyst showed better catalytic performances in FTS (T = 225 °C, P = 8 bar, H_2/CO = 2, GHSV = 3840 mL g^{-1} h^{-1}) than the one reduced in H_2 above 400 °C (Table 9) [91].

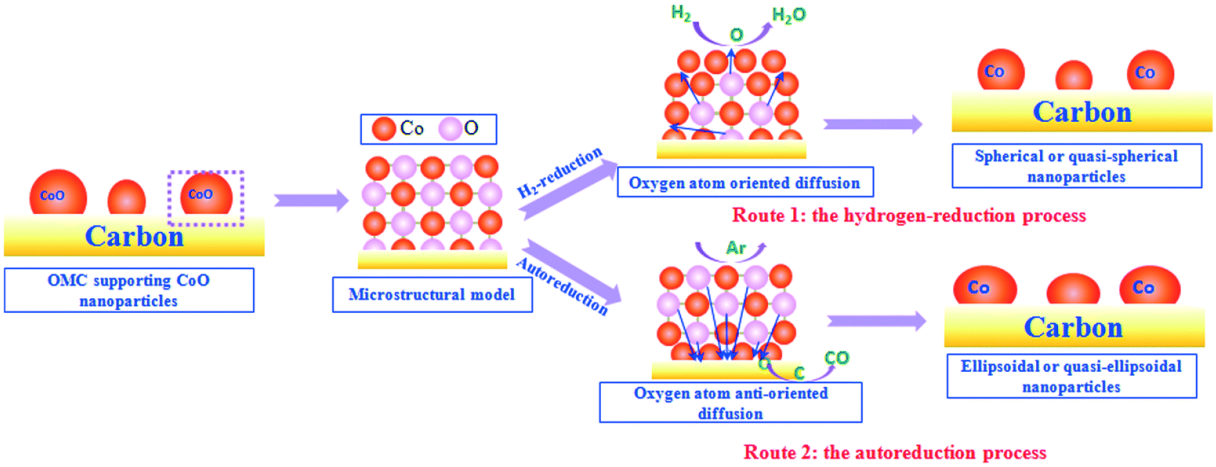

Figure 44. Depiction of structural evolution of as-synthesized Co/C catalysts during the auto-reduction and hydrogen-reduction processes. Reproduced by permission from Ref [107]. Copyright 2017 Royal Society of Chemistry.

Increasing the temperature during H_2 activation can contribute to an optimization of the catalytic performances. Upon reduction at 300 °C for 1 h, a 9%Co/Dia_{ox} catalyst (Dia_{ox} = oxidized diamond) showed a low CO conversion (37.6%) in FTS (T= 250 °C, P = 10 bar, H_2/CO = 2, GHSV = 4500 mL g^{-1} h^{-1}) [80]. By increasing the reduction temperature to 350 °C, the CO conversion reached *ca.* 50% under the same conditions in FTS [80]. In contrast, for the catalysts reduced at 450 and 500 °C, CO conversion decreased to 42.5% and 33.3%, respectively, which could be due to the increase of Co particle size [80].

Table 10. Fischer-Tropsch synthesis performances of carbon supported Co-catalysts pretreated in high-purity H_2, Ar and N_2

Catalyst	Pretreatment	CO conversion (%)/ Co Time Yield[a]	Product selectivity (%)		Ref
			CH_4	C5+	
Co/CNT_{ox}	H_2 at 300°C	12.50	11.1	85.8	[91]
	H_2 at 400°C	25.90	30.6	62.1	[91]
	H_2 at 480°C	3.70	2.9	95.9	[91]
	N_2 at 400°C	3.40	3.5	95.8	[91]
	N_2 at 480°C	13.30	8.9	87.0	[91]
2.3%Co/N-CS	H_2 at 480°C	0.14[a]	28.9	46.8	[160]
	Ar at 480°C	0.27[a]	29.3	47.1	[160]
1.1%Co/CS	H_2 at 480°C	0.05[a]	37.6	37.4	[160]
	Ar at 480°C	0.07[a]	38.1	36.9	[160]

[a] Cobalt-Time-Yield= mol_{CO} g^{-1} h^{-1}

During auto-reduction, the transformation from metal oxide to the metallic phase can determine two crucial parameters: the particle size and the MSI [108,215]. It was reported that the incorporation of nitrogen atoms significantly changes the chemical environment of carbon supports, which results in interfacial electronic interactions [108]. Owing to the strong MSI, the distribution of cobalt particles on the surface of N-doped supports could be affected [108]. The effect of nitrogen on the auto-reduction of supported cobalt particles has been investigated by Yang *et al.* [108] Pristine ordered mesoporous carbon (MC) and nitrogen-doped ordered mesoporous carbons (N-MC) were prepared by using a post-synthesis method with cyanamide (CA) as a nitrogen source. These materials were used as supports for the preparation of cobalt-

based catalysts. These supports were labelled N-MC-x, in which x represents the mass ratio of the CA to the carbon substrate. As expected, the results showed that the incorporated nitrogen amount gradually increased with the increase of CA amount as follows: pristine MC (0 wt.%) < N-MC-1 (6.5 wt.%) < N-MC-2 (8.4 wt.%) < N-MC-3 (10.5 wt.%). At the same time, the average Co particle size decreased from 19.4 to 6.7 nm with an increase in nitrogen content as follows: Co/MC (19.4 nm) > Co/N-MC-1 (12.8 nm) > Co/N-MC-2 (10.6 nm) > Co/N-MC-3 (6.7 nm). Additionally, the cobalt particles were homogeneously dispersed on the all N-doped MC surface as compared to those on the pristine MC surface, which present a bimodal particle size distribution [108]. This indicates that the introduction of nitrogen improves the dispersion of cobalt species and contributes to the formation of regular particles [108]. It was also observed that the auto-reduction in the 15%Co/MC took place at low temperature (496 °C), due to weak MSI. However, for all the catalysts supported on N-doped supports, the auto-reduction of cobalt oxide gradually shifts towards high temperature with the increase in nitrogen amount in this order: Co/N-MC-1 (497 °C) < Co/N-MC-2 (502 °C) < Co/N-MC-3 (505 °C). This was attributed to the strong MSI , which increased with the increase in nitrogen amount [108]. The catalytic performances of the auto-reduced samples were evaluated in a fixed-bed reactor (T = 240 °C, P = 20 bar, H_2/CO = 2 and GHSV = 1000 mL g^{-1} h^{-1}). CTY increased from 2.67 to 3.02 × 10^{-4} mol_{Co} g_{Co}^{-1} s^{-1} by increasing the Co particle size from 6.7 to 10.6 nm. The low CTY observed for the catalyst with small particle size was attributed to the change in the structure of Co [108]. On the other hand, the CTY systematically decreased for catalysts presenting the Co particle size greater than 10 nm, due to the reduced metallic surface exposed by the Co particles [108]. Higher values of S_{C5+} were obtained over 15%Co/MC in comparison with all the catalysts supported on N-doped supports. This tendency was attributed to the Co particle size effect.

We can conclude that the calcination and activation of Co/C catalysts depend on several parameters including heat treatment temperature, the nature of the gas and MSI. The calcination and activation should be performed at low temperature (300-400 °C) to avoid Co sintering and catalyst deactivation. Inert atmosphere such as Ar favors the auto-reduction and preserves the integrity of the carbon support. Furthermore, the auto-reduction (carboreduction) of carbon supported cobalt catalysts improves Co dispersion which enhances FTS performances. However, since the oxygen and nitrogen groups constitute the keys factors, which determine the nature of the MSI and the Co particles size, and thus the catalytic performance of the catalysts, the carboreduction mechanism of the Co_3O_4 or CoO species will be different for N-doped and O-doped carbon catalysts. O-doped carbon catalysts lead to a weak MSI and large Co particle size as compared to N-doped carbon catalysts, which favor a strong MSI and small Co particle size, therefore better stabilizing the Co particles. For that, the carboreduction takes place at low temperature in the case of O-doped carbon catalysts, due to the faster diffusion of oxygen from the cobalt particles to the carbon support to form metallic particles, as compared to nitrogen groups. In the FTS both approaches present advantages and disadvantages, due to the fact that the large Co particle sizes derived from the carboreduction of O-doped carbon catalysts are beneficial only for the improvement of S_{C5+}, while the small Co particle size obtained from N-doped carbon catalysts are useful for the enhancement of activity.

3.8 Effects of promoters

In the hydrogenation of carbon monoxide, the efficient control of the reaction selectivity to methane, olefins, oxygenated products, or long-chain paraffins is a major concern [275]. In

FTS, a major challenge is the suppression of paraffinic byproducts and the promotion of alcohols and olefins [276]. For Co catalysts, the ability of cobalt to be selective with respect to alcohols and olefins strongly depends on properties such as metal dispersion or particle size, MSI and reducibility. Moreover, due to the high cost of cobalt compared to iron, it is important to maximize the availability of active Co^0 surface sites [277]. The use of a promoter can maximize the density of these sites. Many promoters for cobalt catalysts are proposed in the literature [41], including Pt [277], Ru [277], Cu [165,278], K [279], Cr [279], Mn [71,279], CeO_{2-x} [275], Ni [280], V [281], MoK [282], RhMo [283], and Fe [192]. For example, the promotion of Co/CNT_{ox} catalysts with small amounts of Pt or Ru had no significant effect on the size of Co_3O_4 crystallites but contributed to enhance cobalt reducibility and FTS performances [277]. Zhao et *al.* [284] highlighted the impact of chromium on the activity and selectivity of activated carbon-supported cobalt catalysts (CoxCr/AC, where the Co loading was fixed at 15wt.% and Cr loading (x) being 0, 1, 2, 3, and 5 wt%). These catalysts were prepared by IWI using an aqueous solution of both Co and Cr precursors. The average Co particle size obtained on Co/AC, Co1Cr/AC, Co2Cr/AC, and Co3Cr/AC samples was 7.2, 6.6, 6.7, and 6.2 nm, respectively. This shows the beneficial effect of Cr addition to decrease the average Co particle size, and thus to increase Co dispersion. At the same time, the addition of Cr enhanced cobalt reducibility. Interestingly, Cr promotion inhibited the formation of the Co_2C phase, which is less active in FTS [284]. The non-promoted and promoted catalysts were evaluated in FTS (T = 220 °C, P = 30 bar, H_2/CO = 2, and GHSV = 2000 mL g^{-1} h^{-1}). The TOF increased from 47.2 to 119.8 h^{-1} as the Cr loading increased from 0 to 2 wt%, which was attributed to an active interface created between Co and Cr. However, this also facilitated H_2 adsorption, which favored paraffin formation (Figure 45a) [284]. Cr promoted catalysts also exhibited good stability. Also, increasing Cr loading did not significantly affect chain lengthening probabilities for paraffins, olefins and alcohols (Figure 45b for olefins). In particular, the best promotional effect of Cr was found at the maximum contact area between Co and Cr, which, in this study, corresponded to Cr/Co = 0.13 (Figure 45c).

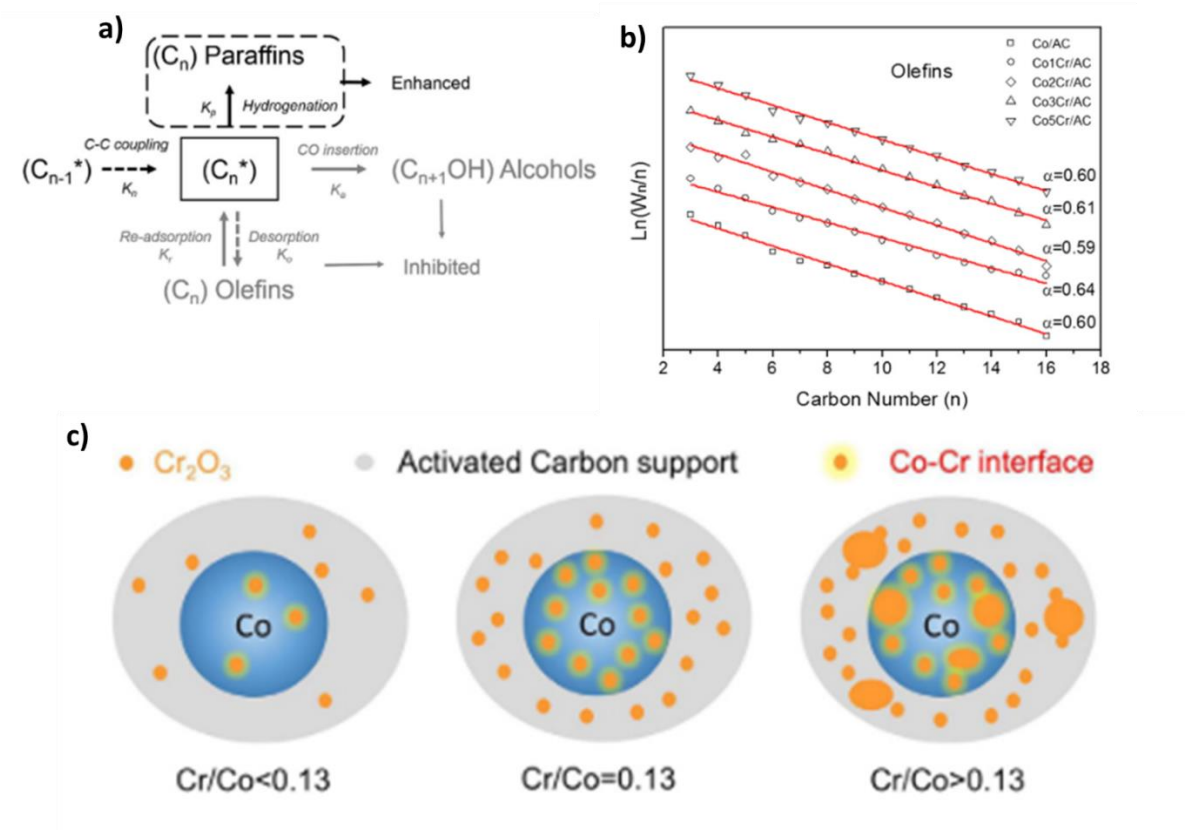

Figure 45. a) ASF distributions of CoxCr/AC catalysts for olefins products formation during FTS reaction (T = 220 °C, P = 30 bar, GHSV = 2000 mL g^{-1} h^{-1}, and H_2/CO = 2); b) schematic figure of reaction routes over CoxCr/AC catalysts; and c) spatial distribution of Cr and Co on the AC support. Reprinted with permission from Ref [284]. Copyright 2019 Elsevier.

Xiong *et al.* [279] investigated the impact of Cr, Mn and K as promoters on the formation of the Co_2C phase in Co/AC supported catalysts. The ratio of Co_2C/*fcc*-Co decreased in the order Cr (0.31) < Mn (1.22) < K (∞). As a conclusion, selected promoters such as Mn and Cr could limit the formation of the Co_2C phase, and consequently favor CO hydrogenation. In another work, Wang *et al.* [275] studied the mechanism of alcohol formation over a series of CNT-supported catalysts, which were promoted by Cu, Ce, Cr and Zr. The catalysts were prepared by the co-impregnation method. For the catalyst promoted by Ce, HRTEM results revealed a strong interaction between CoO and CeO_2, which is essential for the synthesis of alcohols. This interaction was slightly weaker between CuO and CoO. In contrast, Cr and Zr oxides did not favor chain growth termination, leading to long-chain hydrocarbons' formation [275]. Consequently, in FTS for high alcohols synthesis in a fixed-bed reactor (T = 270 °C, P = 25 bar, H_2/CO = 2, and GHSV = 10000 mL g^{-1} h^{-1}), the selectivity towards alcohols was slightly higher with 10Co5Ce/CNT than with 10Co5Cu/CNT, and it was much higher than with other catalysts.

Numerous studies have been devoted to the effect of promoters on catalysts properties and FTS performances, and Table 11 summarizes the most significant results. In these studies, Co played the role of the active metal, while various promoters were investigated, including Ru, Fe and Ni, which can be also used as active metals in FTS. Generally, adding promoters allows improving cobalt dispersion, reducibility, and stability. Using promoters also contributes to tune the MSI, thus increasing the number of active Co^0 surface sites, which enhances FTS rate and increases selectivity into FTS alcohols and olefins products. For example, Pt and Ru as promoters allow boosting FTS rate and S_{C5+} [140,159,186,199,277], Cu and CeO_{2-x} are suitable for alcohol formation [275], while Mn and La are more beneficial for olefins formation [276,285]. >The high selectivity for alcohols, olefins and paraffins for promoted catalysts are attributed to the electronic properties of the promoters [140]. Manganese facilitates the CO dissociative adsorption by the Lewis acid-base interaction between Mn^{2+} and the oxygen atom of CO adsorbed, while La promoter assist both the hydrogenation and the CO insertion, thus, increasing the selectivity into paraffin and alcohol [276,286]. The reduction promoters such as Pt and Ru, affect the electronic structure of cobalt particles and increase the activity and selectivity into heavy paraffins [140]. Based on this, the promotion of cobalt-based supported catalysts resulting in good selectivity for alcohols, olefins and paraffins is due to electronic charge transfer, which modifies the electron density at the interface between active phase and promoter. The contribution of promoters is indisputable in FTS but their choice has to be adapted to the objectives.

Table 11. Effects of promoters on the catalysts properties and FTS performances reported in the literature.

Catalyst	Promoter	Effects on catalyst properties	Effects on FTS performances	Ref.
Co_xMn_yLa/AC **LaZr-Co/AC** **Co-La/AC**	Mn-La La-Zr La	Mn-La prohibits the Co oxide reduction and decreases Co dispersion Mn prohibits H_2 adsorption La increases H_2 uptake and reducibility of the catalyst	Mn-La decreases CO conversion La facilitates the formation of alcohols and C1 products Mn promotes the formation of olefins La-Zr increases both activity and S_{C5+}	[33,276,287,288]
RuCo/CNT_{ox} **PtCo/CNT_{ox}** **RuCo/MHCS**	Ru Pt	Ru and Pt decrease reduction temperature No effect on Co particle size Ru favors hydrogen spillover	Pt is a better promoter for FTS activity than Ru Ru and Pt increase S_{C5+}	[140,159,186,199,277]
CoCu/CNT_{ox} **CoCuZr/CNT_{ox}** **CoMoK/CNT_{ox}** **CoCuMn/AC** **CoMn/CNF** **$CoMnO_x$/C** **$CoMno_x$/CNF**	Cu Mo-K Cu-Zr Cu-Mn MnO_x	Mo-K increases the amount of active species Cu-Mn and MnO_x improve Co^0 active sites	Cu-Mn increases the activity and alcohols selectivity Cu-Zr enhances the activity for CO_2 hydrogenation Cu-Zr promotes methanol formation MnO_x increases TOF and S_{C5+}	[72,165,272,282,289,290]
CoCr/CNT_{ox} **CoMn/CNT_{ox}** **CoK/CNT_{ox}** **CoCr/AC** **Co-K/ZIF-67**	Cr Mn K	K promotes Co_2C formation Mn and Cr restrain Co_2C formation Cr decreases Co particle size and increases reduction degree of the catalyst	K decreases activity and increases S_{CH4} K shifts to higher oxygenate selectivity Mn enhances both FTS activity and S_{CH4} Cr enhances activity, stability and S_{C5+}	[279,284,291]
CoCu/CNT_{ox} **CoCe/CNT_{ox}** **CoZr/CNT_{ox}** **CoK/AC** **CoCe/AC** **CoZr/AC** **K-Co_3O_4**	Ce Zr Cu K	Ce and Zr change slightly the reducibility of Co oxides Ce,K and Zr reduce MSI	Ce is more beneficial for alcohols than Cu Ce promotes long chain hydrocarbons formation	[275,291–293]
CoNi/CNT_{ox}	Ni	Ni increases the Co_3O_4 particle size and Co^0 active sites Ni reduces the reduction temperature	Ni catalyzes the hydrocracking of hydrocarbons	[280]
CoV/AC	V	V increases Co^0 active sites V enhances Co dispersion and reducibility	V increases CO conversion and S_{C5+}	[281]
CoRu/CNT **CoK/CNT**	Ru K	Ru enhances the reducibility of Co_3O_4 and dispersion K increases the reduction temperature	K decreases the FTS rate K increases olefin to paraffin ratio more than Ru	[294]

MnCo/CNT **MnCo/CNF** **PtMnCo/CNT** **RuMnCo/CNT**	Mn Pt-Mn Ru-Mn	Pt-Mn or Ru-Mn enhance the reducibility Pt-Mn reduces the activation energy of CO adsorption	Mn increases activity and decreases S_{CH4} Pt-Mn enhances FTS activity better than Ru-Mn	[59,69, 71,290, 295]
KMoRhCo/CNT **KMoRhCo/AC**	Mo-Rh K	Increases CO chemisorption and Co dispersion	Increases total alcohols yield Enhances the CO hydrogenation	[283]
FeCo/C **K-FeCo/C** **CoFe/CNT** **CoFe/Cs** **CoFe/AC**	Fe K-Fe	K increases the H_2 uptake Fe enhances the reducibility of the catalyst Fe improves both metal dispersion and CO uptake	Fe enhances olefins/paraffin ratios K decreases activity and increases selectivity to olefins Fe-Co prohibits activity	[180,192,211,296–301]
Ni-Co-Fe/C **Au-Ni-Co-Fe/C** **Co-Fe/C** **Mo-Co-Fe/C**	Ni-Fe Au-Ni-Fe Fe Mo-Fe	Ni enhances the Co dispersion Ni increases H_2 adsorption Mo enhances surface acidity of the catalysts	Ni increases CO conversion and S_{CH4} Co-Fe enhances S_{C5+} Au enhances the WGSR Mo-Fe improves the production of gasoline	[302–304]
NbCo/CNT	Nb	Nb increases dispersion and decreases catalyst reducibility	Nb improves CO conversion and enhances S_{C5+}	[305]
Co-SiO_2/AC	SiO_2	Increases the reducibility of Co and dispersion Promote Co_2C formation	SiO_2 increases CO conversion and selectivity for C_1-C_{18} alcohols	[306]
Co-Ca/AC	CaO	Promotes the formation of *hcp*-Co and Co_2C species CaO decreases the quantity of metallic sites	CaO decreases the α value CaO improves selectivity to alcohols	[307]
CoMoS_2NiRh/AC	NiMoS Rh	Ni, Co and Rh improve the reducibility of the catalysts	Ni and Rh enhance the formations of alcohols	[308]

MHCS = mesoporous hollow carbon sphere

3.9 Monolithic structure for carbon supported cobalt catalysts

FTS is a highly exothermic reaction that requires an efficient heat transfer to favor S_{C5+} [229,309]. Multi-tubular fixed-bed and slurry bubble column reactors are currently used on an industrial scale [310]. The fixed-bed reactor is widely used for FTS because it offers many advantages including, low operating costs, easy operation, and easy catalyst separation from liquid products [311]. However, the fixed-bed reactor is subjected to local overheating of the catalyst surface that may lead to a fast deactivation and to high methane selectivity [309]. This behavior was clearly observed in FTS using fixed-bed reactors for carbon supported cobalt catalyst [312]. In this context, the development of novel FTS catalysts with high thermal conductivity for efficient heat transfer is a key challenge in FTS. In order to manage the strong exothermicity of the reaction, monolithic/microstructured reactors present some advantages compared to fixed-bed reactors, such as high gas–liquid mass transfer rates in two phase flow, low pressure drop and external heat removal [81,229]. Microstructured reactors can be found in several forms such as honeycombs [309] or open metallic foams [310]. Chin *et al*. [310] investigated a novel method to fabricate catalysts based on the growth of aligned CNT over FeCrAlY foams for utilization in a microchannel FTS reactor. It was found that the FTS activity was enhanced by a factor of four owing to a potential improvement in mass and heat transfer in the microstructure. Excess heat generated during the FTS reaction can be dissipated away from the Co active sites thanks to the presence of CNT, lowering methane selectivity. The efficient heat removal and the absence of mass transfer limitations in the monolithic catalyst lead to high S_{C5+} (Figure 46) [309,313,314]. Thus, monolithic/microstructured reactors allow limiting diffusional phenomena and hot spots, and thus improving catalytic performances.

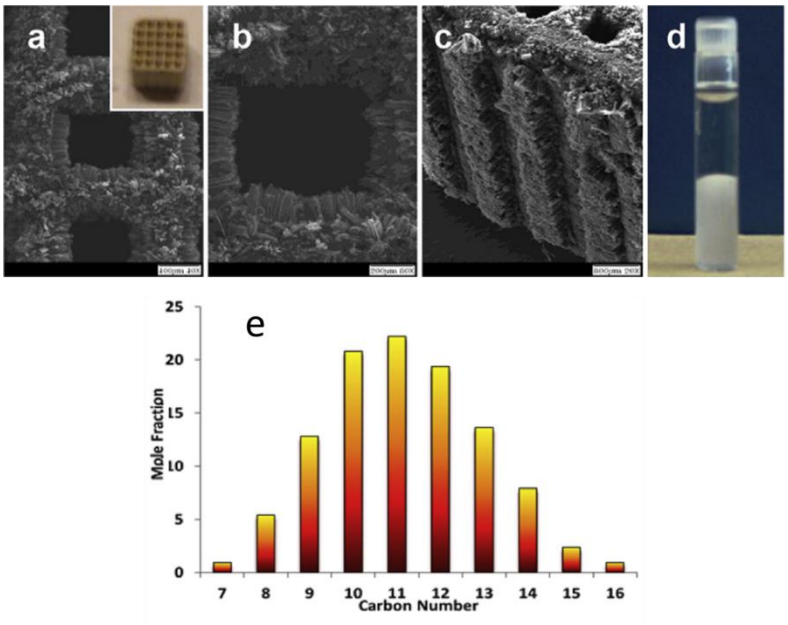

Figure 46. Fischer-Tropsch type synthesis on CNT grown on ceramic monoliths with syngas ratio (H_2:CO = 3:1). a) Shows CNT grown directly on as received coerdite monoliths (inset); b), c) scanning electron microscopy images of different portions of the coerdite monolith showing uniform growth of CNT; d) shows typical liquid collected from FT synthesis on CNT grown on the monoliths; and e) product distribution of the process conducted at 250 °C. Reprinted with permission from Ref [313]. Copyright 2017 Elsevier.

3.10 Summary

In this section, we have presented the different approaches allowing tuning the Co particle size, MSI, reducibility as well as the catalyst deactivation for Co/C catalysts. The goal was to show the influence of the different approaches to modify a catalyst during the preparation step on its catalytic performances. It is clear that different approaches can be properly used to prepare high performance FTS catalysts on carbon materials and carbon-coated materials. The catalytic performances of representative Co/C catalysts modified using different approaches are presented in Table 12.

Table 12. Representative examples of the catalytic performances of Co/C catalysts using different preparation approaches

Catalyst	Conditions	X_{CO} %	Activity/ TOF	CH_4	C5+	Stability	Remarks	Ref
CoCr/AC **CoMn/AC**	T = 230°C, P = 25 bar GHSV = 500 mL g^{-1} h^{-1} H_2/CO = 2	Cr > Mn	Cr > Mn	Cr > Mn	Cr < Mn		Cr-promoted catalysts suppress the formation of Co_2C and enhance FT activity. Mn improves S_{C5+}	[279]
Co/CNS **Co/CNT*ox***	T = 220 °C, P = 18 bar H_2/CO = 2	CNS > CNT_{ox}	CNS > CNT_{ox}	CNS < CNT_{ox}	CNS > CNT_{ox}	CNS > CNT_{ox}	Higher degree of disorder and defect sites in CNS, enhance Co dispersion and reducibility. Subsequently, activity, selectivity, and stability are improved compared to Co supported on CNTox	[218]
Co/CNT-EtOH **Co/CNT-H_2O** **Co/CNT-PrOH**	T = 220 °C, P = 20 bar GHSV = 2000 mL g^{-1} h^{-1} H_2/CO = 2	EtOH > PrOH > H_2O	EtOH > PrOH > H_2O	EtOH ~ PrOH ~ H_2O	EtOH ~ PrOH ~ H_2O		Ethanol and 1-propanol using as a solvent for impregnation, allow avoiding Co_3O_4 agglomeration due to their low surface tension, resulting in well-dispersed and well-distributed Co_3O_4, which enhance FTS performance.	[106]
Co-N/CNT*ox* **Co-A/CNT*ox***	T = 225 °C, P = 8 bar GHSV = 3840 mL g^{-1} h^{-1} H_2/CO = 2	Co-N > Co-A	C-oN > Co-A	Co-N > Co-A	Co-N < Co-A		Co-N enhances Co dispersion compared to Co-A precursor, leading to improved CO conversion.	[91]
Co/CNT **Co/CNT*ox***	T = 220 °C, P = 20 bar GHSV = 4286 mL g-1 h^{-1} H_2/CO = 2	CNT_{ox} > CNT	CNT_{ox} > CNT	CNT_{ox} < CNT	CNT_{ox} > CNT	CNT_{ox} > CNT	The use of CNT_{ox} increases MSI, dispersion, Co confinement and reducibility of cobalt. Functional groups also decrease the sintering of Co particles and enhance the stability and FTS performances.	[173]
Co/CNF-750 **Co/CNF-450**	T = 250 °C, P = 20 bar GHSV = 3000 mL g^{-1} h^{-1} H_2/CO = 2	750 > 450	750 > 450	750 > 450	750 < 450	750 > 450	CNF synthesized at 750 °C exhibit higher average crystalline size (*Lc*) of the graphene sheets and low interlayer spacing (d_{002}). The presence of medium pore diameters leads to higher catalytic activity without further deactivation.	[212]
Co/CNT*ox*-25 **Co/CNT*ox*-100**	T = 220 °C, P = 20 bar Feed = 3600 mL g^{-1} h^{-1} H_2/CO = 2	CNT_{ox}-100 > CNT_{ox}-25	CNT_{ox}-100 > CNT_{ox}-25	CNT_{ox}-100 > CNT_{ox}-25	CNT_{ox}-100 > CNT_{ox}-25		Acid treatment at 100 °C produces more defects and functional groups on CNT_{ox} than that at 25 °C. These are beneficial for designing high performance FTS catalyst.	[128]
Co/CS-IWI **Co/CS-CVD**	T = 220 °C, P = 20 bar SV = 1500 mL g^{-1} h^{-1} H_2/CO = 2	CVD > IWI	CVD > IWI	CVD > IWI	CVD < IWI		The CVD technique produces much higher dispersions of Co catalyst particles and also a more uniform coverage of the CS support surface.	[185]

Co/Al_2O_3 **Co/CN-Al**	T = 220 °C, P = 20 bar H_2/CO = 2	CN-Al > Al_2O_3	CN-Al > Al_2O_3	CN-Al > Al_2O_3	CN-Al < Al_2O_3		The g-C_3N_4 coating on the Al_2O_3 surface slows down the aggregation of Co particles and improves the dispersion. Direct contact of Co and Al_2O_3 is blocked by g-C_3N_4 coating on the CN-Al support, which reduces formation of irreducible cobalt oxide species	[227]
Co/CNF/CF **Co/CNF/CF@ SiO_2**	T = 210 °C, P = 20 bar GHSV = 4300 mL g^{-1} h^{-1} H_2/CO = 2	CNF/CF@ SiO_2 > CNF/CF	CNF/CF@SiO_2 > CNF/CF	CNF/CF @SiO_2 < CNF/CF	CNF/CF@ SiO_2 > CNF/CF	CNF/CF @ SiO_2 > CNF/CF	The SiO_2 layer increases the micropore volume and decreases the oxidation potential of the cobalt species, enhancing FT performances and the stability of the Co catalysts	[229, 230]
Co@C-SiO_2 **Co@SiO_2**	T =230-240 °C, P = 20 bar GHSV = 1000 mL g^{-1} h^{-1} H_2/CO = 2	C-SiO_2 > SiO_2	C-SiO_2 > SiO_2	C-SiO_2 > SiO_2	C-SiO_2 < SiO_2		C-SiO_2, reduces MSI, enhances Co dispersion and reducibility. C content increases also the number of active sites	[252]

CNT = carbon nanotubes ; GNS = graphene nanosheets ; EtOH = ethanol ; PrOH = propanol ; CNT_{ox} = functionalized carbon nanotubes with HNO_3; Co-A = cobalt acetate ; Co-N = cobalt nitrate ; CNF-750 = carbon nanofiber prepared by CVD at 750 °C; CNF-450 = carbon nanofiber prepared by CVD at 450 °C ; CNT_{ox}-100 = CNT treated at 100 °C with HNO_3 solution ; CNT_{ox}-25 = CNT treated at 25 °C with HNO_3 solution.

4. Summary and outlooks

The number of publications related to the use of carbon-supported Co-based catalysts in FTS has grown exponentially in recent years (Figure 1). This is due to the renewed interest in this reaction but also to the potential of this type of support. As for the oxide supports, the research is focused on the development of active, selective and stable catalysts under standard FTS conditions, but research is also needed on the design of catalysts that can provide FT synthesis from syngas derived from biomass, or directly from CO_2 (CO_2-FTS). The choice of a carbon FTS support can be dictated by various requirements.

First, this type of support, as long as its degree of graphitization is sufficient, can allow better thermal conductivity than an oxide of low thermal conductivity. This can of course affect the selectivity of the reaction by limiting the formation of methane, but also the catalyst stability by limiting the formation of hot spots, which contribute to the sintering of the active phase. In this context, the use of monolithic/microstructured reactors, which further allow limiting hot spots but also diffusional phenomena, and thus improving catalytic performances, should be definitively more investigated taking advantages of the numerous methods available to deposit catalysts on structured surfaces [315].

Second, the metal-support interaction is of fundamental importance in FTS, because it influences the reducibility of cobalt, the Co particle size and even the reduced phase obtained (*fcc*-Co or *hcp*-Co), which in turn determines the activity and selectivity in FTS. In this respect, the use of a carbon support can present several advantages. Indeed, the relatively weak interaction of carbon supports with cobalt, as compared to oxides, favors cobalt reduction, which in some cases can occur thanks to the support itself (carboreduction). Thus, this enables to overcome one of the problems associated with the use of oxide supports, that is, the formation of mixed phases between the cobalt and the oxide, which are most of the times very difficult to reduce. Of course, this weak interaction can also be a source of problems, in particular related to the sintering of the active phase. Nevertheless, this review has shown that the rich surface chemistry of carbon materials could remediate this weakness. In fact, carbon supports can be relatively easily functionalized by oxygen or nitrogen surface groups, which contribute to a more intense nucleation of the active phase and therefore to good dispersion and stabilization. Moreover, the addition of dopants makes it possible to stabilize the cobalt on the support.

Third, as the textural properties of the support (surface area, pore volume, pore size distribution, and crystalline phase) have been found to influence the catalyst performances, some carbon materials present peculiar features not present for oxide supports. This is particularly notable in the case of carbon nanotubes, for which confinement effects have regularly been reported. The confinement of the cobalt in the inner cavity of the nanotubes leads to an easy reduction of the metal, a control of the particle size and a stabilization of the active phase. These effects result in catalysts that are more active, more selective but also more stable than in the case of unconfined catalysts. Further studies combining experimental works, detailed characterization and modeling are needed to draw clear correlations between catalytic performances and confinement effects.

In addition to studies based on the specificities of carbonaceous materials, other works focus on issues common for both carbon and oxide supports. Thus, the control of cobalt particle size or cobalt crystalline phase and their influence on the activity, the selectivity and the stability of the catalysts has been the subject of numerous studies. If, similarly to oxide supports, many works indicate that Co/C catalysts with cobalt particle size 6-8 nm are preferred for obtaining both higher TOF and C_{5+} selectivity, a detailed analysis of the published results shows that the

situation is not as clear cut as that on oxide supports (Figure 8). Indeed, the evolution of TOF and S_{C5+} with Co particle size is indeed quite complex, presumably due to the combined effect of different parameters such as hydrogen spillover, cobalt confinement, support surface and textural properties, and cobalt crystallographic phase. Here too, many studies (including through operando techniques) will still be necessary in order to decorrelate these different parameters so as to have a more precise idea of the size effect. The availability of a variety of methods for preparing Co/C catalysts, detailed in this review, should thus make it possible to produce catalysts with better-controlled properties to carry out this type of studies on model catalysts. Finally, it was reported that the limiting factor for the use of carbon-based catalysts in industrial scale is: i) their low density, ii) the inability to regenerate them under oxidizing atmosphere (air, oxygen), and iii) their insufficient mechanical strength. Inorganic/hybrid supports (carbon/oxide) can be developed in order to overcome these limitations.

Declaration of Interest Statement

The authors declare no conflict of interest.

5. Acknowledgements

This work was funded by the “Région Occitanie” and “UFTMiP - Université Fédérale Toulouse Midi-Pyrénées”. This support is gratefully acknowledged.

6. References

[1] A.Y. Krylova, Solid Fuel Chem. 48 (2014) 22–35.

[2] S.S. Ail, S. Dasappa, Renew. Sustain. Energy Rev. 58 (2016) 267–286.

[3] R. Guettel, U. Kunz, T. Turek, Chem. Eng. Technol. 31 (2008) 746–754.

[4] R. Guettel, T. Turek, Chem. Eng. Sci. 64 (2009) 955–964.

[5] A. Delparish, A.K. Avci, Fuel Process. Technol. 151 (2016) 72–100.

[6] J. Xu, Y. Yang, Y.W. Li, Fuel 152 (2015) 122–130.

[7] J.X. Liu, P. Wang, W. Xu, E.J.M.M. Hensen, Engineering 3 (2017) 467–476.

[8] B.C. Enger, A. Holmen, Catal. Rev. - Sci. Eng. 54 (2012) 437–488.

[9] E. de Smit, B.M. Weckhuysen, Chem. Soc. Rev. 37 (2008) 2758.

[10] J. Zhang, J. Chen, Y. Li, Y. Sun, J. Nat. Gas Chem. 11 (2002) 99–108.

[11] B.H. Davis, Ind. Eng. Chem. Res. 46 (2007) 8938–8945.

[12] F. Diehl, A.Y. Khodakov, Oil Gas Sci. Technol. - Rev. l'IFP 64 (2009) 11–24.

[13] M. De Beer, A. Kunene, D. Nabaho, M. Claeys, E. Van Steen, J. South. African Inst. Min. Metall. 114 (2014) 157–165.

[14] Q. Zhang, J. Kang, Y. Wang, ChemCatChem 2 (2010) 1030–1058.

[15] N.E. Tsakoumis, M. Rønning, Ø. Borg, E. Rytter, A. Holmen, Catal. Today 154 (2010) 162–182.

[16] R. Munirathinam, D. Pham Minh, A. Nzihou, Ind. Eng. Chem. Res. 57 (2018) 16137–16161.

[17] C. Hernández Mejía, T.W. van Deelen, K.P. de Jong, Nat. Commun. 9 (2018) 1–8.

[18] D. Vanhove, Z. Zhuyong, L. Makambo, M. Blanchard, Appl. Catal. 9 (1984) 327–342.

[19] G. Prieto, M.I.S. De Mello, P. Concepcion, R. Murciano, S.B.C. Pergher, A. Martinez, ACS Catal. 5 (2015) 3323–3335.

[20] T. Fu, R. Liu, J. Lv, Z. Li, Fuel Process. Technol. 122 (2014) 49–57.

[21] M. Zhong, Y. Guo, J. Wang, Z. Ma, M. Xia, C. Chen, L. Jia, B. Hou, D. Li, Catal. Sci. Technol. 9 (2019) 3482–3492.

[22] D. Wei, J.G. Goodwin, R. Oukaci, A.H. Singleton, Appl. Catal. A Gen. 210 (2001) 137–150.

[23] M. Rahmati, M. Safdari, T.H. Fletcher, M.D. Argyle, C.H. Bartholomew, Chem. Rev. (2019).

[24] G. Jacobs, T.K. Das, Y. Zhang, J. Li, G. Racoillet, B.H. Davis, Appl. Catal. A Gen. 233 (2002) 263–281.

[25] C. Liu, Y. He, L. Wei, Y. Zhao, Y. Zhang, F. Zhao, S. Lyu, S. Chen, J. Hong, J. Li, Ind. Eng. Chem. Res. 58 (2019) 1095–1104.

[26] P. Serp, in: J. Reedijk, K. Poeppelmeier (Eds.), Elsevier, Oxford, 2013, pp. 323–369.

[27] P. Serp, B. Machado, Nanostructured Carbon Materials for Catalysis, Royal Society of Chemistry, Cambridge, 2015.

[28] I.C. Gerber, P. Serp, Chem. Rev. 120 (2020) 1250–1349.

[29] J.H. Bitter, J. Mater. Chem. 20 (2010) 7312–7321.

[30] P. Serp, B. Machado, in: Nanostructured Carbon Mater. Catal., Royal Society of Chemistry, 2015, pp. 1–45.

[31] L.B. Ebert, J. Mol. Catal. 15 (1982) 275–296.

[32] Rosynek, M. P, (1976).

[33] J. Barrault, A. Guilleminot, J.C. Achard, V. Paul-Boncour, A. Percheron-Guegan, Appl. Catal. 21 (1986) 307–312.

[34] A. Guerrero-Ruiz, A. Sepúlveda-Escribano, I. Rodríguez-Ramos, Appl. Catal. A, Gen. 120 (1994) 71–83.

[35] T. Fu, Z. Li, Chem. Eng. Sci. 135 (2015) 3–20.

[36] B. Sun, K. Xu, L. Nguyen, M. Qiao, F.F. Tao, ChemCatChem 4 (2012) 1498–1511.

[37] K. Cheng, J. Kang, D.L. King, V. Subramanian, C. Zhou, Q. Zhang, Y. Wang, Advances in Catalysis for Syngas Conversion to Hydrocarbons, 1st ed., Elsevier Inc., 2017.

[38] C. Il Ahn, Y.M. Park, J.M. Cho, D.H. Lee, C.H. Chung, B.G. Cho, J.W. Bae, Catal. Surv. from Asia 20 (2016) 210–230.

[39] H. Xiong, L.L. Jewell, N.J. Coville, ACS Catal. 5 (2015) 2640−2658.

[40] K.K. Ramasamy, M. Gray, H. Job, Y. Wang, Chem. Eng. Sci. 135 (2015) 266–273.

[41] B.H. Davis, M.L. Occelli, Advances in Fischer-Tropsch Synthesis, Catalysts, and Catalysis, CRC Press, 2009.

[42] M.A. Fahim, T.A. Alsahhaf, A. Elkilani, in: Fundam. Pet. Refin., Elsevier, 2010, pp. 303–324.

[43] J.A. Schaidle, L.T. Thompson, J. Catal. 329 (2015) 325–334.

[44] M. Ojeda, R. Nabar, A.U. Nilekar, A. Ishikawa, M. Mavrikakis, E. Iglesia, J. Catal. 272 (2010) 287–297.

[45] B.T. Loveless, C. Buda, M. Neurock, E. Iglesia, J. Am. Chem. Soc. 135 (2013) 6107–6121.

[46] G.T.K.K.K.K. Gunasooriya, A.P. Van Bavel, H.P.C.E.C.E. Kuipers, M. Saeys, ACS Catal. 6 (2016) 3660–3664.

[47] J.X. Liu, H.Y. Su, D.P. Sun, B.Y. Zhang, W.X. Li, J. Am. Chem. Soc 135 (2013) 16284–16287.

[48] Q. Ge, M. Neurock, J. Phys. Chem. B 110 (2006) 15368–15380.

[49] W. Chen, B. Zijlstra, I.A.W.W. Filot, R. Pestman, E.J.M.M. Hensen, ChemCatChem 10 (2018) 136–140.

[50] B. Zijlstra, R.J.P. Broos, W. Chen, I.A.W. Filot, E.J.M. Hensen, Catal. Today 342 (2020) 131–141.

[51] L. Nie, Z. Li, T. Kuang, S. Lyu, S. Liu, Y. Zhang, B. Peng, J. Li, L. Wang, Chem. Commun. 55 (2019) 10559–10562.

[52] H. Pichler, H. Schulz, Chemie Ing. Tech. 42 (1970) 1162–1174.

[53] S. Storsæter, D. Chen, A. Holmen, Surf. Sci. 600 (2006) 2051–2063.

[54] J. Yang, V. Frøseth, D. Chen, A. Holmen, Surf. Sci. 648 (2016) 67–73.

[55] M. Zhuo, A. Borgna, M. Saeys, J. Catal. 297 (2013) 217–226.

[56] H. Schulz, K. Beck, E. Erich, Stud. Surf. Sci. Catal. 36 (1988) 457–471.

[57] G.P. Van Der Laan, A.A.C.M. Beenackers, Catal. Rev. - Sci. Eng. 41 (1999) 255–318.

[58] R.A. van Santen, A.J. Markvoort, I.A.W. Filot, M.M. Ghouri, E.J.M. Hensen, Phys. Chem. Chem. Phys. 15 (2013) 17038.

[59] A. Rose, J. Thiessen, A. Jess, D. Curulla-Ferré, Chem. Eng. Technol. 37 (2014) 683–691.

[60] M. Trépanier, C.A.D. Dion, A.K. Dalai, N. Abatzoglou, Can. J. Chem. Eng. 89 (2011) 1441–1450.

[61] B. Sarup, B.W. Wojciechowski, Can. J. Chem. Eng. 67 (1989) 62–74.

[62] A. Outi, I. Rautavuoma, H.S. van der Baan, Appl. Catal. 1 (1981) 247–272.

[63] A.N. Pour, M.R. Housaindokht, S. Mehdi, K. Shahri, Ind. Eng. Chem. Res. 57 (2018) 13639–13649.

[64] E. Van Steen, H. Schulz, Appl. Catal. A Gen. 186 (1999) 309–320.

[65] A. Haghtalab, J. Shariati, A. Mosayebi, React. Kinet. Mech. Catal. 126 (2019) 1003–1026.

[66] W. Qian, H. Zhang, W. Ying, D. Fang, Chem. Eng. J. 228 (2013) 526–534.

[67] W. Chen, T.F. Kimpel, Y. Song, F. Chiang, B. Zijlstra, R. Pestman, P. Wang, E.J.M. Hensen, ACS Catal. 8 (2018) 1580–1590.

[68] Z. Shariatinia, M. Abdollahi-moghadam, J. Saudi Chem. Soc. 22 (2018) 786–808.

[69] C.-Y. Liu, E.Y. Li, Sustain. Energy Fuels (2020).

[70] J. Yang, Y. Qi, J. Zhu, Y.A. Zhu, D. Chen, A. Holmen, J. Catal. 308 (2013) 37–49.

[71] J. Thiessen, A. Rose, J. Meyer, A. Jess, D. Curulla-ferré, Microporous Mesoporous Mater. 164 (2012) 199–206.

[72] G.L. Bezemer, P.B. Radstake, U. Falke, H. Oosterbeek, H.P.C.E. Kuipers, A.J. Van Dillen, K.P. De Jong, J. Catal. 237 (2006) 152–161.

[73] A.P. Steynberg., M.E. Dry, in: Stud. Surf. Sci. Catal., 2004, pp. 406–481.

[74] M. Claeys, E. van Steen, in: Stud. Surf. Sci. Catal., Elsevier Inc., 2004, pp. 601–680.

[75] J. Aluha, N.A. Yongfeng Hu, Catalysts (2017) 1–19.

[76] J. Aluha, F. Gitzhofer, N. Abatzoglou, Nanomaterials 8 (2018) 822.

[77] L. Guczi, G. Stefler, O. Geszti, Z. Koppány, Z. Kónya, É. Molnár, M. Urbán, J. Catal. 244 (2006) 24–32.

[78] M. Zaman, A. Khodadi, Y. Mortazavi, Fuel Process. Technol. 90 (2009) 1214–1219.

[79] J. Aluha, N. Abatzoglou, Can. J. Chem. Eng. 96 (2018) 2127–2137.

[80] T.O. Honsho, T. Kitano, T. Miyake, T. Suzuki, Fuel 94 (2012) 170–177.

[81] S. Farzad, A. Rashidi, A. Haghtalab, M.A. Mandegari, Fuel 132 (2014) 27–35.

[82] J.A. Díaz, A.R. De La Osa, P. Sánchez, A. Romero, J.L. Valverde, Catal. Commun. 44 (2014) 57–61.

[83] J. Yang, C. Ledesma Rodriguez, Y. Qi, H. Ma, A. Holmen, D. Chen, Appl. Catal. A Gen. 598 (2020) 117564.

[84] J.H. Boelee, J.M.G. Cüsters, K. Van Der Wiele, Appl. Catal. 53 (1989) 1–13.

[85] J.R. Khusnutdinova, J.A. Garg, D. Milstein, ACS Catal. 5 (2015) 2416–2422.

[86] F. Han, Z. Zhang, N. Niu, J. Li, Chem. Res. Chinese Univ. 34 (2018) 635–642.

[87] V.R.R. Pendyala, W.D. Shafer, G. Jacobs, B.H. Davis, Catal. Letters 144 (2014) 1088–1095.

[88] J. Huang, W. Qian, H. Ma, H. Zhang, W. Ying, RSC Adv. 7 (2017) 33441–33449.

[89] G.L. Bezemer, J.H. Bitter, H.P.C.E. Kuipers, H. Oosterbeek, J.E. Holewijn, X. Xu, F. Kapteijn, A.J. Van Dillen, K.P. De Jong, J. Am. Chem. Soc. 128 (2006) 3956–3964.

[90] T.W. van Deelen, H. Su, N.A.J.M.J.M. Sommerdijk, K.P. De Jong, Chem. Commun. 54 (2018) 2530–2533.

[91] H. Xiong, M.A.M.M. Motchelaho, M. Moyo, L.L. Jewell, N.J. Coville, J. Catal. 278 (2011) 26–40.

[92] A. Nakhaei, P. Mohammadreza, Catal Lett 143 (2013) 1328–1338.

[93] A.N. Pour, E. Hosaini, M. Izadyar, M.R. Housaindokht, Chinese J. Catal. 36 (2015) 1372–1378.

[94] A.N. Pour, M. Housaindokht, Prog. React. Kinet. Mech. 44 (2019) 316–323.

[95] J.P. den Breejen, J.R.A.A. Sietsma, H. Friedrich, J.H. Bitter, K.P. de Jong, J. Catal. 270 (2010) 146–152.

[96] S.A. Chernyak, E. V. Suslova, A.S. Ivanov, A. V. Egorov, K.I. Maslakov, S. V. Savilov, V. V. Lunin, Appl. Catal. A Gen. 523 (2016) 221–229.

[97] T. Fu, J. Lv, Z. Li, Ind. Eng. Chem. Res. 53 (2014) 1342–1350.

[98] Y. Yang, L. Jia, B. Hou, D. Li, J. Wang, Y. Sun, J. Phys. Chem. 118 (2014) 268−277.

[99] Q. Luo, L. Guo, S. Yao, J. Bao, Z.Z. Liu, Z.Z. Liu, J. Catal. 369 (2019) 143–156.

[100] J.P. Den Breejen, P.B. Radstake, G.L. Bezemer, J.H. Bitter, V. Frøseth, A. Holmen, K.P. De Jong, V. Fr{\o}seth, A. Holmen, K.P. De Jong, V. Froseth, A. Holmen, K.P. De Jong, V. Frseth, A. Holmen, K.P. De Jong, J. Am. Chem. Soc. 131 (2009) 7197–7203.

[101] P.B. Radstake, J.P. Den Breejen, G.L. Bezemer, J.H. Bitter, K.P. De Jong, A. Holmen, J. Am. Chem. Soc 167 (2007) 85–90.

[102] A. Nakhaei Pour, E. Hosaini, A. Tavasoli, A. Behroozsarand, F. Dolati, A. Nakhaei, E. Hosaini, A. Tavasoli, A. Behroozsarand, J. Nat. Gas Sci. Eng. 21 (2014) 772–778.

[103] M.K. Gnanamani, G. Jacobs, W.D. Shafer, B.H. Davis, Catal. Today 215 (2013) 13–17.

[104] J. Yang, E.Z. Tveten, D. Chen, A. Holmen, Langmuir 26 (2010) 16558–16567.

[105] R. Pestman, W. Chen, E. Hensen, ACS Catal. 9 (2019) 4189–4195.

[106] T.O. Eschemann, W.S. Lamme, R.L. Manchester, T.E. Parmentier, A. Cognigni, M. Rønning, K.P. De Jong, J. Catal. 328 (2015) 130–138.

[107] Y. Yang, L. Jia, B. Hou, D. Li, J. Wang, Y. Sun, Catal. Sci. Technol. 4 (2014) 717–728.

[108] Y. Yang, L. Jia, B. Hou, D. Li, J. Wang, Y. Sun, ChemCatChem 6 (2014) 319–327.

[109] E. Iglesia, Appl. Catal. A Gen. 161 (1997) 59–78.

[110] E. van Steen, M. Claeys, Chem. Eng. Technol. 31 (2008) 655–666.

[111] E. Rytter, N.E. Tsakoumis, A. Holmen, Catal. Today 261 (2016) 3–16.

[112] S. Lögdberg, M. Lualdi, S. Järs, J.C. Walmsley, E.A. Blekkan, E. Rytter, A. Holmen, J. Catal. 274 (2010) 84–98.

[113] T.O. Eschemann, J.H. Bitter, K.P. De Jong, Catal. Today 228 (2014) 89–95.

[114] M. Zhong, J. Wang, C. Chen, Z. Ma, L. Jia, B. Hou, D. Li, Catal. Sci. Technol. 9 (2019) 6037–6046.

[115] A. Barbier, A. Tuel, G.A. Martin, I. Arcon, I. Arcon, A. Kodre, A. Kodre, J. Catal. 200 (2001) 106–116.

[116] Q. Cheng, Y. Tian, S. Lyu, N. Zhao, K. Ma, T. Ding, Z. Jiang, L. Wang, J. Zhang, L. Zheng, F. Gao, L. Dong, N. Tsubaki, X. Li, Nat. Commun. 9 (2018).

[117] G. Prieto, A. Martínez, P. Concepción, R. Moreno-Tost, J. Catal. 266 (2009) 129–144.

[118] N. Fischer, E. Van Steen, M. Claeys, J. Catal. 299 (2013) 67–80.

[119] H. Li, S. Wang, F. Ling, J. Li, J. Mol. Catal. A Chem. 244 (2006) 33–40.

[120] H. Li, J. Li, H. Ni, D. Song, Catal. Letters 110 (2006) 71–76.

[121] T.T. Nguyen, P. Serp, ChemCatChem 5 (2013) 3595–3603.

[122] V.R. Surisetty, E. Epelde, M. Trépanier, J. Kozinski, A.K. Dalai, Int. J. Chem. React. Eng. 10 (2012).

[123] A. Tavasoli, M. Tre, A.K. Dalai, N. Abatzoglou, J. Chem. Eng. Data. 55 (2010) 2757–2763.

[124] W. Chen, Z. Fan, X. Pan, X. Bao, J. Am. Chem. Soc. 130 (2008) 9414–9419.

[125] P. Serp, M. Corrias, P. Kalck, Appl. Catal. A Gen. 253 (2003) 337–358.

[126] O. Akbarzadeh, N.A.M. Zabidi, Y.A. Wahab, N.A. Hamizi, Z.Z. Chowdhury, Z.M.A. Merican, M.A. Rahman, S. Akhter, E. Rasouli, M.R. Johan, Symmetry (Basel). 10 (2018) 572.

[127] V. Vosoughi, S. Badoga, A.K. Dalai, N. Abatzoglou, Ind. Eng. Chem. Res. 55 (2016) 6049–6059.

[128] M. Trépanier, A. Tavasoli, A.K. Dalai, N. Abatzoglou, Fuel Process. Technol. 90 (2009) 367–374.

[129] W. Xie, Y. Zhang, K. Liew, J. Li, Sci. China Chem. 55 (2012) 1811–1818.

[130] W. Chen, X. Pan, X. Bao, J. Am. Chem. Soc. 129 (2007) 7421–7426.

[131] T. Fu, Z. Li, Catal. Commun. 47 (2014) 54–57.

[132] A. Karimi, A. Mohajeri, A.J. Jolodar, A.M. Rashidi, K. Forsat, J. Pet. Sci. Technol. 6 (2016) 14–27.

[133] M. Trépanier, A.K. Dalai, N. Abatzoglou, Appl. Catal. A Gen. 374 (2010) 79–86.

[134] A. Karimi, B. Nasernejad, A.M. Rashidi, Korean J. Chem. Eng 29 (2012) 1516–1524.

[135] F. Yang, B. Hu, W. Xia, B. Peng, J. Shen, M. Muhler, J. Catal. 365 (2018) 55–62.

[136] W.C. Conner, J.L. Falconer, Chem. Rev. 95 (1995) 759–788.

[137] D. Nabaho, J.W. (Hans. W. (Hans. Niemantsverdriet, M. Claeys, E. van Steen, Catal. Today 275 (2016) 27–34.

[138] D. Nabaho, J.W. Niemantsverdriet, M. Claeys, E. Van Steen, Catal. Today 261 (2016) 17–27.

[139] A.C. Ghogia, S. Cayez, B.F. Machado, A. Nzihou, P. Serp, K. Soulantica, D. Pham Minh, ChemCatChem 12 (2020) 1–13.

[140] T.N. Phaahlamohlaka, D.O. Kumi, M.W. Dlamini, R. Forbes, L.L. Jewell, D.G. Billing, N.J. Coville, ACS Catal. 7 (2017) 1568–1578.

[141] Z. Wang, F.H. Yang, R.T. Yang, J. Phys. Chem. C 114 (2010) 1601–1609.

[142] T.N. Phaahlamohlaka, M.W. Dlamini, D.O. Kumi, R. Forbes, L.L. Jewell, N.J. Coville, Appl. Catal. A, Gen. 599 (2020) 117617.

[143] A.M. Saib, D.J. Moodley, I.M. Ciobîc, M.M. Hauman, B.H. Sigwebela, Catal. Today 154 (2010) 271–282.

[144] G.L. Bezemer, T.J. Remans, A.P. Van Bavel, A.I. Dugulan, J. Am. Chem. Soc. 132 (2010) 8540–8541.

[145] A. Nakhaei, P. Elham, H. Mostafa, J. Iran. Chem. Soc. 13 (2015) 139–147.

[146] M. Trépanier, A. Tavasoli, S. Anahid, A. K.Dalai, Iran. J. Chem. Chem. Eng. 30 (2011) 37–47.

[147] M. Wolf, B.K. Mutuma, N.J. Coville, N. Fischer, M. Claeys, ACS Catal. 8 (2018) 3985–3989.

[148] Ø. Borg, Z. Yu, D. Chen, E.A. Blekkan, E. Rytter, A. Holmen, Top. Catal. 57 (2014) 491–499.

[149] C.G. Okoye-Chine, M. Moyo, X. Liu, D. Hildebrandt, Fuel Process. Technol. 192 (2019) 105–129.

[150] M.M. Keyser, F.F. Prinsloo, in: Stud. Surf. Sci. Catal., Elsevier Inc., 2007, pp. 45–73.

[151] S. Chernyak, A. Burtsev, A. Egorov, K. Maslakov, S. Savilov, V. Lunin, Funct. Mater. Lett. (2020).

[152] M.R. Hemmati, M. Kazemeini, F. Khorasheh, J. Zarkesh, A. Rashidi, J. Nat. Gas Chem. 21 (2012) 713–721.

[153] J. Hong, B. Wang, G. Xiao, N. Wang, Y. Zhang, A.Y. Khodakov, J. Li, ACS Catal. 10 (2020) 5554−5566.

[154] T.W. van Deelen, H. Yoshida, R. Oord, J. Zečević, B.M. Weckhuysen, K.P. de Jong, Appl. Catal. A Gen. 593 (2020).

[155] S. Taghavi, A. Asghari, A. Tavasoli, Chem. Eng. Res. Des. 119 (2017) 198–208.

[156] P. Munnik, P.E. De Jongh, K.P. De Jong, Chem. Rev. 115 (2015) 6687–6718.

[157] J. Aluha, P. Boahene, A. Dalai, Y. Hu, K. Bere, N. Braidy, N. Abatzoglou, Ind. Eng. Chem. Res. 54 (2015) 10661–10674.

[158] H. Almkhelfe, X. Li, P. Thapa, K.L. Hohn, P.B. Amama, J. Catal. 361 (2018) 278–289.

[159] A. Tavasoli, S. Taghavi, J. Energy Chem. 22 (2013) 747–754.

[160] H. Xiong, M. Moyo, M.K. Rayner, L.L. Jewell, D.G. Billing, N.J. Coville, ChemCatChem 2 (2010) 514–518.

[161] T. Fu, Y. Jiang, J. Lv, Z. Li, Fuel Process. Technol. 110 (2013) 141–149.

[162] C. Perego, P. Villa, 34 (1997) 281–305.

[163] K.P. De Jong, Synthesis of Solid Catalysts, Wiley-VCH, 2009.

[164] G.J. Hutchings, J.C. Védrine, Springer Ser. Chem. Phys. 75 (2004) 215–258.

[165] H.-B. Zhang, X.-L. Liang, X. Dong, H.-Y. Li, G.-D. Lin, Catal Surv Asia 13 (2009) 41–58.

[166] H. Bin Zhang, X. Dong, G.D. Lin, X.L. Liang, H.Y. Li, Chem. Commun. (2005) 5094–5096.

[167] X. Dong, X.L. Liang, H.Y. Li, G.D. Lin, P. Zhang, H. Bin Zhang, Catal. Today 147 (2009) 158–165.

[168] J.W. Geus, A.J. Van Dillen, in: Prep. Solid Catal., Wiley Blackwell, Weinheim, Germany, 2008, pp. 460–487.

[169] P. Serp, J.L. Figueiredo, Carbon Material for Catalysis, 2009.

[170] G.L. Bezemer, P.B. Radstake, V. Koot, A.J. Van Dillen, J.W. Geus, K.P. De Jong, J. Catal. 237 (2006) 291–302.

[171] S. Eriksson, U. Nylén, S. Rojas, M. Boutonnet, Appl. Catal. A Gen. 265 (2004) 207–219.

[172] A. Karimi, B. Nasernejad, A. Morad, A. Tavasoli, M. Pourkhalil, Fuel 117 (2014) 1045–1051.

[173] M. Davari, S. Karimi, A. Tavasoli, A. Karimi, Appl. Catal. A Gen. 485 (2014) 133–142.

[174] C.L. Bianchi, F. Martini, P. Moggi, Catal. Letters 76 (2001) 65–69.

[175] A.F. Zainul Abidin, K.S. Loh, W.Y. Wong, A.B. Mohamad, I. Puspasari, Int. J. Hydrogen Energy 43 (2018) 11047–11055.

[176] J. Blanchard, N. Abatzoglou, R. Eslahpazir-Esfandabadi, F. Gitzhofer, Ind. Eng. Chem. Res. 49 (2010) 6948–6955.

[177] F. Guo, J.Q. Xu, W. Chu, Catal. Today 256 (2015) 124–129.

[178] R. Pristavita, N.Y. Mendoza-Gonzalez, J.L. Meunier, D. Berk, Plasma Chem. Plasma Process. 30 (2010) 267–279.

[179] J. Aluha, S. Blais, N. Abatzoglou, Catal. Letters 148 (2018) 2149–2161.

[180] A.S.M. Ismail, M. Casavola, B. Liu, A. Gloter, T.W. Van Deelen, M. Versluijs, J.D. Meeldijk, O. Stéphan, K.P. De Jong, F.M.F. De Groot, ACS Catal. 9 (2019) 7998–8011.

[181] P. Serp, J.C. Hierso, R. Feurer, R. Corratgé, Y. Kihn, P. Kalck, A.E. Aksoylu, J.L. Faria, A.M.T. Pacheco, J.L. Figueiredo, Stud. Surf. Sci. Catal. 130 B (2000) 1001–1006.

[182] P. Serp, P. Kalck, R. Feurer, Chem. Rev. 102 (2002) 3085–3128.

[183] T. Kuang, S. Lyu, S. Liu, Y. Zhang, J. Li, G. Wang, L. Wang, J. Energy Chem. 33 (2019) 67–73.

[184] I. Kazemnejad, A. Feizbakhsh, A. Niazi, A. Tavasoli, Int. J. Ind. Chem. 10 (2019) 321–333.

[185] U.M. Graham, G. Jacobs, M.K. Gnanamani, S.M. Lipka, W.D. Shafer, C.R. Swartz, T. Jermwongratanachai, R. Chen, F. Rogers, B.H. Davis, ACS Catal. 4 (2014) 1662–1672.

[186] J. Shariati, A. Haghtalab, A. Mosayebi, J. Energy Chem. 28 (2019) 9–22.

[187] A.D. Bokare, W. Choi, J. Hazard. Mater. 275 (2014) 121–135.

[188] M. Xie, J. Yang, J. Liang, X. Guo, W. Ding, Carbon N. Y. 77 (2014) 215–225.

[189] M.Y. Nassar, I.S. Ahmed, Polyhedron 30 (2011) 2431–2437.

[190] C. Liu, Y. He, L. Wei, Y. Zhang, Y. Zhao, J. Hong, S. Chen, L. Wang, J. Li, ACS Catal. 8 (2018) 1591–1600.

[191] B. Wang, Y. Han, S. Chen, Y. Zhang, J. Li, J. Hong, Catal. Today (2019) 0–1.

[192] M.W. Dlamini, D.O. Kumi, T.N. Phaahlamohlaka, ChemCatChem 7 (2015) 3000–3011.

[193] S.A. Chernyak, G.E. Selyaev, E. V Suslova, A. V Egorov, K.I. Maslakov, A.N. Kharlanov, Kinet. Catal. 57 (2016) 645–651.

[194] Q. Yang, Q. Xu, H.L. Jiang, Chem. Soc. Rev. 46 (2017) 4774–4808.

[195] W.G. Cui, G.Y. Zhang, T.L. Hu, X.H. Bu, Coord. Chem. Rev. 387 (2019) 79–120.

[196] C. Zhang, X. Guo, Q. Yuan, R. Zhang, Q. Chang, K. Li, B. Xiao, S. Liu, C. Ma, X. Liu, Y. Xu, X. Wen, Y. Yang, Y. Li, ACS Catal. 8 (2018) 7120–7130.

[197] N. Li, C.P. Ma, C.H. Zhang, Y. Yang, Y.W. Li, J. Fuel Chem. Technol. 47 (2019) 428–437.

[198] M. Rivera-Torrente, C. Hernández Mejía, T. Hartman, K.P. de Jong, B.M. Weckhuysen, Catal. Letters 149 (2019) 3279–3286.

[199] A. Panda, E. Kim, Y.N. Choi, J. Lee, S. Venkateswarlu, M. Yoon, Catalysts 9 (2019).

[200] Y. Pei, Z. Li, Y. Li, AIChE J. 63 (2017) 2935–2944.

[201] Y. Chen, X. Li, M.U. Nisa, J. Lv, Z. Li, Fuel 241 (2019) 802–812.

[202] B. Qiu, C. Yang, W. Guo, Y. Xu, Z. Liang, D. Ma, R. Zou, J. Mater. Chem. A 74 (2017) 8081–8086.

[203] H. Janani, A.A. Mirzaei, A. Rezvani, React. Kinet. Mech. Catal. 128 (2019) 205–215.

[204] J. Liu, Z. Wang, X. Yan, P. Jian, J. Colloid Interface Sci. 505 (2017) 789–795.

[205] Z. Ni, S. Kang, J. Bai, Y. Li, Y. Huang, Z. Wang, H. Qin, X. Li, J. Colloid Interface Sci. 505 (2017) 325–331.

[206] N.M. Deraz, J. Ind. Environ. Chem. 2 (2018) 19–21.

[207] J. Aluha, N. Braidy, A. Dalai, N. Abatzoglou, Can. J. Chem. Eng. 94 (2016) 1504–1515.

[208] W. Chu, J. Xu, J. Hong, T. Lin, A. Khodakov, Catal. Today 256 (2015) 41–48.

[209] Z. Yu, Ø. Borg, D. Chen, E. Rytter, A. Holmen, Top. Catal. 45 (2007) 69–74.

[210] Z. Yu, Ø. Borg, D. Chen, C. Enger, V. Frøseth, E. Rytter, Catal. Letters 109 (2006) 2–6.

[211] J. Antonio, A. Romero, A.M. García-minguillán, A. Giroir-fendler, J. Luis, Fuel Process. Technol. 138 (2015) 455–462.

[212] J.A. Díaz, M. Martínez-fernández, A. Romero, J. Luis, J.L. Valverde, J. Luis, J.L. Valverde, J. Luis, Fuel 111 (2013) 422–429.

[213] A. Tavasoli, R.M.M.M. Abbaslou, M. Trepanier, A.K. Dalai, Appl. Catal. A Gen. 345 (2008) 134–142.

[214] K.S. Ha, G. Kwak, K.W. Jun, J. Hwang, J. Lee, Chem. Commun. 49 (2013) 5141–5143.

[215] X. Li, M.U. Nisa, Y. Chen, Z. Li, Ind. Eng. Chem. Res. 58 (2019) 3459–3467.

[216] Y. Zhao, S. Huang, L. Wei, Y. Zhang, A. Lin, C. Liu, J. Li, Ind. Eng. Chem. Res. 59 (2020) 3279–3286.

[217] M. Luo, H. Li, React. Kinet. Mech. Catal. 124 (2018) 279–291.

[218] S. Karimi, A. Tavasoli, Y. Mortazavi, A. Karimi, Chem. Eng. Res. Des. 104 (2015) 713–722.

[219] A.Y. Khodakov, W. Chu, P. Fongarland, Chem. Rev. 107 (2007) 1692–1744.

[220] H. Xiong, M.A.M.M. Motchelaho, M. Moyo, L.L. Jewell, N.J. Coville, Catal. Today 214 (2013) 50–60.

[221] S.A. Chernyak, E. V. Suslova, A. V. Egorov, L. Lu, S. V. Savilov, V. V. Lunin, Fuel Process. Technol. 140 (2015) 267–275.

[222] Z. Jiang, Y. Zhao, C. Huang, Y. Song, D. Li, Fuel 226 (2018) 213–220.

[223] H. Zhang, C. Lancelot, W. Chu, J. Hong, A.Y. Khodakov, P.A. Chernavskii, D. Tong, J. Mater. Chem. (2009) 9241–9249.

[224] J. Jimmy, A. Roesyadi, S. Suprapto, F. Kurniawansyah, W. Anggraini, R. Rahmawati, J. Appl. Eng. Sci. 18 (2020) 1–9.

[225] O. Akbarzadeh, N. Asmawati, M. Zabidi, Y.A. Wahab, N.A. Hamizi, Z.Z. Chowdhury, Z. Merican, A. Merican, Symmetry (Basel). 11 (2019) 7.

[226] C. Xing, G. Yang, D. Wang, C. Zeng, Y. Jin, R. Yang, Y. Suehiro, N. Tsubaki, Catal. Today 215 (2013) 24–28.

[227] H. Park, Y. Kim, H. Youn, H. Choi, Y. Kim, ChemCatChem 9 (2017) 4098–4104.

[228] Y. Liu, T. Dintzer, J. Energy Chem. 22 (2013) 279–289.

[229] J. Zhu, J. Yang, A. Helland, Y. Zhu, Y. Yu, Catal. Today 215 (2013) 121–130.

[230] K. Cheng, V. Subramanian, A. Carvalho, V. V. Ordomsky, Y. Wang, A.Y. Khodakov, J. Catal. 337 (2016) 260–271.

[231] S.A. Chernyak, D.N. Stolbov, A.S. Ivanov, S. V Klokov, T.B. Egorova, K.I. Maslakov, O.L. Eliseev, V. V Maximov, S. V Savilov, V. V Lunin, Catal. Today (2019) 1–10.

[232] J.A. Díaz, M. Martínez-fernández, A. Romero, J. Luis, Fuel 111 (2013) 422–429.

[233] V. Benedetti, S.S. Ail, F. Patuzzi, D. Cristofori, R. Rauch, M. Baratieri, Renew. Energy 147 (2020) 884–894.

[234] H. Zhang, C. Lancelot, W. Chu, J. Hong, A.Y. Khodakov, P.A. Chernavskii, J. Zheng, D.

Tong, J. Zheng, D. Tong, J. Zheng, D. Tong, J. Zheng, D. Tong, J. Mater. Chem. 19 (2009) 9241.

[235] S.A. Chernyak, N.E. Strokova, E.S. Fedorova, A.S. Ivanov, K.I. Maslakov, S. V. Savilov, V. V. Lunin, Phys. Chem. Chem. Phys. 21 (2019) 13243–13249.

[236] M.A. Kazakova, A.S. Andreev, A.G. Selyutin, V. Arcady, A. V Shuvaev, V.L. Kuznetsov, O.B. Lapina, Appl. Surf. Sci. 456 (2018) 657–665.

[237] M. Luo, S. Li, Z. Di, Z. Yang, W. Chou, B. Shi, Appl. Catal. A Gen. 599 (2020) 117608.

[238] H. Oliaei Torshizi, A. Nakhaei Pour, A. Mohammadi, Y. Zamani, New J. Chem. 44 (2020) 6053–6062.

[239] S. Li, N. Yao, F. Zhao, X. Li, Catal. Sci. Technol. 6 (2016) 2188–2194.

[240] M.W. Dlamini, T.N. Phaahlamohlaka, D.O. Kumi, R. Forbes, L.L. Jewell, N.J. Coville, Catal. Today 342 (2020) 99–110.

[241] C. Galeano, J.C. Meier, M. Soorholtz, H. Bongard, C. Baldizzone, K.J.J. Mayrhofer, F. Schüth, ACS Catal. 4 (2014) 3856–3868.

[242] M.A. Fraga, E. Jordão, M.J. Mendes, M.M.A. Freitas, J.L. Faria, J.L. Figueiredo, J. Catal. 209 (2002) 355–364.

[243] J. Li, L. Ma, X. Li, C. Lu, H. Liu, Ind. Eng. Chem. Res. 44 (2005) 5478–5482.

[244] E. V. Suslova, S. V. Savilov, A. V. Egorov, V. V. Lunin, Kinet. Catal. 60 (2019) 87–95.

[245] Q. Cheng, N. Zhao, S. Lyu, Y. Tian, F. Gao, L. Dong, Z. Jiang, J. Zhang, N. Tsubaki, X. Li, Appl. Catal. B Environ. 248 (2019) 73–83.

[246] O.Y. Podyacheva, A.S. Lisitsyn, L.S. Kibis, A.I. Stadnichenko, A.I. Boronin, E.M. Slavinskaya, O.A. Stonkus, S.A. Yashnik, Z.R. Ismagilov, Catal. Today 301 (2018) 125–133.

[247] O. Akbarzadeh, N.A.M. Zabidi, N.A. Hamizi, Y.A. Wahab, Z.M.A. Merican, W.A. Yehya, S. Akhter, M. Shalauddin, E. Rasouli, M.R. Johan, Symmetry (Basel). 11 (2019) 50.

[248] S.A. Chernyak, A.S. Ivanov, K.I. Maslakov, A. V. Egorov, Z. Shen, S.S. Savilov, V. V. Lunin, Phys. Chem. Chem. Phys. 19 (2017) 2276–2285.

[249] A. Tavasoli, M. Irani, A. Nakhaeipour, Y. Mortazavi, A.A. Khodadadi, A.K. Dalai, Iran. J. Chem. Chem. Eng. 28 (2009) 37–48.

[250] C. Qin, B. Hou, J. Wang, G. Wang, Z. Ma, L. Jia, D. Li, ACS Appl. Mater. Interfaces 11 (2019) 33886–33893.

[251] D. Song, J. Li, Q. Cai, J. Phys. Chem. C 111 (2007) 18970–18979.

[252] R. Xie, H. Wang, P. Gao, L. Xia, Z. Zhang, T. Zhao, Y. Sun, Appl. Catal. A Gen. 492 (2015) 93–99.

[253] L. Shi, D. Li, B. Hou, Y. Wang, Y. Sun, Fuel Process. Technol. 91 (2010) 394–398.

[254] L. Shi, D. Li, B. Hou, Y. Sun, Chinese J. Catal. 28 (2007) 999–1002.

[255] Y. Zhang, K. Hanayama, N. Tsubaki, Catal. Commun. 7 (2006) 251–254.

[256] Y.H. Zhao, Y.H. Song, Q.Q. Hao, Y.J. Wang, W. Wang, Z.T. Liu, D. Zhang, Z.W. Liu, Q.J. Zhang, J. Lu, Fuel Process. Technol. 138 (2015) 116–124.

[257] P. Zhai, P.P. Chen, J. Xie, J.X. Liu, H. Zhao, L. Lin, B. Zhao, H.Y. Su, Q. Zhu, W.X. Li,

D. Ma, Faraday Discuss. 197 (2017) 207–224.

[258] D. Schanke, E. Bergene, A. Holmen, WO 98/38147 (1998) Publ. date 03.09.98, Priority data: 28.02.97.

[259] Y. Liu, J. Luo, M. Girleanu, O. Ersen, C. Pham-huu, C. Meny, J. Catal. 318 (2014) 179–192.

[260] H. Koo, G.Y. Han, J.W. Bae, Korean J. Chem. Eng 33 (2016) 1565–1570.

[261] A.Y. Khodakov, Brazilian J. Phys. 39 (2009) 171–175.

[262] A. de la Osa, A. Romero, F. Dorado, J. Valverde, P. Sánchez, Catalysts 6 (2016) 98.

[263] J.W. Bae, S.M. Kim, S.H. Kang, K.V.R.R. Chary, Y.J. Lee, H.J. Kim, K.W. Jun, J. Mol. Catal. A Chem. 311 (2009) 7–16.

[264] M.P. Rosynek, C.A. Polansky, Appl. Catal. 73 (1991) 97–112.

[265] X. Li, H. Almkhelfe, N.M. Bedford, T.C. Back, K.L. Hohn, P.B. Amama, Catal. Today 338 (2019) 40–51.

[266] L. Fratalocchi, C.G. Visconti, L. Lietti, Appl. Catal. A, Gen. 595 (2020) 117514.

[267] J. Panpranot, S. Kaewkun, P. Praserthdam, J.G. Goodwin, Catal. Letters 91 (2003) 95–102.

[268] M. Kraum, M. Baerns, Appl. Catal. A Gen. 186 (1999) 189–200.

[269] A.J. van D. and K.P. de J. G. L. Bezemer, A. van Laak, Stud. Surf. Sci. Catal. 147 (2004) 259–264.

[270] J. Lv, X. Ma, S. Bai, C. Huang, Z. Li, J. Gong, Int. J. Hydrogen Energy 36 (2011) 8365–8372.

[271] J. Lü, C. Huang, S. Bai, Y. Jiang, Z. Li, J. Nat. Gas Chem. 21 (2012) 37–42.

[272] S. Iqbal, T.E. Davies, D.J. Morgan, K. Karim, J.S. Hayward, J.K. Bartley, S.H. Taylor, G.J. Hutchings, Catal. Today 275 (2016) 35–39.

[273] T. Fu, C. Huang, J. Lv, Z. Li, Fuel 121 (2014) 225–231.

[274] S.A. Chernyak, E. V. Suslova, A. V. Egorov, K.I. Maslakov, S. V. Savilov, V. V. Lunin, Appl. Surf. Sci. 372 (2016) 100–107.

[275] P. Wang, S. Chen, Y. Bai, X. Gao, X. Li, K. Sun, H. Xie, G. Yang, Y. Han, Y. Tan, Fuel 195 (2017) 69–81.

[276] Z. Zhao, W. Lu, H. Zhu, W. Dong, Y. Lyu, T. Liu, X. Chen, Y. Wang, Y. Ding, J. Catal. 361 (2018) 156–167.

[277] H. Zhang, W. Chu, C. Zou, Catal Lett 141 (2011) 438–444.

[278] A. Jean-Marie, A. Griboval-Constant, A.Y. Khodakov, F. Diehl, Catal. Today 171 (2011) 180–185.

[279] J. Xiong, Y. Ding, T. Wang, L. Yan, W. Chen, H. Zhu, Y. Lu, Catal. Letters 102 (2005) 265–269.

[280] S. Wang, Q. Yin, J. Guo, L. Zhu, Energy Fuels 27 (2013) 3961−3968.

[281] T. Wang, Y. Ding, J. Xiong, L. Yan, H. Zhu, Y. Lu, L. Lin, Catal. Letters 107 (2006) 47–52.

[282] X. Ma, G. Lin, H. Zhang, Catal. Letters 111 (2006) 3–4.

[283] V.R. Surisetty, A.K. Dalai, J. Kozinski, Ind. Eng. Chem. Res. 49 (2010) 6956–6963.

[284] Z. Zhao, W. Lu, C. Feng, X. Chen, H. Zhu, R. Yang, W. Dong, M. Zhao, Y. Lyu, T. Liu, Z. Jiang, Y. Ding, J. Catal. 370 (2019) 251–264.

[285] F. Jiang, S. Wang, J. Zheng, B. Liu, Y. Xu, X. Liu, Catal. Today (2020) 1–9.

[286] G.R. Johnson, S. Werner, A.T. Bell, ACS Catal. 5 (2015) 5888–5903.

[287] T. Wang, Y. Ding, L. Yuan, H. Zhu, L. Lin, J. Nat. Gas Chem. 17 (2008) 153–158.

[288] G. Jiao, Y. Ding, H. Zhu, X. Li, J. Li, R. Lin, W. Dong, Appl. Catal. A Gen. 364 (2009) 137–142.

[289] Y. Pei, S. Jian, C. Wang, RSC Adv 5 (2015) 76330–76336.

[290] G.L. Bezemer, U. Falke, A. Jos, V. Dillen, K.P. De Jong, Chem. Commun. (2005) 731–733.

[291] Z. Wang, G. Laddha, S. Kanitkar, J.J. Spivey, Catal. Today 298 (2017) 209–215.

[292] J. Wang, P.A. Chernavskii, Y. Wang, A.Y. Khodakov, Fuel 103 (2013) 1111–1122.

[293] W.P. Ma, Y.J. Ding, L.W. Lin, Ind. Eng. Chem. Res 43 (2004) 2391–2398.

[294] M. Trépanier, A. Tavasoli, A.K. Dalai, N. Abatzoglou, Appl. Catal. A Gen. 353 (2009) 193–202.

[295] Z. Zhao, W. Lu, R. Yang, H. Zhu, W. Dong, F. Sun, Z. Jiang, Y. Lyu, T. Liu, H. Du, Y. Ding, ACS Catal. 8 (2018) 228–241.

[296] A.A. Chen, L. Geoffroy, M. Kaminsky, G.L. Geoffroy, M.A. Vannice, J. Phys. Chem. 90 (1986) 4810–4819.

[297] I.B. Catalyst, F. Synthesis, J. Nat. Gas Chem. 15 (2006) 335–339.

[298] H. Du, H. Zhu, T. Liu, Z. Zhao, X. Chen, W. Dong, W. Lu, W. Luo, Y. Ding, Catal. Today 281 (2017) 549–558.

[299] J.A. Díaz, H. Akhavan, A. Romero, A.M. Garcia-Minguillan, R. Romero, A. Giroir-Fendler, J.L. Valverde, Fuel Process. Technol. 128 (2014) 417–424.

[300] A. Tavasoli, M. Trépanier, R.M. Malek, A.K. Dalai, N. Abatzoglou, Fuel Process. Technol. 90 (2009) 1486–1494.

[301] H. Du, H. Zhu, Z. Zhao, W. Dong, W. Luo, W. Lu, M. Jiang, T. Liu, Y. Ding, "Applied Catal. A, Gen. 523 (2016) 263–271.

[302] J. Aluha, N. Abatzoglou, Gold Bull 50 (2017) 147–162.

[303] A.S. Albazzaz, A. Ghassanalsultan, S. Ali, Y.H. Taufiq-yaq, M. Amran, M. Salleh, W. Azlina, W. Abdul, K. Ghani, J. Energy Environ. Chem. Eng. 3 (2018) 40–53.

[304] J. Aluha, N. Abatzoglou, J. Ind. Eng. Chem. 50 (2017) 199–212.

[305] S. Ali, N. Asmawati, M. Zabidi, D. Subbarao, J. Nat. Gas Chem. 20 (2011) 659–663.

[306] Y. Pei, Y. Ding, H. Zhu, H. Du, Chinese J. Catal. 36 (2015) 355–361.

[307] H. Du, H. Zhu, X. Chen, W. Dong, W. Lu, W. Luo, M. Jiang, T. Liu, Y. Ding, Fuel 182 (2016) 42–49.

[308] V.R. Surisetty, I. Eswaramoorthi, A.K. Dalai, Fuel 96 (2012) 77–84.

[309] A. Holmen, H.J. Venvik, R. Myrstad, J. Zhu, D. Chen, Catal. Today 216 (2013) 150–157.

[310] Y. Chin, J. Hu, C. Cao, Y. Gao, Y. Wang, Catal. Today 110 (2005) 47–52.

[311] B. Jager, M.E. Dry, T. Shingles, a. P. Steynberg, Catal. Letters 7 (1990) 293–301.

[312] W. Chen, T.F. Kimpel, Y. Song, F. Chiang, B. Zijlstra, R. Pestman, P. Wang, E.J.M. Hensen, ACS Catal. 8 (2018) 1580−1590.

[313] A. Sims, M. Jeffers, S. Talapatra, K. Mondal, S. Pokhrel, L. Liang, X. Zhang, A.L. Elias, B.G. Sumpter, V. Meunier, M. Terrones, Carbon N. Y. 121 (2017) 274–284.

[314] S. Zarubova, S. Rane, J. Yang, Y. Yu, Y. Zhu, D. Chen, A. Holmen, ChemSusChem 4 (2011) 935–942.

[315] V. Meille, Appl. Catal. A Gen. 315 (2006) 1–17.